2021

Quasilinear Control: Multivariate Nonlinearities, Robustness and Numerical Properties, and Applications

Sarnaduti Brahma
University of Vermont

Follow this and additional works at: https://scholarworks.uvm.edu/graddis

 Part of the Electrical and Electronics Commons

Quasilinear Control: Multivariate Nonlinearities, Robustness and Numerical Properties, and Applications

A Dissertation Presented

by

Sarnaduti Brahma

to

The Faculty of the Graduate College

of

The University of Vermont

In Partial Fulfillment of the Requirements
for the Degree of Doctor of Philosophy
Specializing in Electrical Engineering

October, 2021

Defense Date: August 26th, 2021
Dissertation Examination Committee:

Hamid Reza Ossareh, Ph.D., Advisor
Safwan Wshah, Ph.D., Chairperson
Mads Almassalkhi, Ph.D.
Luis Duffaut Espinosa, Ph.D.
ShiNung Ching, Ph.D., Washington University in St. Louis
Cynthia J. Forehand, Ph.D., Dean of the Graduate College

ABSTRACT

Quasilinear Control (QLC) is a theory with a set of tools used for the analysis and design of controllers for nonlinear feedback systems driven by stochastic inputs. It is based on the concept of Stochastic Linearization (SL), which is a method of linearizing a nonlinear function that, unlike traditional Jacobian linearization, uses statistical properties of the input to the nonlinearity to linearize it. Until now in the literature of QLC, SL was applied only to feedback systems with single-variable nonlinearities that appear only in actuators and/or sensors. In this dissertation, my recent contributions to the literature of QLC are summarized. First, the QLC theory is extended to feedback systems with isolated multivariate nonlinearities that can appear anywhere in the loop and applied to optimal controller design problems, including systems with state-multiplicative noise. Second, the numerical properties of SL, particularly, the accuracy, robustness, and computation of SL, are investigated. Upper bounds are provided for the open-loop relative accuracy and, consequently, the closed-loop accuracy of SL. A comparison of the computational costs of several common numerical algorithms in solving the SL equations is provided, and a coordinate transformation proposed to improve most of their success rates. A numerical investigation is carried out to determine the relative sensitivities of SL coefficients to system parameters. Finally, QLC is applied to the optimal primary frequency control of power systems with generator saturation, and control of virtual batteries in distribution feeders.

The expected impacts of this work are far-reaching. On the technical front, this work provides: *i*) a new set of theoretical and algorithmic tools that can improve and simplify control of complex systems affected by noise, *ii*) information to control engineers on accuracy guarantees, choice of solvers, and relative sensitivities of SL coefficients to system parameters to guide the analysis and design of nonlinear stochastic systems in the context of QLC, *iii*) a new computationally efficient method of addressing saturation in generators or virtual batteries in modern electric power systems, resulting in efficient utilization of resources in providing grid services. On the societal front, this work: *i*) enables technologies that rely on computationally-efficient algorithms for automation of complex systems, e.g., control of soil temperature for agriculture, which depends on multiple factors like soil moisture and net radiation, *ii*) allows effective coordination of controllable smart devices in people's homes, so as not to hamper their quality of service, and *iii*) provides a stepping stone towards key societal challenges like combating climate change by facilitating reliable operation of the grid with significant renewable penetration.

Dedicated to my parents.

ACKNOWLEDGEMENTS

TABLE OF CONTENTS

LIST OF FIGURES

LIST OF TABLES

CHAPTER 1

INTRODUCTION

1.1 BACKGROUND

Actuators and sensors (i.e., instrumentation) in control systems are often nonlinear. One of the most common examples is actuator saturation. While plants are generally nonlinear as well, they can usually be linearized around an operating point if the control system is well-designed. The nonlinear instrumentation, however, cannot. This is because external inputs to the system may be large enough to force the actuators and sensors to operate far from their designed operating point, activating nonlinearities in them.

Nonlinear feedback systems with static nonlinearities have been researched for more than 100 years. The theory of Lyapunov stability and absolute stability ([2–4]) have led to significant developments. Performance analysis of systems with saturation has been discussed in [5,6]. Nonlinear systems with stochastic inputs and randomly varying parameters have been studied in [7–9]. A challenge with most existing methods for nonlinear stochastic systems is that they are, in general, either conservative

or difficult to apply in practice.

1.1.1 Review of Common Techniques for nonlinear systems

Some common techniques for the analysis and design of controllers for nonlinear systems are:

- **Model Predictive Control:** This method involves predicting the future trajectories of the system given different inputs over a horizon, possibly subject to constraints, and selecting the best input trajectory that optimizes an objective function over that horizon [10–14]. Only the first sample of the input trajectory is applied to the system at the next time step and the optimization problem solved again at the next step. The drawback is that this requires a lot of computation at every step of the process, and for nonlinear systems would require solving nonlinear programming problems which may have issues such as lack of uniqueness of a solution.

- **Describing Functions**: It approximates the nonlinear system with an equivalent gain by applying a sinusoidal signal at its input and calculating the ratio of the Fourier coefficient of the first harmonic at the output to the magnitude of the sinusoidal signal [3, 15–19]. The drawback is that this works the best for periodic inputs, especially sinusoidal inputs, and its not suitable for stochastic inputs.

- **Anti-Windup**: This method is used to prevent integral windup in case the

actuator is saturated, and in its standard form, involves using the input and the output of the saturation to modify the integral of the tracking error through an anti-windup gain [20–24]. The drawback is that the anti-windup gain is generally chosen heuristically and does not take into account the saturation limits.

- **Linear Matrix Inequality based methods**: This involves design for stabilization or performance of systems with sector-bounded nonlinearities by forming linear matrix inequalities [25–29]. The drawback of this method is that this leads to conservative controllers as the controllers are designed for any nonlinearity in a sector.

- **Barrier based methods**: These involve using barrier functions (whose values become infinite as the variable approaches the boundary of the set) to ensure stability of the control system [30–34]. These also lead to conservative designs.

- **Perturbation/Averaging**: This is an asymptotic method of analyzing nonlinear systems, and consists of exploiting the "smallness" of a perturbation parameter, a parameter on which the nonlinear function and the solution of the nonlinear system depends on, to construct approximate solutions that are valid for small values of that parameter [35–39]. The drawback is that this requires the nonlinear function to be smooth in the perturbation parameter, which is not available for common nonlinearities like the saturation function.

- **Jacobian Linearization**: This involves selecting an operating point and evaluating the derivative/Jacobian of the nonlinear function at that operating point, and replacing it by an affine approximation [3, 4, 40–42]. However, this is only

a local approximation that fails to be effective when the operating point shifts from the point of linearization.

- **Least Squares**: This involves replacing the nonlinear system by an affine approximation by minimizing the (possibly weighted) mean square error between the outputs of the nonlinear function and the affine approximation [43–47]. The drawback is that this does not consider the input signal for this linearization, e.g., considering which values of the input are more likely to occur, and hence, the linearization may not be effective for all different regions of operation.

- **Gain Scheduling**: This involves linearizing the nonlinear system at several equilibrium points, designing a linear feedback controller at each of those points, and implementing the resulting family of controllers as a single controller whose parameters can be changed by monitoring the scheduling variables (the variables that parameterize the nonlinear system) [48–52]. However, the drawback is that gain scheduling works best when the scheduling variable is constant or varies slowly. Large changes in the scheduling variable, as, for example, in a stochastic input, can result in instability.

- **State Feedback Control in Normal Form:** This involves transforming the nonlinear system into external and internal dynamics by applying a transformation, and then using state feedback control that converts the external dynamics into a chain of integrators and makes the internal dynamics unobservable from the output [53–57]. The difficulty is that this requires the nonlinearities to be sufficiently smooth on a domain and the transformation to be a diffeomorphism on a neighborhood of every point on the domain.

- **Feedback Linearization**: This uses state feedback control to linearize the system [58–62]. However, this requires the existence of a sufficiently smooth function relating the input to the output that is hard to find and involves evaluating the Lie brackets, checking for involutiveness and solving partial differential equations.

- **Sliding Mode Control**: In this control technique, trajectories of the nonlinear system are forced to reach a sliding manifold in finite time and stay on it for all future time, and motion on the manifold is independent of matched uncertainties [63–67]. The drawback is that the system with sliding mode control suffers from "chattering" due to imperfections in switching devices and delays in forcing the solution on the manifold. Chattering results in low control accuracy, high heat losses in electrical circuits, and high wear of moving mechanical parts.

- **Lyapunov Redesign**: This assumes that the nonlinear system is subjected to model uncertainty or parameter uncertainty, and involves using a Lyapunov function to design an additional feedback (on top of an existing feedback law) such that the overall control law stabilizes the actual system in the presence of uncertainty [68–72]. This also suffers from the problem of chattering as it is a discontinuous controller.

- **Backstepping**: It considers systems that are cascade connection of two subsystems. The first subsystem is assumed to be stabilized by smooth state feedback control, and assuming the existence of a Lyapunov function, a change of variable is done by subtracting the control law from the state of the second subsystem [73–77]. This method, however, requires the nonlinear functions to be

smooth in a domain that contains the origin, which is not suitable for saturated systems.

- **Passivity-based Control**: This technique involves using a locally Lipschitz function of the output of the nonlinear system as feedback [78–82]. However, it requires the nonlinear system to be passive with a radially unbounded positive definite storage function and zero state observable.

- **Bumpless Transfer**: This refers to the instantaneous switching between manual and automatic control of a process while retaining a smooth ("bumpless") control signal [24, 83–88]. During tentative evaluation of new controllers, standard bumpless transfer faces some drawbacks, related to safety (the new controller can drive the system unstable), economic feasibility (requiring costly modifications to existing controller), robustness (it is sensitive to the new controller) and generality of the controllers (requires the existing controller to have a particular structure like the velocity form).

In summary, the above methods for the control of nonlinear systems are in general, conservative, difficult to apply in practice, and/or are not suitable for stochastic systems.

1.1.2 OVERVIEW OF QUASILINEAR CONTROL

Quasilinear Control (QLC) is a recently-developed theory that provides a simpler alternative for analyzing and designing controllers for such nonlinear stochastic systems [89]. QLC leverages the method of stochastic linearization (SL) to *approximate* the nonlinear system by replacing each nonlinearity by an equivalent gain and a bias,
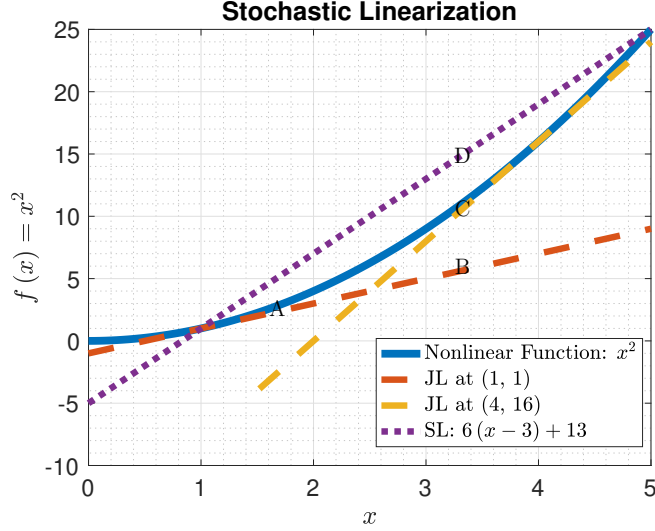
Figure 1.1: Traditional and stochastic linearization applied to $f(x) = x^2$.

based on the statistical properties of the stochastic inputs. This is unlike ordinary Jacobian linearization, which seeks only a local linear approximation to a nonlinear function. SL is similar in principle to the "describing function" methodology [3], as it involves approximating the static nonlinearity by a linear function. However, unlike describing functions, which are intended for the analysis of systems driven by sinusoidal inputs, SL is intended for the analysis of systems driven by stochastic inputs. A visual explanation of the SL procedure is given next.

Consider a nonlinear function $f(x) = x^2$ shown by the solid blue curve in Fig. 1.1, and assume that the input x is a Gaussian random process with mean $\mu = 3$ and standard deviation $\sigma = 2$. The traditional (Jacobian) approach in linearizing such a function is to find the derivative of the function at a suitable operating point and replace the nonlinearity by a local linear approximation. The method of stochastic linearization, on the other hand, is based on minimizing the difference between the nonlinear function and its approximation in a mean-squared sense, taking into account

the probability distribution of the input. The dashed lines in Fig. 1.1 represent two Jacobian linearizations performed at $x = 1$ and $x = 4$, and the dotted line represents the stochastically linearized approximation. If Jacobian linearization is performed at $x = 1$, but the operating point shifts to, say, $x = 4$, the linearization becomes highly inaccurate because the distance between points B and C in Fig. 1.1 is large. However, since stochastic linearization considers the statistical properties of the input, it performs better at D compared to B in predicting the actual value at C.

1.1.3 Literature Review of QLC

There is a significant body of literature in the field of SL. A detailed overview of the prominent works can be found in [90–92]. Stochastic linearization was first introduced as a generalization of the describing function methodology for nonlinear stochastic systems virtually simultaneously by Booton and Kazakov [93, 94]. Subsequent developments are mentioned in [95–98]. The standard criterion of SL in [93, 94] is to minimize the mean squared deviation between the output of the nonlinearity and the SL approximation. An alternative criterion for SL is presented in [99] that requires the mean squares of the function and its nonlinear approximation to be equal. In [100], a third criterion for SL is proposed that minimizes the potential energy of the nonlinear system and its linear equivalent. Similarly, there are other criteria, by demanding other probability functionals be minimal or equal [101].

SL of systems with multivariate nonlinearities is specifically described in [102, 103]. A similar method of linearization of nonlinear elements in a stochastic system, known as "equivalent linearization", but often used interchangeably with SL in the literature, was proposed by Caughey in [104]. As elaborated in [90, 105], it slightly

differs from SL applied in the sense of Kazakov [102] in evaluating the statistical averages. In [106], the existence and uniqueness of solutions generated by equivalent linearization are discussed. In [107], an energy-based version of SL is applied to dynamical systems whose states evolve according to quantum stochastic differential equations. In [108, 109], the methods of SL and harmonic balance are combined to approximate nonlinear stochastic systems with pseudo-harmonic behavior. These references, however, do not apply SL explicitly in the context of *feedback* control systems that are frequently encountered by control engineers.

The theory of QLC seeks to apply the SL procedure to nonlinear *feedback* systems and extend traditional control techniques like the root-locus design to stochastic systems with saturation [89, 110, 111]. While SL for multivariate nonlinearities has been around for long, and indeed also used to analyze and design generic control systems in these works in Russian [112–114], it was not applied in the traditional QLC literature. In the book [89], the nonlinearities under consideration were single-variable, symmetric (which, in QLC literature, refers to odd), and only appearing in the actuators and sensors of the control system. In [110, 111], QLC was extended to asymmetric (which refers to non-odd in context of QLC) nonlinearities, but still single-variable and appearing in actuators and sensors.

1.1.4 Shortcomings in Existing Literature for QLC

There are several shortcomings in the existing literature, as summarized below.

Stochastic Linearization of Systems with Multivariate Nonlinearities

Previous works on SL [89, 110, 115] focused on systems with *univariate* nonlinearities, for example actuator saturation, sensor dead zone, and gear backlash. However, multivariate nonlinearities also arise in practical applications, which necessitates a method of analysis and design capable of dealing with them. Examples of such nonlinearities are bilinear control systems and systems with state multiplicative noise [116]. Furthermore, in previous works, only systems with additive noise entering them were considered. The theory of QLC does not currently consider multiplicative noise.

As another example of multivariate nonlinearities, the author was involved in a power-systems-related project, in which the goal was to control the power grid by leveraging the flexibility provided by an aggregation of consumer-side distributed energy resources (DERs) and solar PV inverters. Such an aggregation typically has *variable/random* power limits, due to devices opting in and out of service and variability in solar irradiance. The behavior of the aggregation can be effectively modeled by a trivariate saturation nonlinearity, where the first input is the power that is desired of the aggregation, the second is the baseline power consumption of the aggregation, and the third is the aggregate power flexibility currently available (i.e., variable saturation bounds) [117].

Investigation of Accuracy, Robustness and Computation of SL

While SL has been successfully applied in many examples in the references mentioned before (for single-variable nonlinearities), there are still many open questions surrounding the accuracy, robustness, and computational aspects of it. All these are important from the perspective of an SL-based controller design for nonlinear

stochastic feedback systems.

The first problem is related to the *accuracy* of SL in approximating the statistics of the signals in nonlinear feedback systems. Specifically, it needs to be investigated how the inaccuracy (i.e., approximation errors) of SL in feedback settings is affected by these causes: the inherent inaccuracy of the approximation itself (i.e., open-loop approximation error), and the inaccuracy due to the assumption of Gaussianity in closed-loop settings (i.e., closed-loop error). While there have been studies (e.g., [90, 118, 119]) on closed-loop accuracy of SL for generic systems, such breakup of the approximation errors was not attempted in the past. This information on the accuracy of SL is valuable from a practical perspective, as the error can then be preemptively accounted for during an SL-based design of controllers for the original nonlinear system.

The second problem is the *computation* of SL of a feedback control system. Since SL involves solving implicit equations that generally contain transcendental functions (e.g., the error function), their solution can be arrived at only numerically. Often in practice, numerically solving this system of SL equations is only an intermediate step in solving a larger problem. An example is optimal controller design using SL for a system with saturation (e.g. [120, 121]). In such an optimization problem, the SL equations need to be solved at every iteration of the solver. Hence, to ensure fast solve times, it is important to employ numerical algorithms that solve the equations as quickly as possible and with low computational overhead. This has further impacts on stability/performance if the optimization needs to be performed in real-time and updates of controller gains in regular intervals are necessary to maintain adequate performance.

The third problem is related to the *robustness* of SL to system parameters. The SL gain and bias in closed loop depends on the statistical properties of the exogenous signals and all other system parameters (including the plant or process being controlled, the controller, and the nonlinear element). If the sensitivity of the SL gain and bias to system parameters is high, a small uncertainty in these parameters may render the linearization (and consequently the designed controller, for example) inaccurate. Hence, it is crucial to quantify which system parameter affects the gain/bias more than others. The sensitivity of SL has been studied in the literature, e.g., in [122]. However, [122] does not compare the relative sensitivities of the SL coefficients to system parameters in a feedback control system and their effect on signal statistics, which could be employed, for example, in optimal controller design.

1.1.5 Limited Applications of QLC in the Existing Literature

QLC has many potential applications that are not explored in the existing literature.

Droop Control of Power Systems with Generator Saturation

Control of frequency in power systems is vital to ensure reliable operation. In a power system, the frequency can deviate from the nominal value when there is a mismatch between supply and demand, which could result from changes in demand, tripping of generators, or isolation of areas with large generation capacity. A poorly controlled power system would result in a low quality of supplied electrical energy that can lead to power system collapse. Hence, power systems are typically equipped with an
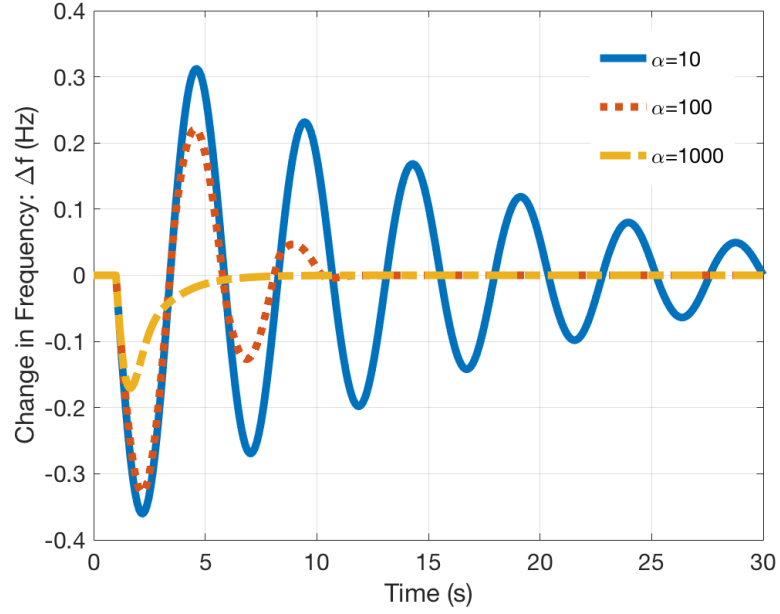
Figure 1.2: Effect of actuator saturation on droop control - A highly saturated actuator (α=10) leads to oscillations in the frequency deviations from the nominal for a step change in load power. A less saturated actuator (α = 100) leads to less oscillations. With negligible saturation (α = 1000), the response is overdamped. Note that a small steady state error is present in this case, although not visible to the naked eye. This is for illustration only, with system parameters taken from [1].

automatic frequency control system that nullifies any change in frequency.

An automatic frequency control system is generally implemented in three parts: primary, secondary and tertiary control [123–125]. Primary Frequency Control (PFC), or droop control, serves to bring the frequency back to an acceptable value locally in a power system area, although leaving a steady state error in frequency due to the purely proportional droop controller. This control task is shared by all generators in the area, irrespective of the location of the disturbance.

The proportional droop controller used in primary control can be chosen optimally. This can ensure, for example, a minimal change in frequency with reduced

13

control effort. Optimized droop control has been studied in the literature. For example, Mallada et. al [126] propose an optimal load-side frequency control mechanism to maintain the grid within operational constraints. In [127] and [128] averaging-based distributed controllers, using communication among the generation units to ensure economic optimization, are explored. A distributed real time frequency control scheme, using reverse and forward engineering, is discussed in [129]. In [130], dynamic droop controllers that improve the dynamics without affecting the steady state solution are proposed. In [131], the tracking of an operating point subject to power balance over the network is optimized. Delays in frequency dependent flexible loads are investigated in [132].

These references, however, do not *systematically* incorporate the issue of generator power saturation, which can take place when, for example, the gate or valve position that influences the flow of steam into a turbine is restricted, leading to specific output power limits. By *systematically*, I mean a design process that explicitly considers all the system parameters including saturation limits and, at the same time, does not lead to overly complex controllers. While neglecting saturation leads to simplification in the controller design and analysis, the results obtained may not accurately reflect the performance when saturation is present.

I illustrate this fact using a simulation analysis, where the same droop controller is used with varying levels of saturation (I used the system given in [1]). As shown in Fig. 1.2 by the orange dashed line, an unsaturated actuator leads to a well-behaved droop response - a momentary change in frequency, caused due to a step change in load power, is brought back to a constant value without oscillations. However, when there is significant generator saturation, the frequency change shows an underdamped

response before being nullified, as shown by the solid line.

The above example motivates the systematic design of an optimal droop controller to account for generator saturation in power systems.

Control of Virtual Batteries

With increased penetration of renewable generation like solar photovoltaic (PV), coordinated control of demand-side distributed energy resources (DERs) in distribution feeders is becoming vital to supporting a clean energy future. Many works in this area propose novel control architectures to coordinate and control these resources. For example, in [133, 134], methods for load frequency control using DERs are described. In [135], the active and reactive power of DERs are controlled using information exchange with neighboring DERs, while in [136], a model predictive control-based approach is taken. Moreover, a virtual battery (VB) is an abstraction, i.e., a modeling tool, to capture the flexibility and dynamics of aggregations of DERs [137–139] that enables analysis and design of controllers. Generally, the objective of VB control (ignoring grid constraints) is to maximize revenue [140]. Hence, if the output power of the VBs are controlled, as we seek to achieve this objective, the VBs may be pushed to their energy or power limits. This requires controller design to be cognizant of power/energy limits.

While most works on hierarchical control of DERs (e.g. [141]) mainly consider using frequency and voltage droop characteristics to generate power set-points for DERs using local measurements of frequency and voltage and compensating for the deviations, in [142], a previous work by the authors, a novel hierarchical framework for control of VBs in distribution feeders was proposed, wherein the deviation in the

head node power of the feeder from an *economic* trajectory was minimized instead. Unlike most local droop-based control strategies that are generally not cognizant of the network, the design of the controller gains was done based on the grid topology and device constraints, using the concept of a VB, with power and energy saturation limits, to represent an aggregation of DERs.

Existing works to tune controller parameters based on saturation limits are either heuristic [142], or the parameters are not optimized [127], which means the full potential of VBs is not unleashed. Furthermore, no work adaptively retunes the controller parameters to take into account variable saturation levels using real-time data. In the case of tuning PID controllers [143], there exist methods like the Cohen Coon, Internal Model Control, and Ziegler Nichols, but they also do not provide a mechanism to include the saturation nonlinearity in the design process. From a technical standpoint, the challenge is that saturation represents a nonlinearity and the grid is driven by stochastic inputs, a class of systems for which control design tools are limited.

1.2 Original Contributions

This dissertation aims to solve the above mentioned problems.

Stochastic Linearization of Systems with Multivariate Nonlinearities and State Multiplicative Noise

In Chapter 3, the theory of QLC is developed for nonlinear functions of multiple variables. The original contributions of Chapter 3 and 4 are as follows. First, the

16

equations for computing the linearization coefficients for SL of multivariate nonlinearities have been derived in detail in the open-loop environment. Second, the existence of these gains and biases for a generic nonlinear feedback system with generic multivariate nonlinearities (not just actuators or sensors) have been discussed, along with a process for finding them. Third, the resulting formulae are applied to find SL of a practical nonlinearity, namely the trivariate saturation, which is motivated by a power systems example, and the practical significance of the SL coefficients is highlighted. Fourth, in Chapter 4, the theory of SL has been extended to systems with multiple input multiple output (MIMO) nonlinearities, and has been applied to the analysis and optimal controller design of systems with randomly varying parameters (i.e., state multiplicative noise), where it is shown that SL can be effectively used to study this class of systems. Development of SL for MIMO nonlinearities also allows systems with multiplicative noise to be considered, apart from only additive noise that was considered till now in the literature. Fifth, a robustness analysis is performed to study the sensitivity of SL coefficients to system parameters. Finally, the theory is applied to a bivariate saturation nonlinearity in the shape of an optimal control problem, which demonstrates that SL is both fairly accurate and is able to adapt systematically based on system parameters.

Investigation of Accuracy, Robustness and Computation of Stochastic Linearization

In Chapter 5, the issue of accuracy of SL is addressed. Specifically, I delineate the breakup of inaccuracy of SL in feedback settings to the open-loop approximation error and the closed-loop error, provide a tight upper bound on the open-loop ap-

proximation error, and discuss the implications of this upper bound on the closed-loop accuracy for systems with saturation nonlinearities. The analyses show that SL of a saturation nonlinearity can produce relative mean squared errors less than 30.1% in the output but relative accuracy improves with a smaller variance in the input. A way to analytically determine the statistics of the actuator input that leads to the largest open-loop mean squared error for a given saturation authority is derived. Finally, it is shown that open-loop relative accuracy being bounded above also results in the closed-loop accuracy being bounded above by a value that is dependent on the saturation authority and the input of the saturation.

The issue of computation of SL has been investigated by comparing, through Monte Carlo simulations, six numerical algorithms (specifically, the Bisection, Newton-Raphson, Broyden, Trust-Region Reflective, Trust Region Dogleg, and Fixed Point Iteration methods) for the number of function evaluations required to converge to a solution of the SL equations. It has been found that, in the case of symmetric saturation, the SL functions for most systems are, in fact, contraction maps, but not in the asymmetric case. The best solver in terms of minimizing the amount of computation for solving the SL equations on average in both the symmetric and asymmetric cases is found to be the Trust Region Reflective method. A novel coordinate transformation is also proposed that can improve the success rate of most of the above-mentioned algorithms.

The issue of robustness of SL is addressed by performing Monte Carlo simulations and showing that the SL gain and bias are more affected by those parameters that directly affect the actuator input or its saturation authorities. Also, the sensitivities are found to be higher for systems with an asymmetric saturation nonlinearity than

for those with symmetric saturation, and the sensitivity of the SL bias is found to be higher than that of the SL gain. However, the signal statistics are usually not affected much by the SL coefficients, although in the case of asymmetric saturation, it is possible to have a higher sensitivity of the mean of the actuator input and the tracking error.

In sum, Chapter 5 investigates issues of accuracy, computation, and robustness of SL in a typical feedback system with a saturating actuator (a system that is commonly analyzed in various existing QLC literature [119, 144, 145]). Thus, the original contributions of Chapter 5 are as follows:

- A novel metric for the relative accuracy of SL is proposed for the open-loop accuracy of SL, along with upper bounds for the open-loop and, consequently, the closed-loop accuracy of SL.

- A comparison of the computational costs of several common numerical algorithms in solving the SL equations is provided.

- A coordinate transformation is proposed to improve the success rate of most of the above-mentioned algorithms.

- A numerical investigation is carried out into the sensitivity of SL coefficients to system parameters.

Optimal Primary Frequency Control of Power Systems with Generator Saturation

In Chapter 6, I leverage the method of QLC to systematically design an optimal droop controller that will dynamically adapt to the parameters of a power system.

Numerical simulations show that the resulting optimal QLC controller reduces the combined state and control costs by as much as 17% compared to a baseline design from the literature. Since QLC depends on all the parameters of the system, any change in a parameter leads to a systematic redesign of the optimal controller to meet performance requirements.

Control of Virtual Batteries

In Chapter 7, the technique of SL is leveraged to optimally control VBs. Specifically, it illustrates the advantages of using an SL-based optimization compared to the optimal VB controller described in [142, 146]. While existing design methods (for linear controller design of systems with saturation) based on Lyapunov functions and LMIs [4, 5] treat the saturation as a sector-bounded nonlinearity and, hence, lead to conservative designs, my goal is to achieve a non-conservative, optimal design, though with a small approximation error due to SL. Specifically, I show in Chapter 7 that compared to a baseline design, SL results in more accurate estimation of signal statistics, SL-based optimization can reduce head node power deviation from nominal while optimizing VB usage, and that SL-based optimization can use updated information to update the controller parameters, i.e., can be made adaptive. Thus, the original contributions of Chapter 7 are:

- An SL-based optimal controller design for control of networked VBs with fixed power limits (i.e., by modeling the limits by a univariate saturation function),

- Adaptive SL-based design of VB controllers using real-time data,

- Analysis on the effect of various system parameters on the optimization, and

- Simulation-based analysis of the SL-based design to VBs with variable power limits (i.e., by modeling the limits by a trivariate saturation function).

1.3   STATEMENT OF IMPACT

The expected impacts of this work are far-reaching. On the technical front, this work provides:

- a new set of theoretical and algorithmic tools that can improve and simplify control of complex systems affected by noise, which are traditionally difficult since the existing methods are heuristic or computationally challenging.

- information to control engineers on accuracy guarantees of SL (specifically, the bounds derived on the open loop and closed loop accuracy provide a means to incorporate them into design, perhaps using a robust control approach), choice of solvers to solve the SL equations as quickly as possible (which is important for an online optimization problem that is dependent on system parameters), and relative sensitivities of SL coefficients to system parameters (which informs which parameters of the physical system need to be estimated more accurately) to guide the analysis and design of nonlinear stochastic systems in the context of QLC.

- a new computationally efficient method of addressing saturation in generators or virtual batteries in modern electric power systems, resulting in efficient utilization of resources in providing grid services. Specifically, QLC provides a way to incorporate constraints like saturation into the design process and leads to more effective controllers.

On the societal front, this work:

- enables technologies that rely on computationally-efficient algorithms for automation of complex systems (especially when they influenced by multiple variables), e.g., control of soil temperature for agriculture, which depends on multiple factors like soil moisture and net radiation,

- allows effective coordination of controllable smart devices like air conditioners and water heaters in people's homes, so as not to hamper their quality of service, when they provide grid services like frequency regulation.

- provides a stepping stone towards key societal challenges like combating climate change by facilitating reliable operation of the grid with significant renewable penetration.

1.4 OUTLINE

The outline of the rest of the dissertation is as follows. In Chapter 2, a brief review of single variable QLC is provided. In Chapter 3, SL is extended to systems with multivariate nonlinearities. Chapter 4 describes the SL process applied to systems with state-multiplicative noise. In Chapter 5, the numerical properties of SL, namely accuracy, robustness and computation are investigated. In Chapter 6, SL is applied for optimal primary control of power systems with generator saturation. In Chapter 7, SL is applied to optimal control of virtual batteries. Finally, Chapter 8 concludes the dissertation.

CHAPTER 2

REVIEW OF SINGLE VARIABLE QUASI-LINEAR CONTROL

This chapter presents a brief review of single-variable QLC theory. For details, please refer to [89, 110]. Section 2.1 reviews SL in open-loop case. Section 2.2 applies SL formulae to the closed-loop case. Section 2.3 concludes this Chapter by providing two examples for SL.

2.1 OPEN LOOP SYSTEM

Consider a piecewise differentiable nonlinear function $f : \mathbb{R} \to \mathbb{R}$, shown in Fig. 2.1, driven by a wide-sense stationary (WSS) Gaussian random input $u(t)$, with the following properties [103]:

1. $\frac{\partial f}{\partial u}$ exists and is continuous almost everywhere;

2. $|f(u)| < A\exp(u^a)$, $a < 2$, for some $A \in \mathbb{R}$ and any $u \in \mathbb{R}$.

SL approximates the above nonlinearity by a linear approximation $\hat{v}(t) = Nu_0(t) + M$, where $u_0(t) = u(t) - E[u(t)]$ is the zero-mean part of $u(t)$, such that the functional:

$$\epsilon(N, M) = E[(v - \hat{v})^2] \tag{2.1}$$

is minimized [110]. Here, N is called the *quasilinear gain*, M the *quasilinear bias*, and $E[\cdot]$ denotes mathematical expectation. It can be shown [91] that the values of N and M are:

$$N = E[f'(u)] = \mathcal{F}_N(\mu_u, \sigma_u) \tag{2.2}$$

$$M = E[f(u)] = \mathcal{F}_M(\mu_u, \sigma_u) \tag{2.3}$$

Because $u(t)$ is Gaussian, (2.2) and (2.3) depend only on its mean, μ_u, and standard deviation, σ_u. This dependency is denoted by functions $\mathcal{F}_N$ and $\mathcal{F}_M$.

Now consider the saturation nonlinearity, which is the most widely studied nonlinearity in the QLC literature:

$$f(u) = \mathrm{sat}_\alpha^\beta(u) := \begin{cases} \beta, & u > \beta \\ u, & \alpha \le u \le \beta \\ \alpha, & u < \alpha \end{cases} \tag{2.4}$$

where $\alpha < 0$ and $\beta > 0$ are constants and indicate the saturation limits. For this function, the quasilinear gain N and bias M are given by [110]:

$$N = \frac{1}{2}\left[\mathrm{erf}\left(\frac{\beta - \mu_u}{\sqrt{2}\sigma_u}\right) - \mathrm{erf}\left(\frac{\alpha - \mu_u}{\sqrt{2}\sigma_u}\right)\right] \tag{2.5}$$

24

(a) Involving $u_0(t)$

(b) Not involving $u_0(t)$
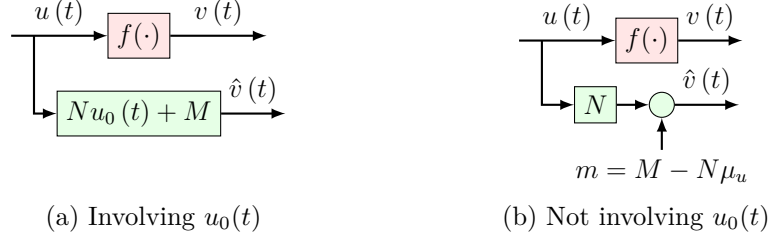
Figure 2.1: The process of single-variable SL. Part (b) shows an arrangement that is equivalent to that in part (a), but is amenable to block diagram manipulation. Here, N is the quasilinear gain defined in (2.2), M the quasilinear bias defined in (2.3), μ_u, the mean of $u(t)$ and $u_0(t) = u(t) - \mu_u$.

$$M = \frac{\alpha + \beta}{2} - \frac{\beta - \mu_u}{2}\mathrm{erf}\left(\frac{\beta - \mu_u}{\sqrt{2}\sigma_u}\right) + \frac{\alpha - \mu_u}{2}\mathrm{erf}\left(\frac{\alpha - \mu_u}{\sqrt{2}\sigma_u}\right) - $$
$$\frac{\sigma_u}{\sqrt{2\pi}}\left[\exp\left(-\left(\frac{\beta - \mu_u}{\sqrt{2}\sigma_u}\right)^2\right) - \exp\left(-\left(\frac{\alpha - \mu_u}{\sqrt{2}\sigma_u}\right)^2\right)\right] \tag{2.6}$$

where $\mathrm{erf}(\cdot)$ is the error function:

$$\mathrm{erf}(x) = \frac{2}{\sqrt{\pi}}\int_0^x e^{-t^2}dt$$

.

Quantitatively, the quasilinear gain N from (2.5) equals the probability that the output, $\mathrm{sat}_\alpha^\beta(u)$, has not been saturated at either its lower limit α or upper limit β [144]. Hence, $0 \le N \le 1$. When the saturation is symmetric, i.e., $\beta = -\alpha$, and u is zero-mean, i.e., $\mu_u = 0$, (2.5) and (2.6) reduce to:

$$N = \mathrm{erf}\left(\frac{\beta}{\sqrt{2}\sigma_u}\right), M = 0 \tag{2.7}$$
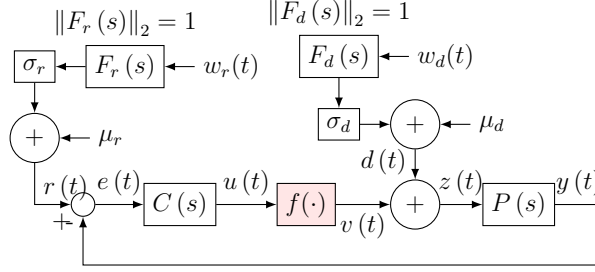
Figure 2.2: Block diagram of control system

2.2 Closed Loop System

The literature of QLC (e.g., [89, 110]) considers feedback systems similar to the one shown in Fig. 2.2. It consists of a plant $P(s)$ whose output is desired to be controlled using a controller $C(s)$ and a nonlinear actuator described by the function $f(\cdot)$. Since I am concerned with performance analysis and not stability, I assume $C(s)$ has been chosen such that the resulting closed-loop system is stable. The reference signal $r(t)$ is modeled as a WSS Gaussian random process, with μ_r and σ_r as the mean and standard deviation of its samples, respectively. To generate $r(t)$, standard Gaussian white noise $w_r(t)$ is passed through a coloring filter $F_r(s)$ having unit $\mathcal{H}_2$ norm (to ensure that the samples of the output of $F_r(s)$ have unit variance). The output of $F_r(s)$ is then scaled by σ_r and shifted by μ_r. The disturbance signal $d(t)$ is also modeled as a WSS Gaussian random process, with μ_d and σ_d as the mean and standard deviation of its samples, respectively, and is generated similarly.

I note that this system can be generalized to that shown in Fig. 3.2, which is consistent with the literature of robust control and absolute stability. This generalization has not been attempted previously in the literature of QLC. Here, $w(t)$, which models all exogenous inputs, including references and disturbances, is a vector
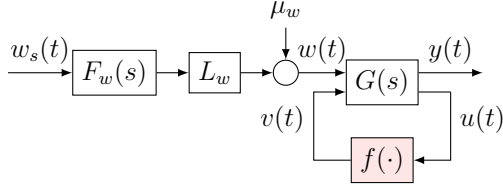
Figure 2.3: Generalized nonlinear feedback system

of WSS Gaussian processes, with a vector of means μ_w and covariance matrix Σ_w. Again, the closed loop system is assumed to be stable. To generate $w(t)$, a vector of standard independent and identically distributed Gaussian white noise processes, $w_s(t)$, is passed through a diagonal transfer matrix $F_w(s)$, with the diagonal elements being coloring filters having unit $\mathcal{H}_2$ norm. The result is scaled by L_w, which is the lower triangular matrix resulting from the Cholesky decomposition of $\Sigma_w = L_w L_w^{\mathrm{T}}$, and is shifted by μ_w. The linear part of the system is denoted by $G(s)$, while $f(\cdot)$ denotes a single-variable nonlinearity in the system. The block diagram in Fig. 2.2 can be redrawn as that in Fig. 3.2, with:

$$w_s(t) = \begin{bmatrix} w_r(t) \\ w_d(t) \end{bmatrix}, w(t) = \begin{bmatrix} r(t) \\ d(t) \end{bmatrix}, y(t) = y(t)$$

$$F_w(s) = \begin{bmatrix} F_r(s) & 0 \\ 0 & F_d(s) \end{bmatrix}$$

$$L_w = \begin{bmatrix} \sigma_r & 0 \\ \frac{\sigma_{rd}}{\sigma_r} & \frac{\sqrt{(\sigma_r \sigma_d)^2 - \sigma_{rd}^2}}{\sigma_r} \end{bmatrix}, \mu_w = \begin{bmatrix} \mu_r \\ \mu_d \end{bmatrix}$$

$$G(s) = \begin{bmatrix} 0 & P(s) & P(s) \\ C(s) & -C(s)P(s) & -C(s)P(s) \end{bmatrix}$$

such that $(y(t), u(t))$ is the output when $(w(t), v(t))$ is input to $G(s)$, and σ_{rd} is the

27
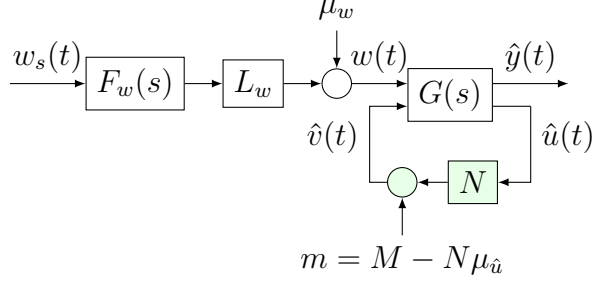
Figure 2.4: SL of the system in Fig. 3.2

covariance between $r(t)$ and $d(t)$. The SL of the system in Fig. 3.2 involves the computation of N and M from (2.2) and (2.3). This requires the probability density function (PDF) of $u(t)$. However, because the system is nonlinear, such PDF is not readily available. To remedy this issue, it is assumed that the system in Fig. 3.2 has been stochastically linearized to that in Fig. 3.3, and the PDF of $\hat{u}(t)$ is instead used for the computation of N and M. Since all inputs in Fig. 3.3 are Gaussian, so is the signal $\hat{u}(t)$, and hence only its mean, $\mu_{\hat{u}}$, and standard deviation, $\sigma_{\hat{u}}$, are required to compute N and M. It is shown in [110] that when the plant is of a low-pass filtering nature, the use of $\hat{u}(t)$ instead of $u(t)$ typically results in only a small error, for example, in their variances.

To explain how $\sigma_{\hat{u}}$ and $\mu_{\hat{u}}$ can be computed, let us first partition $G(s)$ as follows:

$$G(s) = \begin{bmatrix} G_{11}(s) & G_{12}(s) \\ G_{21}(s) & G_{22}(s) \end{bmatrix} \tag{2.8}$$

The standard deviation of $\hat{u}(t)$ is calculated using the $\mathcal{H}_2$ norm $\|\cdot\|_2$ of the transfer matrix from $w_s(t)$ to $\hat{u}(t)$ [147], after setting the exogenous inputs, μ_w and m, to zero:

$$\sigma_{\hat{u}}(N) = \left\| [1 - NG_{22}(s)]^{-1} G_{21}(s) L_w F_w(s) \right\|_2 \tag{2.9}$$

The mean of $\hat{u}(t)$ can be found by evaluating the DC gain of the transfer function/-matrix from m and μ_w to $\hat{u}(t)$:

$$\mu_{\hat{u}}(N, m) = \lim_{s \to 0} (1 - NG_{22}(s))^{-1} (G_{21}(s)\mu_w + mG_{22}(s)) \tag{2.10}$$

Note that previously in the literature of QLC [110], the formulation $\mu_{\hat{u}}(M) = \lim_{s \to 0}[G_{21}(s)\mu_w + MG_{22}(s)]$ was studied instead of (2.10). The novel formulation of $\mu_{\hat{u}}$ in terms of N and m in (2.10) is more amenable to numerical computation as compared to that in terms of only M. This is because the formulation of (2.10) can handle cases where the DC gain of any element of $G_{21}(s)$ or of $G_{22}(s)$ is infinite, which can happen, for example, when there are integrators in the control system. To illustrate this, consider Fig. 2.2, with $C(s) = 5$ and $P(s) = \frac{10}{s(s+1)}$. Then, $\lim_{s \to 0} G_{21}(s) = \lim_{s \to 0} \begin{bmatrix} C(s) & -C(s)P(s) \end{bmatrix} = \begin{bmatrix} 5 & -\infty \end{bmatrix}$ and $\lim_{s \to 0} G_{22}(s) = -\lim_{s \to 0} C(s)P(s) = -\infty$. Then, $\mu_{\hat{u}}(M)$ is not defined, unless $M = -\mu_d$. On the other hand, from (2.10), $\mu_{\hat{u}}(N, m) = -\frac{m+\mu_d}{N}$ is defined for all m and $N \neq 0$.

The values of N and M $(= m + N\mu_{\hat{u}})$ can be found by solving (2.2) and (2.3), with $\sigma_{\hat{u}}$ and $\mu_{\hat{u}}$ given by (2.9) and (2.10), respectively, resulting in the following equations with two unknowns, N and m:

$$N = \mathcal{F}_N(\mu_{\hat{u}}(N, m), \sigma_{\hat{u}}(N)) \tag{2.11}$$

$$m + N\mu_{\hat{u}}(N, m) = \mathcal{F}_M(\mu_{\hat{u}}(N, m), \sigma_{\hat{u}}(N)) \tag{2.12}$$

Note the resulting circularity in these equations. In general, the equations are transcendental and hence, only numerically solvable. They can be solved using, for example, MATLAB's `fsolve`, which uses the Trust Region Dogleg method [148]. This

completes the process of SL of systems with univariate nonlinearities.

2.3   EXAMPLES

In this section, I illustrate the process of SL through two examples, one for an open-loop and another for a closed-loop system.

2.3.1   EXAMPLE 1

Problem: Consider the nonlinear function $f(x) = x^2$. Suppose the input process is known to follow a Gaussian distribution with mean 3 and standard deviation 0.1. Find the SL of f, i.e., find the gain N and the bias M.

The probability density function of x is given by:

$$p(x) = \frac{1}{\sqrt{2\pi(0.1)^2}} e^{-\frac{(x-3)^2}{2(0.1)^2}}$$

The value of the quasilinear gain N can then be obtained from (2.2):

$$N = E\left[f'(x)\right] = \int_{-\infty}^{\infty} 2xp(x)\, dx = \int_{-\infty}^{\infty} 2x \frac{1}{\sqrt{2\pi(0.1)^2}} e^{-\frac{(x-3)^2}{2(0.1)^2}}\, dx = 6$$

The value of quasilinear bias M can be obtained as:

$$M = E\left[f(x)\right] = \int_{-\infty}^{\infty} x^2 p(x)\, dx = \int_{-\infty}^{\infty} x^2 \frac{1}{\sqrt{2\pi(0.1)^2}} e^{-\frac{(x-3)^2}{2(0.1)^2}}\, dx = 9.01$$

Thus, the SL of $f(x) = x^2$ is $Nx_0 + M = 6(x-3) + 9.01$.
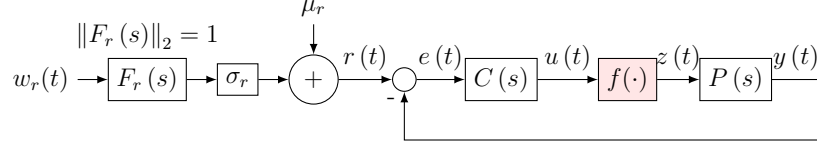
Figure 2.5: Block diagram of control system
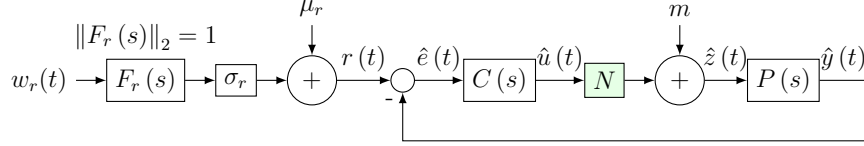
Figure 2.6: Stochastic Linearization of System in Fig. 2.5

2.3.2 EXAMPLE 2

Problem: Consider a feedback system as shown in Fig. 2.5, which $C(s) = 5$, $P(s) = \frac{1}{s+1}$, $\mu_r = 0.1$, $\sigma_r = 1$, $f(\cdot) = \text{sat}^2_{-1}(\cdot)$. Let $F_r(s) = \frac{\sqrt{3}}{s^3 + 3s^2 + 3s + 1}$ (3rd order Butterworth filter). Stochastically linearize this system to that shown in Fig. 2.6 and obtain N and m.

To stochastically linearize the system, we need to find the mean and standard deviation of the input to N, $\hat{u}$. The standard deviation of $\hat{u}$ is evaluated using the $\mathcal{H}_2$-norm of the transfer function from $w_r(t)$ to $\hat{u}(t)$, after setting exogenous biases to zero, i.e., $\mu_r = m = 0$:

$$
\begin{aligned}
\sigma_{\hat{u}}(N) &= \left\| \frac{F_r(s)\, C(s)}{1 + N C(s)\, P(s)} \right\|_2 \sigma_r \\
&= \left\| \frac{5\sqrt{3}}{(s+1)^2 (5N + s + 1)} \right\|_2
\end{aligned}
\tag{2.13}
$$

Similarly, the mean of $\hat{u}$ is computed by considering the DC gain of the transfer functions from μ_r and m to $\hat{u}$:

$$\mu_{\hat{u}}(N,m) = \frac{C_0\left(\mu_r - mP_0\right)}{1 + NP_0C_0} = \frac{5(0.1 - m)}{1 + 5N} \tag{2.14}$$

where P_0 and C_0 are the DC gains of $P(s)$ and $C(s)$ repsectively.

Now, for the saturation function, N and m are given by (2.5)-(2.6) and $m = M - N\mu_u$, with $\alpha = -1$ and $\beta = 2$, and σ_u and μ_u replaced by $\sigma_{\hat{u}}$ and $\mu_{\hat{u}}$ respectively from (2.13) and (2.14). This results in a system of two equations in N and m. By solving the resulting equations using MATLAB's `fsolve` (Version 2021a, Windows) for m and N, we obtain $N = 0.9092$ and $m = 0.0339$.

CHAPTER 3

STOCHASTIC LINEARIZATION OF SYSTEMS WITH MULTIVARIATE NONLINEARITIES

This chapter introduces multivariable stochastic linearization. The outline of this chapter is as follows: Section 3.1 introduces expressions for SL of a multivariate nonlinearity. The expressions introduced in Section 3.1 are then used in Section 3.2 to find the SL of a general feedback control system. Section 3.3 introduces a recipe for evaluating robustness of stochastic linearization coefficients. Finally, in Section 3.4, a practical example of an optimal controller design is provided.

3.1 Multivariable Stochastic Lineariza-tion

In this section, the idea of SL is presented for multivariate nonlinearities, i.e., non-linearities having multiple inputs and a single output. The case of multiple outputs is considered in Section 4.1. Note that SL for multivariate nonlinearities has been presented in an alternative form in [102, 149, 150]. A contribution of this section is to provide its derivation for completeness.

Consider a function $f : \mathbb{R}^n \to \mathbb{R}$ evaluated at n jointly stationary Gaussian inputs $u_1(t), u_2(t), \ldots, u_n(t)$, forming a stationary Gaussian random vector $u(t)$ with mean vector μ_u. The problem is to approximate $v(t) = f(u(t))$ by the linear function $\hat{v}(t) = N^\top u_0(t) + M$, where $u_0(t) = u(t) - \mu_u$ is the zero-mean part of $u(t)$. Here, N and M are constants and are referred to as the *quasilinear gain* and the *quasilinear bias* respectively. Our objective is to choose N and M to minimize the mean square difference between the two outputs $v(t)$ and $\hat{v}(t)$. This is carried out in Theorem 1 below. Before I state the theorem, I note that since $u(t)$ and $u_0(t)$ are assumed to be stationary processes, their probability distributions are independent of time. Thus, in the following Theorem, I omit the time argument t after u and u_0. Furthermore, for convenience, I denote ∂_θ to mean partial derivative with respect to θ.

Theorem 1. *Let u_0 be a zero-mean stationary jointly-Gaussian process with a positive definite covariance matrix $E[u_0 u_0^\top]$, and let $u = u_0 + \mu_u$, where μ_u is a constant mean vector. Let $f(u) : \mathbb{R}^n \to \mathbb{R}$ be a function with the following properties:*

    1. the first partial derivative of f with respect to $u_i, i = 1, 2, ..., n$, exists and is

continuous almost everywhere;

2. $|f(u)| < A exp\left(\sum_{j=1}^{n} u_j^a\right)$, $a < 2$ *for some* $A \in \mathbb{R}$ *and any* $u \in \mathbb{R}^n$.

Then, the functional $\epsilon(N, M) = E\{[f(u) - N^{\mathrm{T}} u_0 - M]^2\}$ *is minimized over* $N \in \mathbb{R}^n$ *and* $M \in \mathbb{R}$ *by:*

$$N = E\left[\nabla f(u)\right] \tag{3.1}$$

$$M = E\left[f(u)\right] \tag{3.2}$$

Proof. I prove this theorem by completing the square and noting that the functional,

$$\begin{aligned}
\epsilon(N, M) &= E\{[f(u) - N^{\mathrm{T}} u_0 - M]^2\} \\
&= ||N - \Sigma_{u_0}^{-1} E[f(u) u_0]||_{\Sigma_{u_0}}^2 + (M - E[f(u)])^2 \\
&\quad + E[(f(u) - E[f(u)])^2] - ||E[f(u) u_0]||_{\Sigma_{u_0}^{-1}}^2
\end{aligned} \tag{3.3}$$

where $\Sigma_{u_0} = \text{cov}(u_0) = E[u_0 u_0^\top]$ is the covariance matrix of u_0, and $||w||_\Sigma = w^\top \Sigma w$ is the weighted Euclidean norm. The minimum of this functional is clearly attained at

$$N = \Sigma_{u_0}^{-1} E[f(u) u_0] \tag{3.4}$$

and $M = E[f(u)]$. The term $E[f(u) u_0]$ in (3.4) can be expanded using the following result from [103]: $E\left[g(\eta)\eta\right] = E\left[\eta\eta^{\mathrm{T}}\right] E\left[\nabla g(\eta)\right]$, where η is any jointly Gaussian vector with zero mean, i.e., $E[\eta] = 0$, ∇ is the gradient operator, and g is a function that satisfies properties 1) and 2) in the Theorem statement. In this case, $\eta = u_0$ (which is indeed zero-mean) and $g(\eta) = f(\eta + \mu_u)$. The substitution of $E[u_0 u_0^\top] E[\nabla f(u)]$

35

(a) Involving $u_0(t)$ (b) Not involving $u_0(t)$
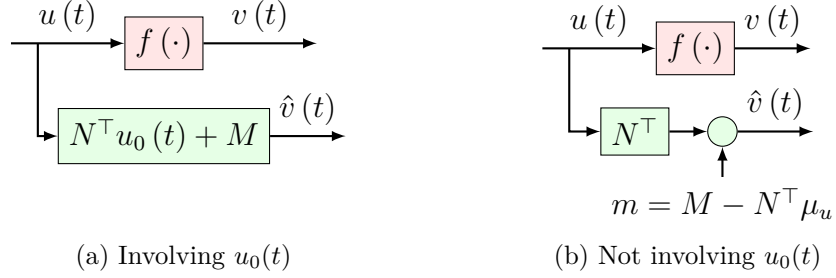
Figure 3.1: The process of multi-variable SL for multivariate nonlinearities. Part (b) shows an arrangement that is equivalent to that in part (a), but is amenable to block diagram manipulation. Here, N is the vector of quasilinear gains defined in (3.1), M the quasilinear bias defined in (3.2), μ_u the mean of $u(t)$ and $u_0(t) = u(t) - \mu_u$.

for $E[f(u)u_0]$ in (3.4) completes the proof.   □

Equations (3.1) and (3.2) provide the necessary expressions for obtaining the equivalent gains and bias for the case of multivariable SL. The process is illustrated in Fig. 3.1, where the right-hand block diagram is an equivalent representation that is more amenable to block diagram manipulation.

Because $u(t)$ is Gaussian, the right-hand side of (3.1) and (3.2) depend only on its mean, μ_u, and covariance matrix, Σ_u. I denote this dependency by functions $\mathcal{G}_N$ and $\mathcal{G}_M$ in the following equations:

$$N = \mathcal{G}_N\left(\mu_u, \Sigma_u\right) \tag{3.5}$$

$$M = \mathcal{G}_M\left(\mu_u, \Sigma_u\right) \tag{3.6}$$

Remark 1. *In the most general formulation of SL [90], what enters the SL procedure is the joint probability distribution of the inputs to the nonlinearity at the current time only, and thus theoretically, it does not matter if the inputs are stationary or not. However, for the N and M to be independent of time, which is a practical*

requirement for QLC, at least a wide sense stationarity (WSS) assumption must be imposed on the random inputs to the nonlinearity (in the case of Gaussian inputs, as assumed above, this implies strict sense stationarity also).

Application to Trivariate Saturation To illustrate the use of the above formulae for the SL of a practical nonlinearity that arises in control of power systems with DERs [117], consider, as an example, a trivariate saturation nonlinearity, with three jointly Gaussian inputs, $p(t)$, $n(t)$ and $u(t)$, whose standard deviations are small compared to their mean values. The input $p(t)$ represents the nominal or baseline power consumed by an aggregate of DERs. The signal $n(t)$ represents the aggregate flexibility of the DERs on top of the nominal power in both the positive and negative direction, while the input $u(t)$ represents the power that is desired from the aggregation. Clearly, the aggregate of DERs can only supply power that is between $p(t) - n(t)$ and $p(t) + n(t)$. Thus the input $u(t)$ is saturated dynamically by these time-varying, stochastic limits. Moreover, if for some reason, the value of $n(t)$ is zero or negative, it signifies that there is no flexibility in these resources, implying that the DERs only supply nominal power $p(t)$. This nonlinearity is defined as follows:

$$\text{sat}(u, p, n) = \begin{cases} p+n, & u > p+n \\ u, & p-n \leq u \leq p+n \\ p-n, & u < p-n \end{cases} \tag{3.7}$$

when $n \geq 0$, and $\text{sat}(u, p, n) = p$ when $n < 0$.

On substituting the nonlinear function (3.7) for $f(\cdot)$ in (3.1), the values of N_1, N_2 and N_3 can be found as follows: $N = \begin{bmatrix} N_1 & N_2 & N_3 \end{bmatrix}^\top = E\left[\nabla \text{sat}(u(t), p(t), n(t))\right].$

37

Note that since the saturation function is not differentiable at certain points, the gradient ∇ has to be taken piecewise.

Since this nonlinearity is of importance to us, I delve deeper into its properties. Specifically, I show that the quasilinear gains are significant in informing how likely it is that the input $u(t)$ to the saturation nonlinearity is saturated or by how much. This is summarized in the following Theorem.

Theorem 2. *Consider the trivariate saturation with jointly Gaussian inputs $u(t)$, $p(t)$, and $n(t)$, as described above. The probability that the primary input $u(t)$ is not saturated is quantified by the first element of N, i.e., N_1. That is, $N_1 = \Pr(p(t) - n(t) < u(t) < p(t)+n(t))$. Similarly, the probability that either the primary input $u(t)$ is saturated, or $n(t) < 0$, is quantified by N_2, i.e., $N_2 = \Pr(u(t) < p(t) - n(t) \vee u(t) > p(t)+n(t) \vee N < 0)$, which can be shown to satisfy $N_2 = 1 - N_1$. The quasilinear gain N_3 represents how much more the input $u(t)$ is likely to be saturated by the upper limit than by the lower limit, i.e., $\Pr(u(t) > p(t) + n(t)) - \Pr(u(t) < p(t) - n(t)) = N_3$.*

Proof. By definition of the joint PDF,

$$\Pr\left(p(t) - n(t) < u(t) < p(t) + n(t)\right)$$
$$= \int_{-\infty}^{\infty} \int_{-\infty}^{\infty} \int_{p-n(t)}^{p+n(t)} \Phi\left(u, p, n\right) \ du \ dp \ dn$$

Since, by the definition of the trivariate saturation in (3.7), the output is zero when $n(t) < 0$,

$$\Pr\left(p(t) - n(t) < u(t) < p(t) + n(t)\right)$$
$$= \int_{0}^{\infty} \int_{-\infty}^{\infty} \int_{p-n}^{p+n} \Phi\left(u, p, n\right) \ du \ dp \ dn$$

which is exactly N_1. Similarly,

$$\Pr\left(u(t) < p(t) - n(t) \vee u(t) > p(t) + n(t) \vee n(t) < 0\right)$$
$$= \int_0^\infty \int_{-\infty}^\infty \int_{-\infty}^{p-n} \Phi\left(u, p, n\right) \; du \; dp \; dn$$
$$+ \int_0^\infty \int_{-\infty}^\infty \int_{p+n}^\infty \Phi\left(u, p, n\right) \; du \; dp \; dn$$
$$+ \int_{-\infty}^0 \int_{-\infty}^\infty \int_{-\infty}^\infty \Phi\left(u, p, n\right) \; du \; dp \; dn$$

which is exactly N_2 and also matches $1 - N_1$. Also,

$$\Pr\left(u(t) > p(t) + n(t)\right) - \Pr\left(u(t) < p(t) - n(t)\right)$$
$$= \int_0^\infty \int_{-\infty}^\infty \int_{p+n}^\infty \Phi\left(u, p, n\right) \; du \; dp \; dn$$
$$- \int_0^\infty \int_{-\infty}^\infty \int_{-\infty}^{p-n} \Phi\left(u, p, n\right) \; du \; dp \; dn = N_3.$$

$\square$

The above theorem thus enables us, by noting the values of the quasilinear gains, to qualitatively assess "how nonlinear" the system is, how much the inputs are saturated, and what the contributions are from the upper and lower limits in saturating the input. This insight can be valuable not only for analysis but also for controller synthesis.
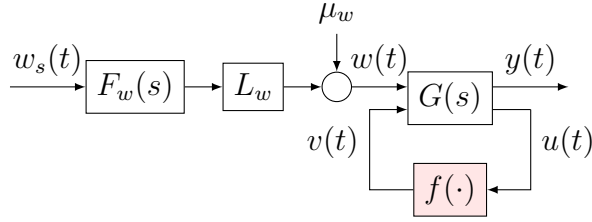
Figure 3.2: Generalized nonlinear feedback system
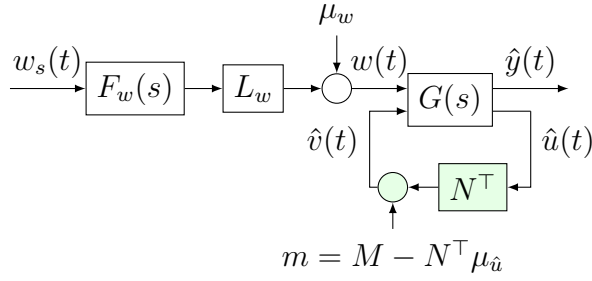
Figure 3.3: SL of the system in Fig. 3.2

3.2 STOCHASTIC LINEARIZATION OF FEEDBACK SYSTEMS WITH MULTIVARIATE NONLINEARITIES

In this section, the procedure of multivariable SL, applied to a generic feedback control system with a multivariate nonlinearity, is described.

Consider a generic nonlinear feedback control system depicted in Fig. 3.2. In this system, the nonlinear part $f(\cdot)$ has been isolated from the linear part $G(s)$. The nonlinearity $f : \mathbb{R}^n \to \mathbb{R}$ is assumed to have the properties 1) and 2) mentioned in the Theorem 1 statement. I showed in [144] that this is a generic structure that can represent a wide variety of nonlinear systems, including the standard feedback control

system that contains a single linear time-invariant plant and controller. Here, $w(t)$ models all the exogenous stochastic inputs, including references and disturbances, entering the control system. It is a vector of stationary Gaussian processes, with a vector of means μ_w and a covariance matrix Σ_w. The closed-loop system is assumed to be stable. To generate $w(t)$, a vector of standard independent and identically distributed Gaussian white noise processes, $w_s(t)$, is passed through a diagonal transfer matrix $F_w(s)$, with the diagonal elements being coloring filters having unit $\mathcal{H}_2$ norm. The result is scaled by L_w, any matrix square root of $\Sigma_w = L_w L_w^\top$, and is shifted by μ_w.

Note that this system (Fig. 3.2) can be equivalently represented as a stochastic differential equation (SDE) containing a nonlinear function of states (in fact, as shown below, I will employ the SDE of its linearized version to find the SL of this system). In this work, I assume that a stationary solution to the nonlinear SDE exists, has a well-defined PDF, and is stochastically bounded [151]. I also consider that the class of controllers that generate $u(t)$ in Fig. 3.2 are linear, stabilizing controllers.

To apply SL to this system, it is necessary to find N and M from (3.1) and (3.2). This requires analytic expressions for the multivariate probability density function (PDF) of $u(t)$. However, because the system is nonlinear, such PDF is not readily available. Hence, it is assumed that the system has been stochastically linearized to the system shown in Fig. 3.3 and that the moments arising in the calculation of linearization coefficients from (3.1) and (3.2) are approximated by corresponding moments of the linearized system in Fig. 3.3 (this procedure is similar to the one used in [90]). Because the input $w(t)$ is Gaussian, so is $\hat{u}(t)$; thus, its mean, $\mu_{\hat{u}}$, and its covariance matrix, $\Sigma_{\hat{u}}$, can now be used instead for the computation of N and

M. This approximation is generally fairly accurate for the systems with plants of a low-pass filtering nature [110].

The process of computation of the mean and the covariance matrix of $\hat{u}(t)$ can be simplified by decomposing the input $w(t)$ into its zero-mean random part and a constant part that is its mean, and passing those parts separately as inputs to the system. This is illustrated below.

Consider a linear time-invariant (LTI) system, with transfer matrix $G(s)$ and impulse response $g(t)$, as shown in Fig. 3.4, with a WSS input $p(t)$ and WSS output $q(t)$. Let $p_0(t)$ and μ_p be the zero-mean part and the mean of $p(t)$, respectively. If the input to the system is $p_0(t)$, the output is $q_0(t) = g(t) * p_0(t)$. If the input is μ_p, the output is $\mu_q = g(t) * \mu_p$. Then, because the system is LTI,

$$q(t) = g(t) * p(t) = g(t) * [p_0(t) + \mu_p]$$
$$= g(t) * p_0(t) + g(t) * \mu_p = q_0(t) + \mu_q$$

Since $p_0(t)$ is zero-mean, so is $q_0(t)$, and since μ_p is a constant, so is μ_q. Hence, in the equation $q(t) = q_0(t) + \mu_q$, the variability in $q(t)$ must come from $q_0(t)$, or, $\Sigma_q = E\left[q(t)q^{\mathrm{T}}(t)\right] = E\left[q_0(t)q_0^{\mathrm{T}}(t)\right] = \Sigma_{q0}$, where Σ_q and Σ_{q0} are the covariance matrices of $q(t)$ and $q_0(t)$, respectively. Also, the mean of $q(t)$ must equal μ_q, or $E\left[q(t)\right] = \mu_q$.

Thus, by treating $w(t)$ as the input $p(t)$ in the above discussion, and $\hat{u}(t)$ as the output $q(t)$, I can decompose $w(t)$, which greatly simplifies the calculation of the statistical properties of $\hat{u}(t)$ required for SL. In the following, I use the zero-mean part of $w(t)$ for computing the covariance matrix of $\hat{u}(t)$, and the constant mean

42
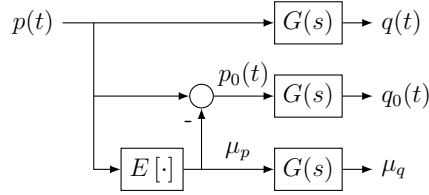
Figure 3.4: Decomposition of a vector input $p(t)$ to system S into its zero-mean part $p_0(t)$ and its mean μ_p, in order to calculate the statistical properties of the output $q(t)$. Here $E[\cdot]$ denotes mathematical expectation. This arrangement results in the stationary mean of $q(t)$ being equal to μ_q, and the covariance matrix of $q(t)$ being equal to that of $q_0(t)$.

part, i.e., μ_w, for computing the expected value of $\hat{u}(t)$.

I now discuss the computation of $\mu_{\hat{u}}$ and $\Sigma_{\hat{u}}$. To do that, let us first partition $G(s)$ as follows:

$$G(s) = \begin{bmatrix} G_{11}(s) & G_{12}(s) \\ G_{21}(s) & G_{22}(s) \end{bmatrix} \tag{3.8}$$

This partitioning is meant to correspond to the inputs/outputs of Fig. 3.3. The value of $\mu_{\hat{u}}$ can then be computed by evaluating the DC gains of the transfer matrices from m and μ_w to $\hat{u}(t)$:

$$\mu_{\hat{u}}(N, m) = \lim_{s \to 0} (I_n - G_{22}(s)N^{\mathrm{T}})^{-1} (G_{21}(s)\mu_w + mG_{22}(s)) \tag{3.9}$$

where I_n is the $n \times n$ identity matrix. To compute $\Sigma_{\hat{u}}$, I consider the following stochastic state-space equation as a general representation of the stochastically linearized system:

$$d\hat{x} = A\hat{x}(t)dt + Bd\beta, \quad \hat{u}(t) = C\hat{x}(t)$$

where $\hat{x}(t)$ is the vector of system states and β is a vector of Wiener processes, such that the white noise $w_s(t)$ in Fig. 3.3 is the formal (or weak) derivative of

β [152]. I assume that the matrix A is Hurwitz (i.e., all eigenvalues satisfy $\text{Re}(\lambda_i) <$ 0). This state-space model, which I assume is minimal, corresponds to the transfer function from $w_s(t)$ to $\hat{u}(t)$ in Fig. 3.3, with $m = \mu_w = 0$, i.e., $C(sI - A)^{-1}B :=$ $[1 - NG_{22}(s)]^{-1} G_{21}(s) L_w F_w(s)$. Then, the stationary covariance matrix of $\hat{x}(t)$, $\Sigma_{\hat{x}} := \lim_{t \to \infty} E\left[\hat{x}(t)\hat{x}^\top(t)\right]$, is the solution of the algebraic Lyapunov equation [153]:

$$A\Sigma_{\hat{x}} + \Sigma_{\hat{x}}A^\top + BB^\top = 0 \tag{3.10}$$

To solve this equation, the following formula can be used [154]: $(I_n \otimes A + A \otimes I_n)\text{vec}(\Sigma_{\hat{x}}) = -\text{vec}(BB^\top)$, where vec $(\cdot)$ is the vectorization operator. Because $\hat{u}(t) = C\hat{x}(t)$, the stationary covariance matrix of $\hat{u}(t)$ is:

$$\Sigma_{\hat{u}} = C\Sigma_{\hat{x}}C^\top \tag{3.11}$$

Remark 2. *Matrix A is a function of N, implying that $\Sigma_{\hat{x}}$ and $\Sigma_{\hat{u}}$ are also functions of N. I thus denote $\Sigma_{\hat{u}}$ by $\Sigma_{\hat{u}}(N)$ to show this dependency. Also, from (3.9), $\mu_{\hat{u}}$ is a function of N and m. Note that m enters into the system as an additive constant input (Fig. 3.1). Hence, these parameters are interrelated.*

Thus, from (3.5) and (3.6), it follows that:

$$N = \mathcal{G}_N\left(\mu_{\hat{u}}(N, m), \Sigma_{\hat{u}}(N)\right) \tag{3.12}$$

$$m + N^\top\mu_{\hat{u}}(N, m) = \mathcal{G}_M\left(\mu_{\hat{u}}(N, m), \Sigma_{\hat{u}}(N)\right) \tag{3.13}$$

where I have used $M = m + N^T\mu_{\hat{u}}$, as shown in the alternative representation of Fig. 3.1. This is a system of equations in the unknowns N and m. Note, however,

that solutions may or may not be unique, similar to the case of single variable SL described in [89]. Non-unique solutions generally lead to "jumping" between possible regimes of operation but are rare in practice for the saturation nonlinearity.

A sufficient condition for the existence of solutions is discussed in the following theorem.

Theorem 3. *Let $\mathcal{N}$ and $\mathcal{M}$ denote the ranges of $\mathcal{G}_N$ and $\mathcal{G}_M$ respectively in (3.12)-(3.13), and let $\overline{\mathcal{N}}$ and $\overline{\mathcal{M}}$ denote their closures. Assume that the following hold:*

1. *The system is asymptotically stable $\forall\, N \in \mathcal{N}$.*

2. *The pair (A, B) is controllable.*

3. *$\overline{\mathcal{N}}$ and $\overline{\mathcal{M}}$ are compact and convex sets.*

4. *$\mathcal{G}_N$ and $\mathcal{G}_M$ are continuously differentiable.*

5. *If any element of $\lim_{s\to 0} G_{21}(s)$ or of $\lim_{s\to 0} G_{22}(s)$ is infinite, then*

   - *$\nu\,(\xi, v) := \lim_{s\to 0}[\xi + v^{\mathrm{T}} \left(I_n - G_{22}(s)v^{\mathrm{T}}\right)^{-1}$ $(G_{21}(s)\mu_w + \xi G_{22}(s))]$ is a constant $k \in \mathcal{M}$ for all $\xi \in \mathbb{R}$, $v \in \mathbb{R}^n$, where n is the number of elements in $u(t)$, and*

   - *there exists a constant $d > 0$ such that:*

   $$\left| \frac{\partial}{\partial \mu_{\hat{u}j}} \left[\mathcal{G}_M \left(\mu_{\hat{u}}, \Sigma_{\hat{u}}(N) \right) \right] \right| \geq d, \ \forall j = 1, 2, \ldots, n$$

   where $\mu_{\hat{u}j}$ denotes the jth element of $\hat{u}(t)$.

Then, (3.12)-(3.13) has a solution (N, m) in $\overline{\mathcal{N}} \times \mathbb{R}$.

Proof. I consider two cases. For the first case, assume that all the elements of $\lim_{s \to 0} G_{21}(s)$ and $\lim_{s \to 0} G_{22}(s)$ are finite. This implies that $\mu_{\hat{u}}(M) = \lim_{s \to 0}[G_{21}(s) \mu_w + M G_{22}(s)]$ is finite. Substituting $\mu_{\hat{u}}(M)$ for $\mu_{\hat{u}}(N, m)$ and M for $m + N^{\mathrm{T}} \mu_{\hat{u}}(N, m)$ in (3.12)-(3.13), I get:

$$N = \mathcal{G}_N \left(\mu_{\hat{u}}(M), \Sigma_{\hat{u}}(N) \right) \tag{3.14}$$

$$M = \mathcal{G}_M \left(\mu_{\hat{u}}(M), \Sigma_{\hat{u}}(N) \right) \tag{3.15}$$

The first assumption implies that for any value of $N \in \mathcal{N}$, the solution $\Sigma_{\hat{x}}$ of (3.10) exists, and with the second assumption, is positive definite. Hence, from (3.11) and Theorem 1, $\Sigma_{\hat{u}}$ exists, is positive definite, and is a continuous function of N. In addition, $\mu_{\hat{u}}$ is a continuous function of M. Therefore, both sides of (3.14) and (3.15) form continuous functions of N and M. By the second assumption, and Brouwer's fixed point theorem [155], (3.14)-(3.15) has a solution $(N, M) \in \overline{\mathcal{N}} \times \overline{\mathcal{M}}$, implying that a solution (N, m) of (3.12)-(3.13) exists in $\overline{\mathcal{N}} \times \mathbb{R}$.

For the second case, let us assume that some elements of $\lim_{s \to 0} G_{21}(s)$ and/or $\lim_{s \to 0} G_{22}(s)$ are infinite. The first part of the fourth assumption, i.e., $\nu(\xi, v) = k \in \mathcal{M}, \ \forall \ \xi \in \mathbb{R}, v \in \mathbb{R}^n$ reduces the LHS of (3.13) to a constant, i.e., k. Since the range of $\mathcal{G}_M$ is $\mathcal{M}$, the assumption $k \in \mathcal{M}$ ensures a necessary condition for (3.13) to have a solution. To prove that the resulting (3.12)-(3.13) has a solution, I first show the existence of an implicit relation $\mu_{\hat{u}} = \varsigma \left(\Sigma_{\hat{u}} \right)$ between $\mu_{\hat{u}}$ and $\Sigma_{\hat{u}}$ in (3.13). Let $p_1 = \mathrm{vec} \left(\Sigma_{\hat{u}} \right)$ and $p_2 = \mu_{\hat{u}}$. Since $\mu_{\hat{u}}$ and $\Sigma_{\hat{u}}$ are continuous functions of m and N respectively, so are p_1 and p_2. Since $\mathcal{G}_M$ is continuously differentiable with respect to $\mu_{\hat{u}}$, $\psi \left(p_1, p_2 \right) := \mathcal{G}_M \left(\mu_{\hat{u}}, \Sigma_{\hat{u}} \right)$ is a continuous mapping from $\mathbb{R}^{n^2} \times \mathbb{R}^n \to \mathbb{R}$, and is

46

continuously differentiable in p_2, where the function ψ has been introduced in order to express $\mathcal{G}_M(\mu_{\hat{u}}, \Sigma_{\hat{u}})$ in terms of p_1 and p_2. By the second part of the fourth assumption and Theorem 1 in [156], for any value of $N \in \overline{\mathcal{N}}$, and hence for any $\Sigma_{\hat{u}}$ (which is a continuous function of N), there exists a unique $\mu_{\hat{u}} = p_2 = \varphi(p_1) = \varsigma(\Sigma_{\hat{u}})$, where φ and ς are continuous functions. On substituting $\varsigma(\Sigma_{\hat{u}})$ for $\mu_{\hat{u}}$ in (3.12), both the sides of (3.12) become continuous functions of N. By the second assumption and Brouwer's fixed point theorem, the result follows. $\qquad\square$

In practice, condition 1) of Theorem 3 can be checked by examining the eigenvalues of the system matrix A as a function of N, and ensuring they are all in the open left half plane. Condition 2) is similarly straightforward to check. Conditions 3) and 4) of Theorem 3 can be checked by examining the ranges of the functions $\mathcal{G}_N$ and $\mathcal{G}_M$, and depend specifically on the nonlinearity $f(\cdot)$. They are both usually satisfied, as in the case of the bivariate saturation nonlinearity. Finally, condition 5) takes care of those cases when some elements of $G(s)$ are infinite. This arises in classes of systems containing, for example, integrators in the controller or poles at origin of the plant. The first part of condition 5) essentially utilizes the infinitude of the elements of $G(s)$ and arranges them in a form such that *in ratio*, they yield a *finite* quantity in the limiting case that can be used in a fixed point equation. The second part of condition 5) essentially ensures that the function $\mathcal{G}_M$ does not become flat with respect to the mean of the control input $\mu_{\hat{u}}$, and allows for the existence of an implicit relation, as mentioned in the proof. For practical systems, this condition is also typically met.

There is no closed-form solution for (3.12) and (3.13), but they can be numerically arrived at by using an algorithm like Trust-Region Dogleg [157], which is used in, for example, MATLAB®'s `fsolve`. After solving those equations, M can be found using

(3.9) and $M = m + N^\top \mu_{\hat{u}}$. This completes the SL procedure for a generic closed-loop system with a multivariate nonlinearity.

Monte Carlo studies have been done with different nonlinear feedback systems (with 1st and 2nd order plants and trivariate saturation nonlinearities) and their stochastic linearizations to evaluate the accuracy of multivariable SL. Results indicate that SL is fairly accurate in approximating the response of the nonlinear system even with multivariate nonlinearities. For example, the median of the relative root-mean-squared differences between the tracking errors, $e(t)$, of the simulated nonlinear systems, and those of the stochastically linearized systems, $\hat{e}(t)$, i.e., $(\sqrt{\sum_{t=1}^{t_n} \{e(t) - \hat{e}(t)\}^2})/\sigma_e$, was found to be less than 7%, where σ_e are the standard deviations of the tracking errors, and t_n is the total number of samples.

3.3 ROBUSTNESS ANALYSIS OF SL

As seen from (3.12) and (3.13), the SL gains and bias depend on all the system and signal parameters. Hence, it is important to study the robustness of SL, i.e., the sensitivity of the quasilinear gains and bias to any change in system or signal parameters. Note that similar sensitivity studies have been conducted in the literature. For example, in [122], the sensitivities of the moments of state variables to parameters present in an SDE with a polynomial nonlinearity are evaluated. However, [122] does not consider a generic nonlinear function and does not specifically compute sensitivity to SL coefficients themselves. These are investigated in this section.

Let θ denote an uncertain system/signal parameter, e.g., plant time constant, plant gain, or the standard deviation of the input signal. To study the robustness of

SL to θ, I study $\partial_\theta N$, where, as before, ∂_θ denotes the partial derivative with respect to θ. Since θ affects the output variance, both directly and indirectly through the quasilinear gain N, I also study $\partial_\theta \sigma_{\hat{y}}$, where $\sigma_{\hat{y}}$ is the standard deviation of $\hat{y}(t)$. While these expressions can be found for very simple systems, they are generally difficult to obtain analytically. Below I provide a recipe to perform this robustness analysis and illustrate the recipe using a numerical example. Note that $\partial_\theta m$ can be studied as well using a similar approach.

Consider the nonlinear stochastic system shown in Fig. 3.2 and its stochastic linearization in Fig. 3.3, both with an uncertain parameter θ as described above. The values of $\mu_{\hat{u}}$ and $\Sigma_{\hat{u}}$ for the stochastically linearized system, as used in (3.12)-(3.13), depend on the uncertain parameter, θ. Let this dependence be denoted by $\mu_{\hat{u}}(N, m, \theta)$ and $\Sigma_{\hat{u}}(N, \theta)$. To simplify notation, let $\mathcal{H}_N(N, m, \theta) := \mathcal{G}_N(\mu_{\hat{u}}(N, m, \theta), \Sigma_{\hat{u}}(N, \theta))$, and $\mathcal{H}_M(N, m, \theta) := \mathcal{G}_M(\mu_{\hat{u}}(N, m, \theta), \Sigma_{\hat{u}}(N, \theta)) - N^{\mathrm{T}} \mu_{\hat{u}}(N, m, \theta)$, where $\mathcal{G}_N$ and $\mathcal{G}_M$ are as in (3.12)-(3.13). Equations (3.12)-(3.13) thus become

$$N = \mathcal{H}_N(N, m, \theta) \tag{3.16}$$

$$m = \mathcal{H}_M(N, m, \theta) \tag{3.17}$$

The sensitivity of N and m (and hence, of M) to θ can be found by finding the derivative of (3.16) and (3.17) with respect to θ using the chain rule and the total derivative of calculus, and evaluating the result at the solution (N, m) of (3.16) and (3.17). This leads to:

$$\partial_\theta N = [I - \partial_N \mathcal{H}_N - \partial_m \mathcal{H}_N (1 - \partial_m \mathcal{H}_M)^{-1} \partial_N \mathcal{H}_M]^{-1}$$
$$[\partial_m \mathcal{H}_N (1 - \partial_m \mathcal{H}_M)^{-1} \partial_\theta \mathcal{H}_M + \partial_\theta \mathcal{H}_N]$$
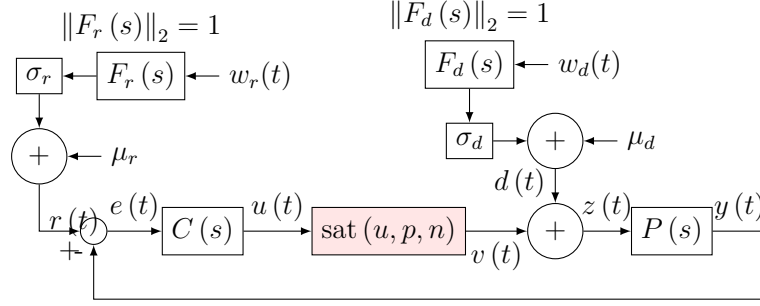
Figure 3.5: Block diagram of feedback control system

where I denotes the $n \times n$ identity matrix. Using $\partial_\theta N$ thus found, $\partial_\theta m = (1 - \partial_m \mathcal{H}_M)^{-1}(\partial_N \mathcal{H}_M \partial_\theta N + \partial_\theta \mathcal{H}_M)$.

To illustrate this process with an example, consider a standard unity feedback control system shown in Fig. 3.5 with plant $P(s) = 1/(Ts+1)$, controller $C(s) = 37.7$, and a trivariate saturation nonlinearity, $\mathrm{sat}(u, p, n)$ (defined in (3.7)), representing actuator saturation. The reference, $r(t)$, and the disturbance, $d(t)$, along with $n(t)$ and $p(t)$, which are inputs to the trivariate saturation nonlinearity other than $u(t)$ (but not shown explicitly as input signals in Fig. 3.5), are assumed to be stationary Gaussian processes that are separately generated by passing standard white Gaussian noises through coloring filters with unit $\mathcal{H}_2$-norm, scaling the respective outputs by the desired standard deviations, and adding biases that are equal to the desired mean values (similar to generation of $w(t)$ in Fig. 3.2). Fig. 3.6 shows the sensitivity of the quasilinear gain N_1 to the plant parameter T (time constant). In this case, at around $T = 0.12$ s, I see that the quasilinear gain N_1 is most sensitive to change in the plant parameter, T. A similar sensitivity is observed in the output standard deviation, $\sigma_{\hat{y}}$. However, for this example, the sensitivity observed in $\sigma_{\hat{y}}$ is not due to SL as such, but due to the underlying structure of the control system (this was
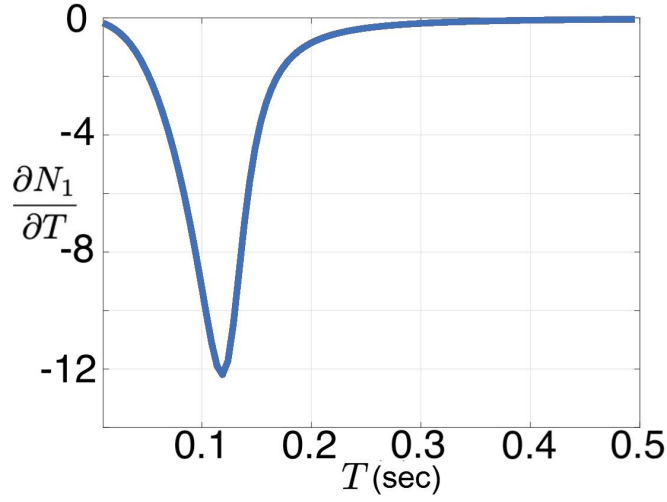
Figure 3.6: Sensitivity of N_1 with respect to plant time constant T for the control system of Fig. 2.2. The plant is $1/(Ts+1)$. The other (constant) parameters are: $C(s) = 37.7, \sigma_r = 1, \mu_r = \sigma_d = \mu_d = \rho_{pn} = 0, \sigma_n = 0.28, \mu_n = 3.40, \sigma_p = 0.66, \mu_p = 0.16$.

verified by forcing $N_1 = 1$, $N_2 = 1 - N_1 = 0$ and $N_3 = 0$ as T was varied). In another experiment, the standard deviation of $n(t)$ (in the trivariate saturation function), σ_n, was varied, and the magnitude of the sensitivity of $\sigma_{\hat{y}}$ to σ_n was found to increase linearly with increase in σ_n. This indicates that with increasing variability in actuator bounds, it becomes more important to get an accurate estimate of the statistics of the actuator inputs to avoid sensitivity issues. As a final remark, note that the sensitivity analysis outlined in this section can inform the selection of the stopping criteria for the numerical root-finding algorithm that solves the SL equations.

3.4 Optimal Controller Design Example

QLC can be used to design optimal controllers. In this section, I consider the design of a static optimal controller, but the process can be applied to dynamic controllers as well. To elaborate, consider the system in Fig. 3.2. I can formulate the following optimization problem to optimize a desired performance measure related to the system:

$$\text{minimize} \quad f_{\text{obj}}$$

where f_{obj} is the objective function that is a function of system and signal parameters. However, since the statistics of the signals in this nonlinear system are difficult to obtain analytically, and time-consuming using numerical simulations, the system needs to be stochastically linearized to that in Fig. 3.3. Therefore, I recast the objective function based on the signals in the stochastically linearized version, and add the equations of gains and bias as equality constraints:

$$\begin{aligned} \text{minimize} \quad & \hat{f}_{\text{obj}} \\ \text{subject to (3.11)-(3.12)} \end{aligned} \tag{3.18}$$

By doing so, I am assuming that SL is accurate in the sense that the two objectives f_{obj} and $\hat{f}_{\text{obj}}$ are close near the solution. While numerical examples show that this is indeed the case, a formal investigation of accuracy of SL is a topic for future publication. In general, however, SL is reliable, and I can obtain conclusions regarding the original system from the stochastically linearized system, when: 1) the system is driven by
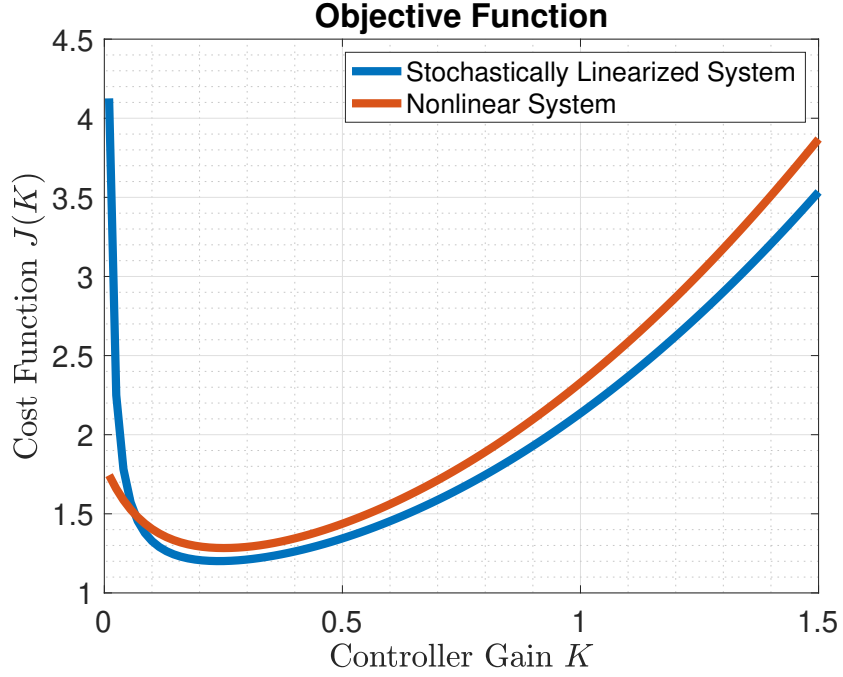
Figure 3.7: Plot of the objective function for the system described in Section 3.4.1. The cost has been evaluated for both the nonlinear system and the stochastically linearized approximation.

random exogenous inputs that have attained stationarity, 2) the open-loop system is of a low pass filtering nature [110], 3) the nonlinearity is not even with respect to any input. I can check for accuracy by comparing the statistics of the outputs of both systems, using numerical simulations. The resulting problem (3.18) is non-convex, with transcendental constraints, and hence should be solved numerically starting from several initial conditions. An example is provided below.

3.4.1 EXAMPLE

Consider Fig. 2.2, but where the actuator $f(\cdot)$ is a bivariate saturation defined as follows: when $u_2 \geq \max(-\beta, \alpha)$,

$$
\text{sat}_{\alpha,\beta}(u_1, u_2) =
\begin{cases}
\beta + u_2, & u_1 > \beta + u_2 \\
u_1, & \alpha - u_2 \leq u_1 \leq \beta + u_2 \\
\alpha - u_2, & u_1 < \alpha - u_2
\end{cases}
\tag{3.19}
$$

and $\text{sat}_{\alpha,\beta}(u_1, u_2) = 0$ when $u_2 < \max(-\beta, \alpha)$, with the second input, i.e., the noise in actuator bounds, modeled as a Gaussian process $u_2(t)$ with mean μ_2 and standard deviation σ_2. It is generated in the same manner as $d(t)$ and $r(t)$ were in Section 2.2. Let $C(s) = K$ and $P(s) = \frac{10}{s(s+10)}$. The actuator bounds are chosen to be $\alpha = -2$, $\beta = 1$, and the input parameters, $\mu_2 = 0$, $\sigma_2 = 1$, $\mu_r = 0$, $\sigma_r = 1$, $\mu_d = 0$ and $\sigma_d = 1$. The bandwidth for all coloring filters is chosen to be 48 rad/s, which is close to the system bandwidth for the range of K considered. Let the objective function be the sum of the second moment of the tracking error, $\hat{e}(t)$, and that of the primary actuator input, $\hat{u}_1(t)$. The following optimization problem can be formulated:

$$
\begin{aligned}
&\text{minimize} && E[\hat{e}^2(t)] + \gamma E[\hat{u}^2(t)] \\
&\text{subject to } (3.12) - (3.11)
\end{aligned}
\tag{3.20}
$$

$$
\begin{aligned}
&\text{minimize} && E[e^2(t)] + \gamma E[u^2(t)] \\
&\text{subject to } (3.12) - (3.11)
\end{aligned}
\tag{3.21}
$$

where $\gamma > 0$ is a control penalty. Fig. 3.7 shows the objective function for both the nonlinear system and the stochastically linearized system. The cost for the nonlinear system was obtained numerically by simulating the system for each K, and that for the stochastically linearized system by solving (3.12)–(3.11) for the same K's. Each case has a well-defined minimum. The difference between the two curves is small, particularly at the minima, indicating the fairly high accuracy of SL. The small error is in part due to the assumptions of SL and in part due to the linear approximation.

The optimization (3.21) was performed using the interior-point algorithm [158] of `fmincon` in MATLAB® with default tolerance of 1×10^{-6}, the initial value of $C(s) = 100$, and $\gamma = 1$. The optimal controller was found to be $C(s) = 0.24$. The cost reduced from 12445.2 to 1.2.

The system was simulated in MATLAB/Simulink® with an initial value of $C(s) = 100$, the results of which are shown in Fig. 3.8a. The upper subplot displays the tracking error in the nonlinear system, $e(t)$, and that in the stochastically linearized system, $\hat{e}(t)$. The lower subplot shows the actuator output from the nonlinear system, $v(t)$, and that from the stochastically linearized system, $\hat{v}(t)$, bounded by the actuator limits: $\alpha - u_2(t)$ and $\beta + u_2(t)$. The value of $v(t)$ can clearly be seen to be saturated by the bounds. Fig. 3.8b shows the same system after optimization. It can be seen that the standard deviation of the nonlinear error, σ_e, reduced from 1.096 to 1.085 and the absolute value of its mean, μ_e, reduced from 0.25 to 0.24. Since the optimization also reduced the primary actuator input, it is no longer saturated, and hence, $e(t)$ and $\hat{e}(t)$ coincide.

Because of the dependency of (3.12)-(3.11) on all system and input parameters, any change in these parameters would result in a change in N and M, and hence in the
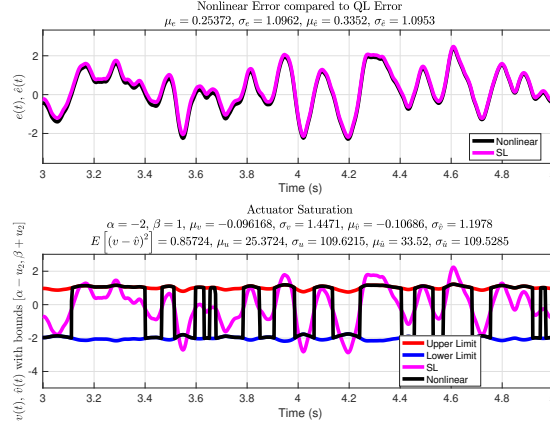
(a) Time series plot for baseline controller
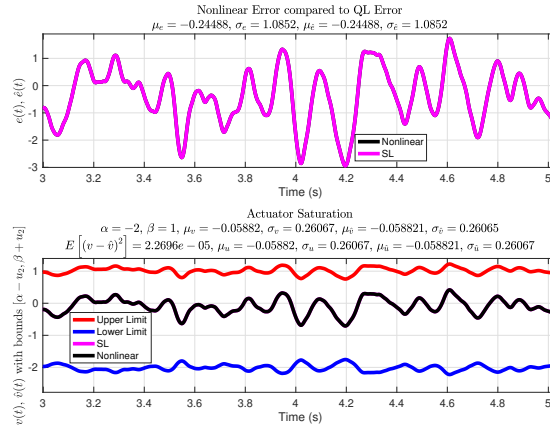
(b) Time series plot for optimal controller

Figure 3.8: Results of Optimization Problem

constraints of the optimization problem. By including N and M in the optimization problem, the method of SL allows for the system to *optimally adapt* to any change in its parameters.

CHAPTER 4

SYSTEMS WITH STATE MULTIPLICATIVE

NOISE

In this chapter, the process of SL is applied to systems with state-multiplicative noise. In Section 4.1, the process of SL is extended to MIMO nonlinearities, which occur in systems with state-multiplicative noise. In Section 4.2, the results of Section 4.1 are applied to the SL of systems with state-dependent noise.

4.1   EXTENSION TO MIMO NONLINEARITIES

The process of SL can be extended to multiple-input multiple-output (MIMO) non-linearities described by $v(t) = f(u(t))$, where $f : \mathbb{R}^n \to \mathbb{R}^m$. This can model systems with nonlinearities having multiple outputs or systems with multiple nonlinearities located in different parts of the control systems. While there can be various objective functions to minimize the error between the output of the multivariate nonlinearity and that of its SL [112, 113], including minimizing the L^2-norm of the error, as done

in [91, 103], the approach used here involves minimizing the mean squared error of each output of the nonlinearity with the corresponding output of its SL, using the results of Section 3.1. In the following theorem, the Jacobian of the function $f(\cdot)$ is denoted as $J_f(\cdot)$ and, for a matrix L, $L^{\circ 2} = L \circ L$, where $\circ$ denotes the Hadamard (i.e., element-by-element) product. Similar to Theorem 1, I drop the argument t after $u(t)$ and $u_0(t)$ for convenience.

Theorem 4. *Let u_0 be a zero-mean stationary jointly-Gaussian process with a positive definite covariance matrix $E\left[u_0 u_0^\top\right]$, and let $u = u_0 + \mu_u$, where μ_u is a constant mean vector. Let $f(u) : \mathbb{R}^n \to \mathbb{R}^m$ be a function such that $f(u) = [f_1(u) \ f_2(u) \ \cdots \ f_m(u)]^\top$, where each $f_j(u) : \mathbb{R}^n \to \mathbb{R}$ satisfies properties 1) and 2) mentioned in Theorem 1. Then, the functional: $\epsilon(N, M) = E\{[f(u) - Nu_0 - M]^{\circ 2}\}$ is minimized over $N \in \mathbb{R}^{m \times n}$ and $M \in \mathbb{R}^m$ by:*

$$N = E\left[J_f(u)\right] \tag{4.1}$$

$$M = E\left[f(u)\right] \tag{4.2}$$

Proof. Let N_j denote the jth row of N, N_{ij} the ijth element of N, and M_j the jth element of M. The jth output of the nonlinearity $f(\cdot)$ can be written as $v_j = f_j(u)$, where $f_j : \mathbb{R}^n \to \mathbb{R}$. Let $\epsilon_j(N_j^\top, M_j)$ be the jth element of $\epsilon(N, M)$. Then $\epsilon(N, M)$ is minimized when for all $j \in \mathbb{N}$, $1 \leq j \leq m$, $\epsilon_j(N_j^\top, M_j)$ is minimized. Using Theorem 1, the functional: $\epsilon_j(N_j^\top, M_j) = E\{[f_j(u) - N_j u_0 - M_j]^2\}$ is minimized when $N_j^\top = E[\nabla f_j(u)]$ and $M_j = E[f_j(u)]$. Hence, it follows that $N = E[J_f(u)]$ and $M = E[f(u)]$. $\square$

Eqns. (4.1) and (4.2) are similar to (3.1) and (3.2) respectively, with some differ-

ences. There are now *nm* quasilinear gains forming a *matrix N*, and *m* biases forming a *vector M*. Also, the gradient in (3.1) is replaced by a *Jacobian* in (4.1).

4.2 STOCHASTIC LINEARIZATION OF SYSTEMS WITH STATE-DEPENDENT NOISE

SL can be used for analyzing and designing optimal controllers for systems with stochastic parameters, or state-multiplicative noise. This application does not appear in the existing literature of SL and is one of the important contributions of this dissertation. Reference [159] describes a somewhat similar application of SL to systems with random parameters excited by random noise, but the parameters are assumed to be random variables (not random processes), the random process excitation does not multiply the state, and the SL has been done by equating the second moments of the nonlinear process and stochastically linearized process (not by minimizing the mean squared error). References [112, 113, 160], which are in Russian, also contain similar other works on the application of SL to systems with parametric noise. In [161] and other literature reviewed in [90], while SL is applied for optimal control of nonlinear stochastic systems, systems with state multiplicative noise are not considered. Control systems with state multiplicative noise, as investigated here, find applications in many areas, for example, control of pH processes [162], oil catalytic cracking [163], and altitude estimation from altimeter measurements [164]. For the sake of presentation, I focus this section on a specific differential equation with random parameters that are stochastic processes. Other forms can be handled similarly.

Consider the following differential equation and output equation as a representation of a system with stochastic parameters:

$$\dot{x}(t) = (A + A_1 w(t)) \, x(t) + (B + B_1 w(t)) \, u(t) \tag{4.3}$$

$$y(t) = Cx(t) + Du(t) \tag{4.4}$$

where $x(t) \in \mathbb{R}^n$ represents the state of the system, $w(t) \in \mathbb{R}$ is a white noise process with intensity σ^2, $A_1 w(t) \in \mathbb{R}^{n \times n}$ and $B_1 w(t) \in \mathbb{R}^{n \times m}$ represent noises in the system matrices $A \in \mathbb{R}^{n \times n}$ and $B \in \mathbb{R}^{n \times m}$ respectively, $u(t) \in \mathbb{R}^m$ is the control input and $y(t) \in \mathbb{R}^p$ is the output. Note that the product of $x(t)$ and $w(t)$ represents a nonlinearity (in fact, bilinearity) in this system. It is assumed, for simplicity, that there is no variability in the matrices $C \in \mathbb{R}^{p \times n}$ and $D \in \mathbb{R}^{p \times m}$. One of the objectives when designing controllers for such systems is to minimize the adverse effect of variability in parameters on some performance measure. In this section, I seek to design an optimal state feedback law $u(t) = Kx(t) + Gr(t)$ such that (4.3)-(4.4) tracks the deterministic reference $r(t)$ on average, and that the sum of the variance of the output and the control effort is a minimum. This is also the standard LQR cost function [165]. I achieve this goal using two approaches. First, I directly design K and G using the original nonlinear system. Second, I use SL to do so. Then, I compare the optimal gains and the output accuracy obtained by both methods. The purpose of this illustration is to establish that SL is an effective method for designing and analyzing nonlinear systems subjected to stochastic inputs.

4.2.1 Nonlinear System

Substituting $u(t) = Kx(t) + Gr(t)$ in (4.3)-(4.4), I obtain:

$$\dot{x} = (A + BK)\, x + BGr + [(A_1 + B_1 K)\, x + B_1 Gr]\, w$$

$$y = (C + DK)x + DGr$$

Since I assume that the system is in the stationary regime, the mean of the state is given by [152]:

$$E[x] = -(A + BK)^{-1} BGr \tag{4.5}$$

Similarly, the covariance matrix of $x(t)$ can be obtained from:

$$E\{[(A + BK)x + BGr](x - E[x])^\top\}$$
$$+ E\{[(A + BK)x + BGr]^\top (x - E[x])\} \tag{4.6}$$
$$+ E\{[(A_1 + B_1 K)x + B_1 Gr]\sigma^2[(A_1 + B_1 K)x + B_1 Gr]^\top\} = 0$$

where $E[x]$ is as in (4.5). Equation (4.6) can be expanded, and then solved for $E[xx^\top]$ by vectorizing both sides and using the property that for conformable matrices P, Q and X, $\text{vec}\,(PXQ) = \left(Q^\top \otimes P\right)\text{vec}\,(X)$. The output covariance, Σ_y, and the input covariance, Σ_u, can thus be found to be:

$$\Sigma_y = (C + DK)\left(E\left[xx^\top\right] - E[x]E[x]^\top\right)(C + DK)^\top \tag{4.7}$$

$$\Sigma_u = K\left(E\left[xx^\top\right] - E[x]E[x]\right)^\top K^\top \tag{4.8}$$

where $E[xx^\top]$ is obtained from (4.6) and $E[x]$ from (4.5).

Finally, since I am designing the system to track the reference $r(t)$, I set the expected value of the output equal to $r(t)$ and compute G:

$$G = [-(C + DK)(A + BK)^{-1}B + D]^{-1} \tag{4.9}$$

The optimization problem is thus stated to be:

$$\begin{aligned} \text{minimize} \quad & \text{tr}(\textstyle\sum_y + \textstyle\sum_u) \\ \text{over } & K \\ \text{subject to } & (4.5)\text{-}(4.9) \end{aligned} \tag{4.10}$$

where tr denotes trace of matrix. This problem can be solved numerically, for example, using a trust-region-reflective algorithm based on the interior-reflective Newton method [166], which is implemented by `lsqnonlin` in MATLAB®.

4.2.2 STOCHASTICALLY LINEARIZED SYSTEM

To find the SL of system (4.3)-(4.4), similarly, I plug in $u(t) = Kx(t) + Gr(t)$ in (4.3)-(4.4), but rewrite the equations in this form:

$$\begin{aligned} \dot{x} &= (A_1 + B_1 K)\, wx + (A + BK)\, x + BGr + B_1 Grw \\ y &= (C + DK)x + DGr \end{aligned} \tag{4.11}$$

To ensure that the nonlinear system tracks the reference on average, I again assume here that G is given by (4.9). It can be seen that the nonlinearity in this system is $f : \mathbb{R}^{n+1} \to \mathbb{R}^n$, given by $f(w, x) = wx$, which is a multi-input, multi-output nonlinearity. Such nonlinearities depending on w and x are considered in open-loop

systems in [112, 113] and in closed-loop systems in [160]. Using (4.1) and using the notation $x = [\ x_1\quad x_2\quad \ldots\quad x_n\ ]^\top$, it can be shown that N is given by:

$$N = \begin{bmatrix} E\left(x_1\right) & 0 & 0 & \cdots & 0 \\ \vdots & \vdots & \ddots & \ddots & \vdots \\ E\left(x_n\right) & 0 & \cdots & 0 & 0 \end{bmatrix}$$

since $E[w] = 0$. Also, from (4.2), $M = E[wx]$. Then, by Theorem 4, the nonlinearity $v = wx$ can be stochastically linearized to: $\hat{v} = E[x]w + E[wx]$. Denoting the states of the stochastically linearized system as $\hat{x}$, (4.11) can thus be stochastically linearized to:

$$\dot{\hat{x}} = (A_1 + B_1K)\left(E\left[\hat{x}\right]w + E\left[w\hat{x}\right]\right) + (A + BK)\hat{x} + \tag{4.12}$$
$$BGr + B_1Grw, \quad \hat{y} = (C + DK)\hat{x} + DGr$$

As before, assuming that the system is in the stationary regime, the mean of $\hat{x}$ can be found from:

$$(A + BK)E[\hat{x}] + (A_1 + B_1K)E\left[w\hat{x}\right] + BGr = 0 \tag{4.13}$$

The above equation has two unknowns, $E[\hat{x}]$ and $E\left[w\hat{x}\right]$. Out of them, $E\left[w\hat{x}\right]$ can be found out separately using system properties. To illustrate the process of finding $E[w\hat{x}]$, I first show how it can be obtained for a general LTI system in the following theorem, and then use the result in this specific case.

Theorem 5. *Consider a stable LTI system with the state-space equation: $\dot{x} = \tilde{A}x + \tilde{R} + \tilde{B}w$, where $\tilde{A}$, $\tilde{B}$, and $\tilde{R}$ are constant matrices, $\tilde{A}$ being non-singular, x is the state, and w is a white noise process with intensity σ^2. Then, assuming the system is*

(a) A scatter plot of $\frac{\hat{\sigma}_{\min} - \sigma_{\min}}{\sigma_{\min}} \times 100\%$ in the x-axis vs. $(A_1 + B_1K)^2\sigma^2/(A + BK)$ in the y-axis.

(b) Scatter plot of optimal controller gain obtained from SL method, $\hat{K}_{\min}$, vs. that from the nonlinear method, $K_{\min}$. The green line indicates the $\hat{K}_{\min} = K_{\min}$ line.
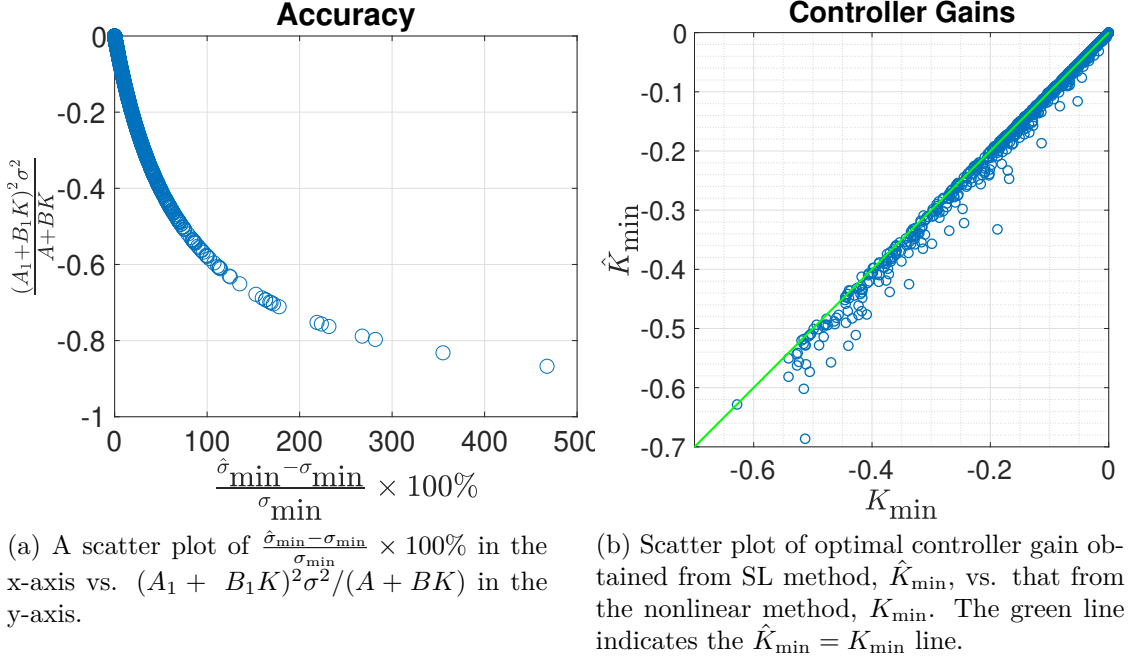
Figure 4.1: Scatter Plots for Accuracy and Controller Gains

in the stationary regime, $E[wx] = \sigma^2 \widetilde{B}$.

Proof. To find $E[wx]$, I make the change of coordinates $z = \widetilde{A}x + \widetilde{R}$ to bring the state equation into a standard form for which I can easily prove the results. In the z coordinates, the dynamics are given by: $\dot{z} = \widetilde{A}z + \widetilde{A}\widetilde{B}w$. This is a system with transfer matrix from w to z given by $G(s) = (sI - \widetilde{A})^{-1}\widetilde{A}\widetilde{B}$. From the theory of LTI systems driven by random processes [167], the cross-power spectral density between the output and the input, S_{zw}, is related to the power spectral density of the input, $S_w = \sigma^2$, by $S_{zw} = G(j\omega)S_w = G(j\omega)\sigma^2$. Also, S_{zw} is given by the Fourier transform of the cross-correlation function, $R_{zw}(\tau)$, between z and w, i.e., $S_{zw} = \mathcal{F}\{R_{zw}(\tau)\}$. Since $E[wz] = R_{zw}(0)$, it follows that: $E[wz] = \mathcal{F}^{-1}\{S_{zw}\}_{t=0} = \mathcal{F}^{-1}\{G(j\omega)\sigma^2\}_{t=0}$. Using the Initial Value Theorem, this can be simplified to: $E[wz] = \sigma^2 \lim_{s\to\infty} sG(s) =$

$\sigma^2 \lim_{s \to \infty} s(sI - \widetilde{A})^{-1}\widetilde{A}\widetilde{B} = \sigma^2 \widetilde{A}\widetilde{B}$. Finally, in the original coordinates, $E[wz] = E(\{\widetilde{A}x + \widetilde{R}\}w) = \widetilde{A}E[wx]$, which implies that $E[wx] = \sigma^2 \widetilde{B}$. $\qquad\square$

Note that the state-space equation assumed in the theorem statement is of the same form as the first equation in (4.12). Thus, using the result of Theorem 5 on (4.12), I obtain:

$$E\left[w\hat{x}\right] = \sigma^2 \left[(A_1 + B_1 K) E\left[\hat{x}\right] + B_1 Gr\right] \tag{4.14}$$

Solving (4.13) and (4.14) for $E[\hat{x}]$ and $E\left[w\hat{x}\right]$, I obtain:

$$E\left[\hat{x}\right] = \sigma^2 P B_1 Gr, \quad E\left[w\hat{x}\right] = -\sigma^2 Q B_1 Gr \tag{4.15}$$

where: $P = [(A_1 + B_1 K)^{-1}(A + BK) + \sigma^2(A_1 + B_1 K)]^{-1}$ and $Q = (I + \sigma^2\{(A_1 + B_1 K)(A + BK)^{-1}(A_1 + B_1 K)\})^{-1}$.

The covariance matrix of $\hat{x}$, $\Sigma_{\hat{x}}$, can be obtained by solving the Lyapunov equation:

$$(A + BK)\Sigma_{\hat{x}} + \Sigma_{\hat{x}}(A + BK)^\top + VV^\top = 0 \tag{4.16}$$

where $V = \sigma\left[(A_1 + B_1 K) E\left[\hat{x}\right] + B_1 Gr\right]$. Similar to (4.7), the output covariance $\Sigma_{\hat{y}}$ and the input covariance $\Sigma_{\hat{u}}$ can be obtained thus:

$$\Sigma_{\hat{y}} = (C + DK)\Sigma_{\hat{x}}(C + DK)^\top \tag{4.17}$$

$$\Sigma_{\hat{u}} = K\Sigma_{\hat{x}}K^\top \tag{4.18}$$

where $\Sigma_{\hat{x}}$ is obtained from (4.16) and $E[\hat{x}]$ from (4.15). The mean of the output is $E[\hat{y}] = (C + DK)E[\hat{x}] + DGr$. Similar to (4.10), the optimization problem can be

65

stated to be:

$$\text{minimize} \qquad \text{tr}(\textstyle\sum_{\hat{y}} + \sum_{\hat{u}})$$

$$\text{over } K \tag{4.19}$$

$$\text{subject to } (4.9), (4.15)\text{-}(4.18)$$

4.2.3 COMPARISON OF THE TWO METHODS

To investigate the effectiveness of SL in predicting the behavior of such a system with stochastic parameters, a Monte Carlo experiment was conducted. Specifically, 1000 first-order systems were randomly generated, with the system matrices being selected randomly and uniformly from the following ranges: $A \sim U[-2, 0]$, $B, C, D, A_1, B_1 \sim U[0, 1]$. Standard white Gaussian noise $w(t)$ was assumed to be the perturbing agent. The reference to be tracked was $r(t) = 1$. Systems with $A + A_1 > 0$ were rejected since noise in such systems might drive them to instability. After experimenting, the computed standard deviation of the output of the nonlinear system was compared with that of the corresponding stochastically linearized system, both the systems having the optimal controller gain that was derived using the SL method described in the previous subsection. This study was conducted to investigate the accuracy of SL for this class of systems. Fig. 4.1a shows a scatter plot of the percentage difference between the standard deviation of output of the stochastically linearized system, $\hat{\sigma}_{\min}$, and that of the nonlinear system, $\sigma_{\min}$, both simulated using the optimal SL gains, $K = \hat{K}_{\min}$. The percent difference in standard deviation is shown in the x-axis and the quantity $\eta := (A_1 + B_1 K)^2 \sigma^2 / (A + BK)$ is in the y-axis. It can be seen that the error (i.e., accuracy) depends highly on the value of η. To intuitively understand this, note from (4.11) that $(A_1 + B_1 K)$ multiplies both the state and noise (with intensity

66

σ^2), and $(A + BK)$ multiplies the state only. Hence, as η becomes closer to -1, or as the noisy component becomes comparable to the no-noise component, the accuracy of SL degrades. For $|\eta| < 10\%$, the error is less than 8%.

Fig. 4.1b shows a scatter plot of the optimal controller gains K for the same set of systems as above, obtained separately from both the methods, namely optimization of the nonlinear system in (4.10), and that of the stochastically linearized system in (4.19). It can be seen that for most of these systems, the optimal gains reported by both methods are close, indicating the effectiveness of SL in designing optimal controllers for systems with stochastic parameters. Note that in this case, the analytical solution to the nonlinear system was readily available, but in many cases, it is not. The above analysis shows that SL is an alternative method of design and analysis that is also effective for such systems.

CHAPTER 5

INVESTIGATION OF ACCURACY, ROBUSTNESS AND COMPUTATION OF SL

This chapter investigates the accuracy, robustness and computation of SL. It is organized as follows. Section 5.1 defines the feedback system considered here, which is commonly used in the literature of QLC. Section 5.2 discusses open-loop accuracy of SL and its effect on closed-loop accuracy. In Section 5.3, the computational costs of different numerical algorithms for computing the SL coefficients for systems with symmetric actuator saturation are compared. In Section 5.4, a sensitivity analysis is performed on the SL coefficients, again for systems with symmetric saturation. Section 5.5 extends the above investigation to systems with asymmetric saturation nonlinearities.
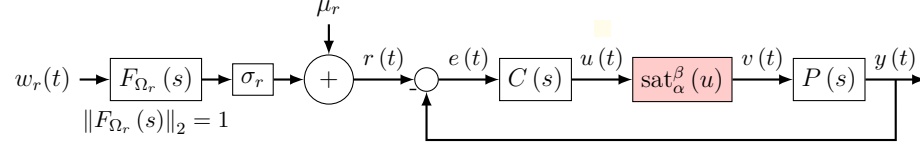
(a) Nonlinear Feedback Control System
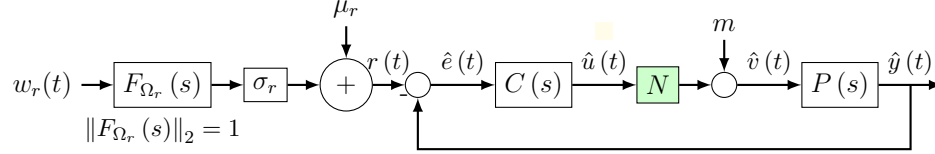
(b) SL of the System in Fig. 5.1a

Figure 5.1: SL of a feedback system

5.1 FEEDBACK SYSTEM

The feedback control system on which the rest of the chapter will be based is described is depicted in Fig. 5.1a, where the symbols have the same meaning as in Section 2.2, and $\text{sat}_\alpha^\beta(u)$ is as in (2.4). Applying the process of SL as described in Chapter 2 to this system, I obtain the system of Fig. 5.1b, where:

$$\sigma_{\hat{u}} = \left\| \frac{F_r(s)C(s)}{1 + NP(s)C(s)} \right\|_2 \sigma_r \tag{5.1}$$

$$M = \frac{1}{P_0}\mu_r - \frac{1}{C_0 P_0}\mu_{\hat{u}} \tag{5.2}$$

$$N = \mathcal{F}_N\left(\mu_{\hat{u}}, \left\| \frac{F_r(s)C(s)}{1 + NP(s)C(s)} \right\|_2 \sigma_r \right) \tag{5.3}$$

$$\frac{1}{P_0}\mu_r - \frac{1}{C_0 P_0}\mu_{\hat{u}} = \mathcal{F}_M\left(\mu_{\hat{u}}, \left\| \frac{F_r(s)C(s)}{1 + NP(s)C(s)} \right\|_2 \sigma_r \right) \tag{5.4}$$

where $\mathcal{F}_N(\cdot, \cdot)$ and $\mathcal{F}_M(\cdot, \cdot)$ are as in (2.2)-(2.3). After solving (5.3) and (5.4), M can be found by using $M = \frac{1}{P_0}\mu_r - \frac{1}{C_0 P_0}\mu_{\hat{u}}$ and m from $m = M - N\mu_{\hat{u}}$. This completes the process of SL of the nonlinear system in Fig. 5.1a to that in Fig. 5.1b.

It can be seen that (5.3) and (5.4) comprise a system of two transcendental equations in two unknowns. Thus, these equations are only numerically solvable. In this chapter, I am thus concerned with investigating the numerical solution of these equations and their properties. Specifically, I have considered two types of nonlinear feedback systems (consistent with the literature of QLC [110, 145]): 1) systems having symmetric saturation nonlinearity (i.e., $\alpha = -\beta$) and zero-mean reference input ($\mu_r = 0$), and 2) systems with asymmetric saturation $\alpha \neq -\beta$ and non-zero mean reference input ($\mu_r \neq 0$). For convenience, systems of the first type are henceforth referred to as "symmetric", and those of the second type are referred to as "asymmetric".

5.2 Analysis of Accuracy of Stochastic Linearization

I begin by investigating the accuracy of SL in this section. Since SL approximates the nonlinear system in a mean-squared sense, there is inevitably an error in the response of the stochastically linearized system compared to that of the original nonlinear system. Consistent with the minimization problem in Eq. (2.1), this error can be quantified as the mean-squared difference between the stationary response of the original nonlinear system and that of its SL. There are mainly two sources that contribute to the error: 1) the SL of the nonlinearity itself (as in (2.1), referred to as the open-loop accuracy herein), and 2) the assumption that the input to the nonlinearity in the closed-loop setting is Gaussian and equal to $\hat{u}$ (in Fig. 5.1b) instead of u (in Fig. 5.1a). Inspired by Eq. (2.1), in this section, I introduce a new metric

to quantify the open-loop relative accuracy of SL for a saturation nonlinearity. I term this metric the "relative approximation error" and provide its relationship to the actuator authority and the statistics of the input to the nonlinearity. I determine the upper bound on this relative error and show its effect on bounding the closed-loop accuracy. This information on the accuracy of SL is valuable to have from a practical perspective, as the error can then be properly accounted for during an SL-based design of controllers for the original nonlinear system.

5.2.1 SYMMETRIC CASE

First, I consider the case of symmetric systems. Recall that the objective of open-loop SL is to minimize the functional (2.1). Let $f(u) = \text{sat}_{-\beta}^{\beta}(u)$, which is the standard symmetric saturation function with upper limit $\beta > 0$ and lower limit $-\beta$, and $u(t) = u_0(t)$ be a zero-mean stationary Gaussian input. Then, substituting for $f(u)$ and $u_0(t)$ as above and N from (2.7) in (2.1), the following expression for the mean squared error, ε, can be obtained in terms of β and σ_u (recall that $M = 0$ in the symmetric case):

$$\varepsilon\left(N,0\right) = -\beta^2 \text{erf}\left(\frac{\beta}{\sqrt{2}\sigma_u}\right) + \beta^2 - \frac{\sqrt{2}\beta\sigma_u e^{-\frac{\beta^2}{2\sigma_u^2}}}{\sqrt{\pi}} - \sigma_u^2 \text{erf}^2\left(\frac{\beta}{\sqrt{2}\sigma_u}\right) + \sigma_u^2 \text{erf}\left(\frac{\beta}{\sqrt{2}\sigma_u}\right) \quad (5.5)$$

It can be observed from (5.5) that if I normalize the above by the variance of the input, σ_u^2, the term $\frac{\beta}{\sqrt{2}\sigma_u}$ can be collected and the expression simplified. In addition, this normalization provides a sense of scale of the accuracy relative to the input variance. Thus, letting $U = \frac{\beta}{\sqrt{2}\sigma_u}$, which I term the "saturating factor", I can define

(a) Symmetric Case   (b) Asymmetric Case
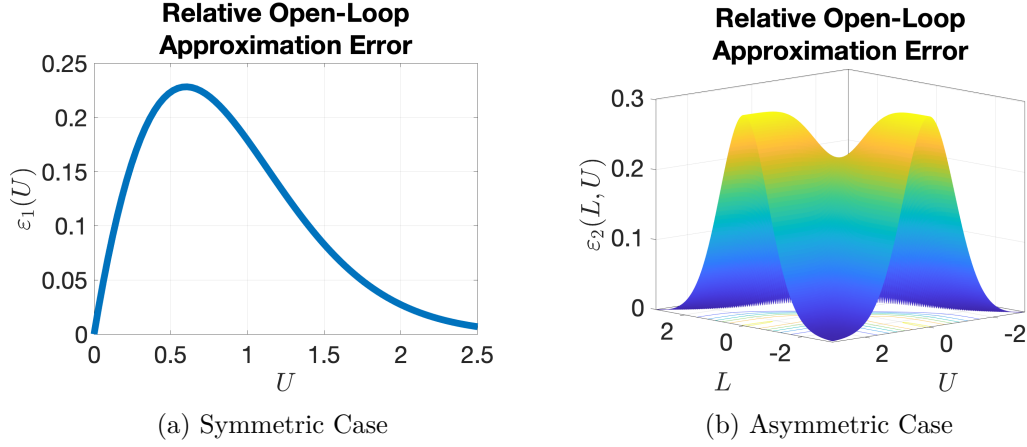
Figure 5.2: Relative Open-Loop Accuracy of SL

the "relative approximation error", ε_1, to be:

$$\varepsilon_1(U) := \sqrt{\frac{\varepsilon(N,0)}{\sigma_u^2}} = \sqrt{2U^2 - \frac{2Ue^{-U^2}}{\sqrt{\pi}} + (1 - 2U^2)\operatorname{erf}(U) - \operatorname{erf}^2(U)} \qquad (5.6)$$

Fig. 5.2a shows the variation of $\varepsilon_1(U)$ with U. It can be seen that ε_1 has a maximum value and is thus bounded above. To find the maximum, I evaluate the derivative $\varepsilon_1(U)$ and set it equal to zero. The maximum is found to occur around $U = 0.600$ and the maximum value is around 0.228. The sensitivity of this relative approximation error to changes in system parameters in the feedback case is remarked upon in Section 5.2.

The bell-shaped nature of Fig. 5.2a can be explained as follows. When $U \gg 0.6$, or the standard deviation of input is very small *compared* to the saturation authority, i.e., $\sigma_u \ll 1.1785\beta$, the error is low (i.e., accuracy is high). This is expected, since in such a case, the output of the saturation function remains practically unsaturated, i.e., $\operatorname{sat}_{-\beta}^{\beta}(u) \to u$. Also, $N = \operatorname{erf}\left(\frac{\beta}{\sqrt{2}\sigma_u}\right) \to 1$ as $\sigma_u \to 0$. Thus, for large U, it can

be mathematically shown that the relative error converges to:

$$\varepsilon_1(U) \to \sqrt{\lim_{\sigma_u \to 0} E\left[\frac{\left(\text{sat}_{-\beta}^{\beta}(u) - Nu\right)^2}{\sigma_u^2}\right]} = \lim_{\sigma_u \to 0} \sqrt{E\left[\frac{(u - Nu)^2}{\sigma_u^2}\right]}$$

$$= \sqrt{\lim_{\sigma_u \to 0} (1 - N)^2 \frac{E\left[u^2\right]}{\sigma_u^2}} = \lim_{\sigma_u \to 0} \sqrt{(1 - N)^2} = 0$$

where I used the fact that $E\left[u^2\right] = \sigma_u^2$.

As can be seen from Fig. 5.2a, the relative accuracy is good even when $U \ll 0.6$, i.e., $\sigma_u \gg 1.1785\beta$ (or the standard deviation of input is very large compared to the saturation authority). This is due to the definition of relative accuracy – the division by a large input variance makes the relative accuracy tend toward zero. This makes physical sense as well: the error is small *compared* to the size of the input. In other words, the standard deviation of the actuator input u is much higher than that what is allowed to propagate through the saturation nonlinearity. Since the bounds of the saturation nonlinearity are finite, the error is small *compared* to the size of the input. I now show this mathematically. Consider $\sigma_u \to \infty$. Then $N = \text{erf}(U) \to 0$, and thus:

$$\varepsilon_1(U) \to \lim_{\sigma_u \to \infty} \sqrt{E\left[\frac{\left(\text{sat}_{-\beta}^{\beta}(u) - Nu\right)^2}{\sigma_u^2}\right]}$$

$$= \lim_{\sigma_u \to \infty} \sqrt{E\left[\frac{\left\{\text{sat}_{-\beta}^{\beta}(u)\right\}^2}{\sigma_u^2}\right] + \lim_{\sigma_u \to \infty} E\left[\frac{N^2 u^2}{\sigma_u^2}\right] - 2 \lim_{\sigma_u \to \infty} E\left[\frac{\text{sat}_{-\beta}^{\beta}(u) Nu}{\sigma_u^2}\right]} = 0$$

In the last line, the first limit is zero because $\{\text{sat}_{-\beta}^{\beta}(u)\}^2$ is bounded but σ_u^2 is unbounded. The second limit is zero because $E[u^2] = \sigma_u^2$ and $N \to 0$. Finally, the third limit is zero because $E[\text{sat}_{-\beta}^{\beta}(u)u] = \text{erf}(\beta/(\sqrt{2}\sigma_u)) \to 0$, as $\sigma_u \to \infty$.

Thus, in the symmetric case, the open-loop relative error of SL for a saturation function is found to be always better than about 0.228, or 22.8%. Thus, the accuracy is high relative to the size of the input. As shown later, this has consequences in the closed-loop accuracy of SL as well, as it provides an upper bound on how inaccurate the SL approximation can be in a feedback system.

5.2.2   Asymmetric Case

For the case of asymmetric systems, the accuracy is obtained by evaluating the expectation in (2.1), with $f(u)$ substituted from (2.4), u_0 as $u - \mu_u$, and N and M substituted from (2.5) and (2.6) respectively. Similar to the symmetric case, the expression for accuracy is simplified if I normalize it by the variance of the input u, and define:

$$L := \frac{\alpha - \mu_u}{\sqrt{2}\sigma_u}, \quad U := \frac{\beta - \mu_u}{\sqrt{2}\sigma_u} \tag{5.7}$$

where L can be termed as the "lower saturation factor" and U the "upper saturation factor" respectively, such that the "relative approximation error" is given by:

$$\varepsilon_2(L, U) := \sqrt{\varepsilon(N, M)/\sigma_u^2}$$

$$= \left(-\frac{L^2 \operatorname{erf}^2(L)}{2} + \frac{L^2}{2} + LU \operatorname{erf}(L) \operatorname{erf}(U) - LU \operatorname{erf}(L) + LU \operatorname{erf}(U) - LU \right.$$

$$+ \frac{Le^{-U^2} \operatorname{erf}(L)}{\sqrt{\pi}} + \frac{Le^{-U^2}}{\sqrt{\pi}} - \frac{Le^{-L^2} \operatorname{erf}(L)}{\sqrt{\pi}} - \frac{U^2 \operatorname{erf}^2(U)}{2} + \frac{U^2}{2} - \frac{Ue^{-U^2} \operatorname{erf}(U)}{\sqrt{\pi}}$$

$$+\frac{Ue^{-L^2}\operatorname{erf}(U)}{\sqrt{\pi}} - \frac{Ue^{-L^2}}{\sqrt{\pi}} + \frac{e^{-L^2-U^2}}{\pi} - \frac{\operatorname{erf}^2(L)}{4}$$

$$+\frac{\operatorname{erf}(L)\operatorname{erf}(U)}{2} - \frac{\operatorname{erf}(L)}{2} - \frac{\operatorname{erf}^2(U)}{4} + \frac{\operatorname{erf}(U)}{2} - \frac{e^{-2U^2}}{2\pi} - \frac{e^{-2L^2}}{2\pi}\Bigg)^{\frac{1}{2}} \qquad (5.8)$$

Fig. 5.2b shows a plot of the above expression for permissible values of L and U, i.e., $L < U$. It can be seen that similar to the symmetric case, the relative open-loop accuracy is always better than a certain level, which in this case, is observed to be the supremum of (5.8). It can be observed from Fig. 5.2b that this supremum can be approached asymptotically along either $L = 0$ or $U = 0$. Specifically, it can be found to be:

$$\lim_{U \to \infty} \varepsilon_2(0, U) = \lim_{L \to -\infty} \varepsilon_2(L, 0) = \sqrt{\frac{1}{4} - \frac{1}{2\pi}}$$

which has a numerical value of around 0.301, or 30.1%. The sensitivity of this relative approximation error to changes in system parameters in the feedback case is remarked upon in Section 6.4.

The observation can be explained as follows: when $\mu_u \approx \alpha$ or $\mu_u \approx \beta$, the input to the saturation is situated, on average, near the boundary of the regions of the saturation function (which are: $u > \beta$, $\alpha \leq u \leq \beta$, and $u < \alpha$), and thus the output is more likely to switch between two linear regions, making the resulting linear approximation less accurate. On the other hand, when $\alpha \ll \mu_u \ll \beta$, $\mu_u \ll \alpha$, or $\mu_u \gg \beta$, the input is situated, on average, in a linear region of the function, and hence, the resulting linear approximation is more accurate. The good accuracy for large σ_u, when L and U both approach zero, is due to division by σ_u^2, which makes

the relative accuracy smaller (similar to the symmetric case).

Thus, the relative accuracy of open-loop SL for an asymmetric saturation is also bounded above and always better than 30.1%, which is higher than the 22.8% in the symmetric case. Moreover, as the magnitude of L or U increases, which can be brought about by a decrease in σ_u, the accuracy improves. As shown next, this has consequences in the closed-loop system, as it bounds the closed-loop accuracy of SL as well.

5.2.3 IMPLICATIONS FOR CLOSED-LOOP ACCURACY

Consider the closed-loop system shown in Fig. 5.1a and its SL in Fig. 5.1b. Analogous to the previous subsections, I can define the closed-loop "relative approximation error" of SL as the square root of the mean squared error between the output of the nonlinearity in Fig. 5.1a and its SL in Fig. 5.1b, normalized by the actuator input variance:

$$\varepsilon_3 := \sqrt{\frac{E\left[\left(\operatorname{sat}_\alpha^\beta(u) - N\hat{u}_0 - M\right)^2\right]}{\sigma_{\hat{u}}^2}} \tag{5.9}$$

I choose to normalize by the variance of the actuator input $\hat{u}(t)$ from the stochastically linearized system as opposed to the nonlinear system since its value is readily available in terms of system parameters, whereas the PDF of the $u(t)$ in the nonlinear system is not readily available. I now proceed to show that this closed-loop relative approximation error is bounded above, leveraging the results from the previous subsections. First, through the algebraic manipulations shown below, it can be observed

that the closed-loop RMSE satisfies:

$$\sqrt{E\left[\left(\mathrm{sat}_{\alpha}^{\beta}(u) - N\hat{u}_0 - M\right)^2\right]}$$

$$= \sqrt{E\left[\left(\left\{\mathrm{sat}_{\alpha}^{\beta}(u) - \mathrm{sat}_{\alpha}^{\beta}(\hat{u})\right\} + \left\{\mathrm{sat}_{\alpha}^{\beta}(\hat{u}) - N\hat{u}_0 - M\right\}\right)^2\right]}$$

$$\leq \sqrt{E\left[\left\{\mathrm{sat}_{\alpha}^{\beta}(u) - \mathrm{sat}_{\alpha}^{\beta}(\hat{u})\right\}^2\right]} + \sqrt{E\left[\left\{\mathrm{sat}_{\alpha}^{\beta}(\hat{u}) - N\hat{u}_0 - M\right\}^2\right]} \tag{5.10}$$

by Minkowski inequality [168]. The last line of (5.10) is profound, as it prominently delineates the breakup of the closed-loop approximation error into two components: the first represents the error due to the Gaussianity assumption on the input to the nonlinearity in the closed-loop setting (i.e., $\hat{u}$ in Fig. 5.1b is equal to u in Fig. 5.1a), while the second represents the open-loop approximation error due to the SL of the nonlinearity itself. I now further simplify the right hand side as follows. Since $\alpha \leq \mathrm{sat}_{\alpha}^{\beta}(u) \leq \beta$ and $\alpha \leq \mathrm{sat}_{\alpha}^{\beta}(\hat{u}) \leq \beta$, $\left|\mathrm{sat}_{\alpha}^{\beta}(u) - \mathrm{sat}_{\alpha}^{\beta}(\hat{u})\right| \leq \beta - \alpha$. Hence,

$$\sqrt{E\left[\left\{\mathrm{sat}_{\alpha}^{\beta}(u) - \mathrm{sat}_{\alpha}^{\beta}(\hat{u})\right\}^2\right]} \leq \beta - \alpha \tag{5.11}$$

Dividing (5.10) by $\sigma_{\hat{u}}$ and using (5.11) and (5.7), I obtain:

$$\varepsilon_3 \leq \sqrt{2}\,(U - L) + \varepsilon_2 \tag{5.12}$$

Thus, the closed-loop relative approximation error ε_3 is found to be bounded above by the sum of the open-loop relative approximation error, ε_2 (in the symmetric case, $\varepsilon_2 = \varepsilon_1$), and a term that depends on the difference of the saturation factors. Since ε_3 depends directly on ε_2, for the same value of $\sigma_{\hat{u}}$, a smaller value of ε_2 leads to a smaller

upper bound for ε_3. In other words, if the open-loop relative accuracy is good, so will the closed-loop relative accuracy. The open-loop relative approximation error ε_2 has already been shown to be bounded above in previous subsections, while the term $\sqrt{2}(U - L)$ provides a bound on the closed-loop relative approximation error due to the Gaussianity assumption on u. Moreover, as $\sigma_{\hat{u}}$ becomes larger, or the saturation authorities become more restrictive, the upper bound of the relative approximation error in closed-loop approaches that in the open-loop case.

In summary, the analyses in the preceding subsections show that SL of a saturation nonlinearity can produce relative mean squared errors less than 30.1% in the actuator output but relative accuracy improves with a smaller variance in the input. Equations (5.6) and (5.8) provide a way to analytically determine the statistics of the actuator input that leads to the largest open-loop mean squared error for a given actuator authority. Finally, it is shown that open-loop relative accuracy being bounded above also results in the closed-loop accuracy being bounded above by a value that is dependent on the saturation authority and the actuator input. This information can be used to design controllers that take into account the possible error in the closed-loop case, for example, involving a robust optimization problem whose solution is robust to linearization error. This is a topic of future research.

5.3 Computation of Stochastic Linearization

I investigate the computation of SL coefficients in this section. As mentioned in Section 5.1, the SL Equations (5.3) and (5.4) are transcendental and, hence, only

numerically solvable. For practical considerations, it is important to employ numerical solvers that can solve them as quickly and efficiently as possible. In this section, some common numerical algorithms are compared for the number of function evaluations until convergence. Since analytic solutions are not possible, I rely on Monte Carlo simulations (similar to [110, 145]) to carry out this investigation.

Only symmetric systems are considered in this section since asymmetric systems give rise to unique computational challenges and results. They are analyzed separately in Section 5.5. Specifically,

- The case of asymmetric saturation requires solving a set of *two* simultaneous equations, and is thereby more complicated, whereas the case of symmetric saturation requires solving only *one* equation.

- When the equation-solving (i.e., root finding) algorithms are applied to the asymmetric case (Section 6.2), most of the systems require many "extra tries" (see below), indicating that this case is not numerically robust. This prompts the coordinate transformation in Section 6.3 so that the number of extra tries required is lowered.

5.3.1 ALGORITHMS EXAMINED

The numerical algorithms that are considered, both in this section and the next for the asymmetric case, are briefly described below:

Bisection Method: The bisection method [169, 170] finds a root of an equation (or a system of equations) by reducing the search interval in half in an iterative manner, based on the function values at the endpoints of the interval. Since the

quasilinear gain $N \in [0,1]$, this algorithm naturally has a bounded initial search interval and can be applied to find SL of symmetric systems. However, the bisection algorithm cannot be applied to the case of asymmetric systems because $\mu_{\hat{u}}$ does not belong to a compact set, which means that the initial search space is unknown. The QLC literature has historically been using this method to solve SL equations [89].

Newton-Raphson Method: The Newton-Raphson method is an iterative algorithm that uses the gradient of the function to choose a step direction for the next iteration, with the weight of this direction decided by the functional value at that point [171]. This algorithm works for any sized system of equations, making it applicable for both symmetric and asymmetric cases. The downsides are that the gradient must be available for computation at every iteration and that convergence is guaranteed only when the initial guess is sufficiently close to the solution.

Broyden's Method: This is a quasi-Newton method that uses the same procedure as the Newton-Raphson method, but with the gradient being approximated by the slope of the line segment between the current and previous guesses [172]. Therefore, it typically has a lower computational overhead as compared with Newton-Raphson, since it does not need to evaluate the gradient explicitly, nor must it evaluate the system of functions more than once at each iteration.

Trust-Region Reflective Method: This method is similar to the Newton-Raphson Method but is more robust in situations where the gradient is singular, or the initial guess is far from the solution. It involves solving a quadratic program around the current best solution (i.e, around a *trust region*) to determine the next step. It is used for solving an unconstrained optimization problem [173]. This algorithm is used by default in MATLAB's `lsqnonlin`. Recall that a root-finding

problem $g(x) = 0$ for a vector function $g : \mathbb{R}^n \rightarrow \mathbb{R}^n$ can be posed equivalently as an unconstrained optimization problem of minimizing $\sum_{i=1}^{n} g_i(x)^2$, where $g_i(x)$ is the ith component of $g(x)$ [174]. Hence, this algorithm is applied by reformulating the SL root-finding problem as an unconstrained minimization problem and solving the resulting optimization problem using this algorithm. Note that other trust-region techniques can be used as well. For example, the Trust Region Dogleg is a similar algorithm used for solving equations [157]. However, since in our studies, the results obtained with the Trust Region Dogleg algorithm were similar to that obtained using the Trust Region Reflective method, I have omitted the former.

Fixed Point Iteration: This method leverages the fact that for a contractive function with a fixed point, repeated function evaluations can be used to converge to the fixed point [175]. Specifically, given the fixed point problem $x = g(x)$, where g a contraction, the following iterative procedure can be used to find the solution: $x_{n+1} = g(x_n)$ starting from any initial guess.

5.3.2   Problem Setup

Systems of the form shown in Fig. 5.1a were chosen for the Monte Carlo study, with only the symmetric cases being considered (for now). A random controller $C(s)$ and plant $P(s)$ were generated for each system, along with random saturation authorities (keeping $\alpha = -\beta$) and reference standard deviation σ_r (with $\mu_r = 0$). To incorporate a variety of situations, three combinations of plant and controller classes were considered: 1) a constant controller with a first-order plant (5.13), 2) a first-order controller with a first-order plant (5.14), and 3) a constant controller with a

Table 5.1: Parameter Ranges used For Random System Generation

Parameter	Value Range
Controller Gain, K_c	$(0, 50)$
Plant Gain, K_p	$(0, 5)$
Saturation Boundary, β	$(0, 10)$
1st Order Controller Time Constant, τ_c	$(0.01, 100)$
1st order Plant Time Constant, τ_p	$(0.01, 100)$
2nd order Plant Natural Frequency, ω_p	$(0.01, 100)$
2nd order Plant Damping Factor, ζ_p	$(0, 2)$
Reference Signal Standard Deviation, σ_r	$(0, 5)$

second-order plant (5.15).

$$C(s) = K_C, \quad P(s) = \frac{K_P}{\tau_P s + 1} \tag{5.13}$$

$$C(s) = \frac{K_C}{\tau_C s + 1}, \quad P(s) = \frac{K_P}{\tau_P s + 1} \tag{5.14}$$

$$C(s) = K_C, \quad P(s) = \frac{K_P \omega_p^2}{s^2 + 2\zeta_p \omega_p s + \omega_p^2} \tag{5.15}$$

Table 5.1 lists the sampling ranges for all these parameters. They were chosen such that the distribution of the quasilinear gain N was more-or-less equally skewed towards both $N = 0$ and $N = 1$, fairly representing systems ranging from both highly nonlinear to fully linear systems. For example, it was observed through a Monte Carlo simulation that values of $\beta = -\alpha < 5$ result in N being more closer to 0 and $\beta = -\alpha > 15$ result in N being more closer to 1. All parameters were sampled uniformly, except for the first-order time constants and the second-order natural frequency, which were sampled logarithmically. To obtain data from a large number of systems, each class of system was sampled 10,000 times; thus a total of 30,000 systems were considered. For each system, (5.3) was solved for the unknown, N (note that (5.4) is not required to be solved since the saturation is assumed to

be symmetric), with a relative convergence tolerance of 1×10^{-8} on the unknown variable, i.e., $(|N_2 - N_1|)/(1 + |N_1|) < 1 \times 10^{-8}$, where N_2 is the value of N at the current iteration and N_1 that at the previous iteration. Systems with phase margin (which is a metric used to quantify the stability and robustness of a control system), PM $< 40°$ were rejected, as they are not indicative of a well-designed control system (see Remark 1 in the next subsection). For algorithms that require the gradient (i.e., the Newton-Raphson and Trust-Region Reflective methods), the gradient was provided by finite differencing. This was done by small perturbations, unlike the finite differencing performed in the Broyden method. For all the algorithms, the numbers of function evaluations (including Jacobian evaluations) were collected. The number of iterations was capped to 400, and if an algorithm was unable to find a solution with a given initial condition, it was allowed to retry with a different random initial condition. The number of such "retries" was capped to 100; if an algorithm failed even after 100 tries, that system was considered a "failure" for the algorithm (since the algorithm would effectively be unusable for practical purposes if it requires many number of tries).

5.3.3 RESULTS

The Monte Carlo experiment revealed that the SL equation for symmetric feedback systems is, in fact, a contraction map (for all randomly generated systems). This is an important and profound discovery into the nature of the SL equations and paves the way for future research into the topological and algebraic properties of this equation. Also, it highlights that the fixed-point iteration can be successfully employed to solve the SL equation.

(a) Box Plot of Function Evaluations (b) Systems requiring extra tries
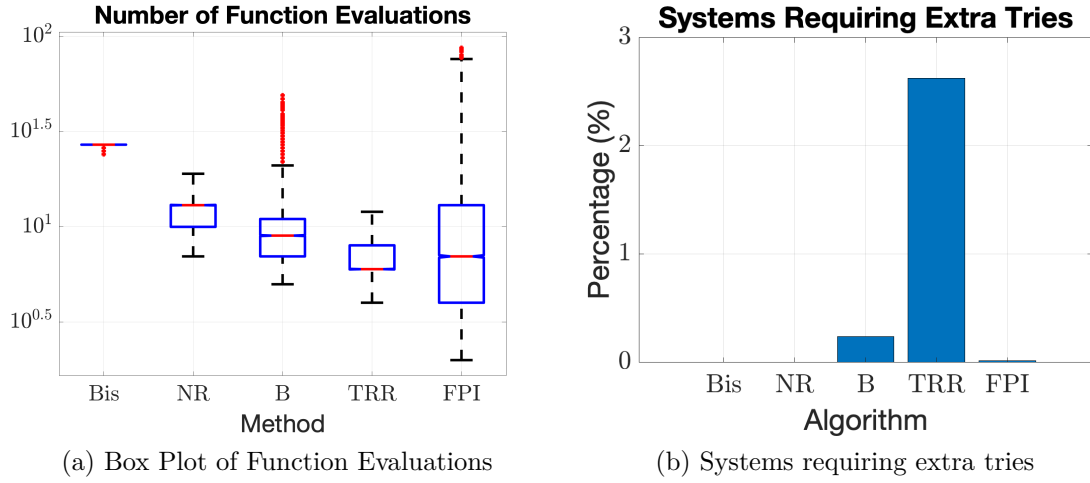
Figure 5.3: Computation of SL

The results from the Monte-Carlo simulation are illustrated in Figs. 5.3a and 5.3b. Fig. 5.3a shows a box plot of the number of function evaluations for different algorithms and Fig. 5.3b shows the number of systems that required extra tries to converge to a solution. All algorithms eventually found the solution, i.e., there were no "failures". From 5.3b, it can be seen that less than 3% of the systems required extra tries. In the x-axis of Fig. 5.3a, "Bis" stands for bisection, "NR" for Newton-Raphson, "TRR" for Trust-Region Reflective, and "FPI" for Fixed Point Iteration. On each box, the central mark indicates the median, and the bottom and top edges of the box indicate the 25th and 75th percentiles, respectively. The whiskers extend to the most extreme data points not considered outliers, and the outliers are plotted individually using the red '∘' symbol. Any data point that is greater than $x + 1.5y$ or less than $x - 1.5y$ is considered an outlier, where x is the median and y the inter-quartile range. From Fig. 5.3a, it can be seen that the bisection algorithm (which is commonly used in the QLC literature) performs significantly worse than all of the other algorithms on average, with mean iterations being more than two times greater
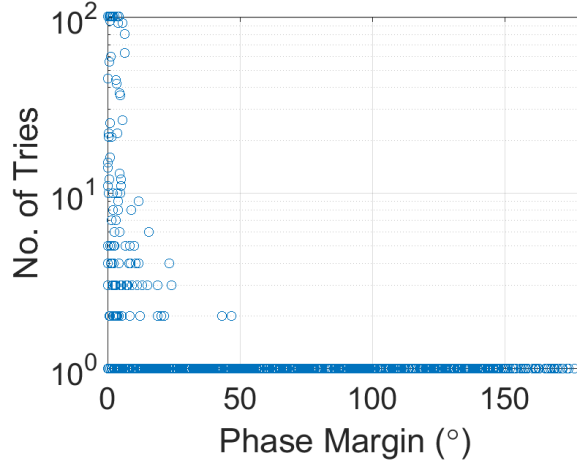
Figure 5.4: Number of Tries for Fixed Point Iteration Method

than those of others, although it has the smallest spread. On average, the Trust-Region Reflective method requires the least number of function evaluations, followed closely by Fixed Point Iteration. However, the Fixed Point Iteration method has a bigger spread in the number of evaluations. This is because the gradients of the functions are close to one, although they are always contractions. From Fig. 5.3b, it can be seen that the Trust Region Reflective method requires more tries in some cases, whereas the Newton Raphson method does not, although both have almost the same spread in the number of function evaluations. I conclude that, if the goal is to ensure certainty of a solution, the Newton-Raphson method is the best, and if the goal is to ensure computational speed most of the time, the Trust Region Reflective is the best.

Remark 3. *In a separate study, I considered systems with PM < 40°. I found that, while none of the algorithms failed (i.e., required tries more than 100) for PM > 40°, in the case of PM < 40°, a few (about 0.3%) of the systems simulated failed to converge for Fixed Point Iteration, indicating that they may not be contraction maps.*

The number of tries for some systems increased for PM < 40°, as shown in Fig. 5.4, and more tries were required for those systems which have smaller phase margin.

5.4 ROBUSTNESS OF SL

Recall that the quasilinear gain N and bias M found by solving (5.3) and (5.4) depend on system components like the plant $P(s)$ and the controller $C(s)$, as well as on exogenous signal statistics like the mean and standard deviation of the reference, $r(t)$. This dependence on various parameters may render these SL coefficients sensitive to these parameters, which may be problematic. For example, in optimal control settings (e.g., the linear quadratic regulator or LQR [176]), the variance of the actuator input, σ_u^2 (or $\sigma_{\hat{u}}^2$ in the SL reformulation), is often penalized in the objective function of the optimal control problem. If the SL coefficients are highly sensitive to system parameters, it may render the optimal control problem numerically sensitive (or even inaccurate) to these parameters as well. Thus, the knowledge of these sensitivities can help to understand which parameters of the system must be estimated/measured more accurately for reliable computation of the quasilinear gain/bias and, hence, the optimal controller. To obtain sensitivity data for a large range of feedback systems, a Monte Carlo investigation was performed. This was done since an analytic investigation of comparative sensitivities is not possible due to the highly transcendental and nonlinear nature of the SL equations. Similar to the previous section, again, only symmetric systems are studied here, and asymmetric systems are separately investigated in Section 5.5. This is because in the case of robustness for asymmetric systems, the sensitivities to *both* the quasilinear gain N and bias term, m, need to be

considered rather than only N in the symmetric case. Also, since in the asymmetric case, the exogenous signals have a non-zero mean, the sensitivities of the *means* of the signals must be considered apart from only the *standard deviations,* as considered in this section. Finally, it is found in Section 6 that the sensitivities in the case of asymmetric saturation are, in general, larger.

5.4.1 Problem Setup

The same systems as in Section 6.2a were considered here for the Monte Carlo study. A 1% change in various system parameters was applied (representing, for example, typical numerical tolerance in the measurement or estimation of the parameters), the quasilinear gain N was re-calculated, and the change from the previous value recorded. Further, to investigate the effect of a change of N on the computation of the statistical properties of the various signals, the standard deviations of the tracking error, $\sigma_{\hat{e}}$, the actuator input, $\sigma_{\hat{u}}$, the actuator output, $\sigma_{\hat{v}}$, and the plant output, $\sigma_{\hat{y}}$, were recorded, both with the original value of N at the solution of the SL equations and with a 1% increase in that value of N.

5.4.2 Results

Fig. 5.5a shows a box plot of the percentage change in the solved quasilinear gain N, i.e., $|\Delta N/N| \times 100\%$, where ΔN refers to the change in N after *re-solving* the SL equations, for a 1% change in various system parameters, i.e., $|\Delta\theta/\theta| \times 100\% = 1\%$, where $\Delta\theta$ is a change in the system parameter θ.

I have removed cases where $N < 0.1$ since the percentage change metric (i.e.,

(a) Sensitivity of Quasilinear Gain to System Pa-
rameters

(b) Sensitivity of Signal Statistics to Quasilinear
Gain
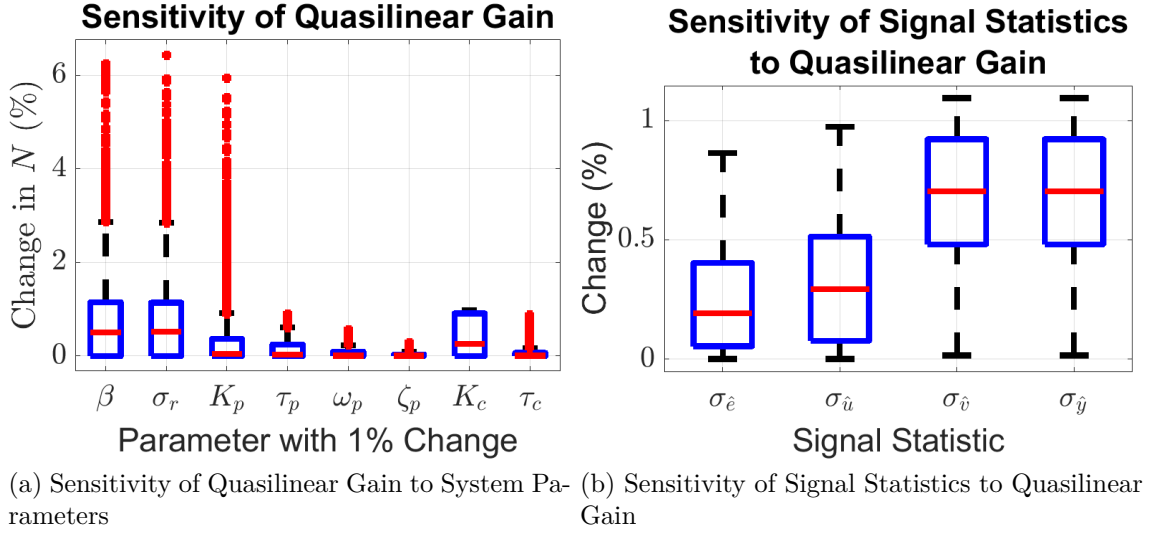
Figure 5.5: Sensitivity of SL Coefficients

$|\Delta N/N| \times 100\%$) does not convey useful information when the original value N is zero or close to zero (also, I am interested only in the *comparative* sensitivities of N to various parameters). From Fig. 5.5a, it can be seen that the overall change in N is less than 1% on average for all parameters (note that this is less than the 1% change introduced in the parameters). Also, while there is not much effect of the plant or controller dynamics (i.e., the time constant, damping factor, or natural frequency), there is a considerable effect of the reference standard deviation σ_r, actuator author-ity β, and the controller and plant gain on the quasilinear gain. This observation can be explained by the fact that these parameters directly affect the magnitude of the input to the saturation, or the bounds of saturation. The probability of saturation is therefore directly influenced by these parameters. Moreover, since β, σ_r, K_c, and τ_c are usually known, it is the plant gain K_p that needs to be accurately measured/es-timated. Knowing these sensitivities, one essentially also knows the level of potential variability in the quasilinear gain due to uncertainties in the model parameters. This

88

can further be leveraged in, for example, an optimization problem to design robust controllers, which is a topic for future work.

Fig. 5.5b shows the effect of a 1% change in N at the solution (i.e., $|\Delta N/N| \times 100 = 1\%$, where ΔN is a change *introduced* in the quasilinear gain N at the solution) on standard deviations of various signals (again, removing instances where the original value of the standard deviation is less than 0.1). That is, the y-axis of Fig. 5.5b shows $|\Delta\sigma_q/\sigma_q| \times 100\%$, where $\Delta\sigma_q$ refers to the change in the standard deviation of the particular signal q, σ_q, due to a 1% change in N. It can be observed that the standard deviations of the signals are affected by less than 1% on average (note that this is less than the 1% change introduced in the parameters). This indicates that even if the quasilinear gain is sensitive to system parameters, this will generally contribute even lesser to a change in the signal statistics. This is a useful property to have for an optimization problem that may involve such statistics for designing optimal controller gains.

Remark 4. *The trends for sensitivity for different parameters do not change for systems with PM $< 40°$, although it was noticed that for some systems the sensitivities were higher than in the case with PM$> 40°$.*

Remark 5. *The sensitivity of the open-loop approximation error* (5.6) *for the stochastically linearized system was found to be, in general, close to zero for all system parameters, except for the plant time constants, in which case, the sensitivity was higher.*

5.5 THE CASE OF ASYMMETRIC SATURATION

In this section, the investigation of robustness and computational efficiency of SL is continued for nonlinear stochastic systems with asymmetric saturation and a nonzero mean reference signal.

5.5.1 PROBLEM SETUP

For investigating the computation and robustness of SL in the following subsections, Monte Carlo studies were conducted on the same classes of systems that were generated in Section 6.2a, but with $\alpha \neq \beta$, α being generated uniformly from $(-10, 0)$. The reference mean μ_r was sampled uniformly from $(-5, 5)$. Both (5.3) and (5.4) were now solved for N and $\mu_{\hat{u}}$. For assessing computational performance, all algorithms mentioned in Section 5.3.1 were considered except the Bisection algorithm (as explained in Section 5.3.1). Moreover, in the case of Fixed Point Iteration, (5.4) was not used in the form shown since it is not a fixed point equation. Instead, $\mu_{\hat{u}}$ was replaced by $C_0(\mu_r - P_0 M)$ and $\sigma_{\hat{u}}$ by RHS of (5.1) in (5.3) and (5.4), and the resulting equations were instead solved for the fixed point (N, M). Systems in which $L > 0$ or $U < 0$ (where L and U are defined in (5.7)) were removed since, for a well-designed control system, it is expected that the nonlinear actuator will not be affected by signals whose values are outside the saturation bounds on *average*. Also, as before, systems with a phase margin of $< 40°$ were rejected, as they are not typically employed in practical settings.

5.5.2 Results for Computation of Stochastic Linearization

Fig. 5.6a shows the number of function evaluations required for convergence for different algorithms and Fig. 5.6b the number of systems that required extra tries, including failed systems (i.e., no. of tries > 400). It can be seen that the number of systems requiring extra tries significantly increased from the symmetric case (Fig. 5.3b). This is expected since the asymmetric case has a more complicated system of transcendental equations. Although from Fig. 5.6a, the number of function evaluations is found to be the least on average in the Fixed Point Iteration method (for systems where the method converged successfully), more than 95% of the systems failed (i.e., required tries more than 400) using this method, indicating that the RHS of (2.5) and (2.6) are not contractions for most systems. This is in contrast to the symmetric case, where the SL equation is a contraction for all systems. The Newton-Raphson method requires a comparatively lesser number of tries but the most number of function evaluations. Upon analyzing the cause of a large number of tries or failures in the Newton-Raphson method, it was found that in some iterations, the quasilinear gain was negative (as previously shown, N must satisfy $0 \leq N \leq 1$). Negative values of N are non-physical and are an artifact of the numerical solver. To remedy this, a co-ordinate transformation is proposed to prevent the solver from choosing non-physical values, as mentioned in the next subsection.

(a) Box Plot of Function Evaluations (b) Systems requiring extra tries
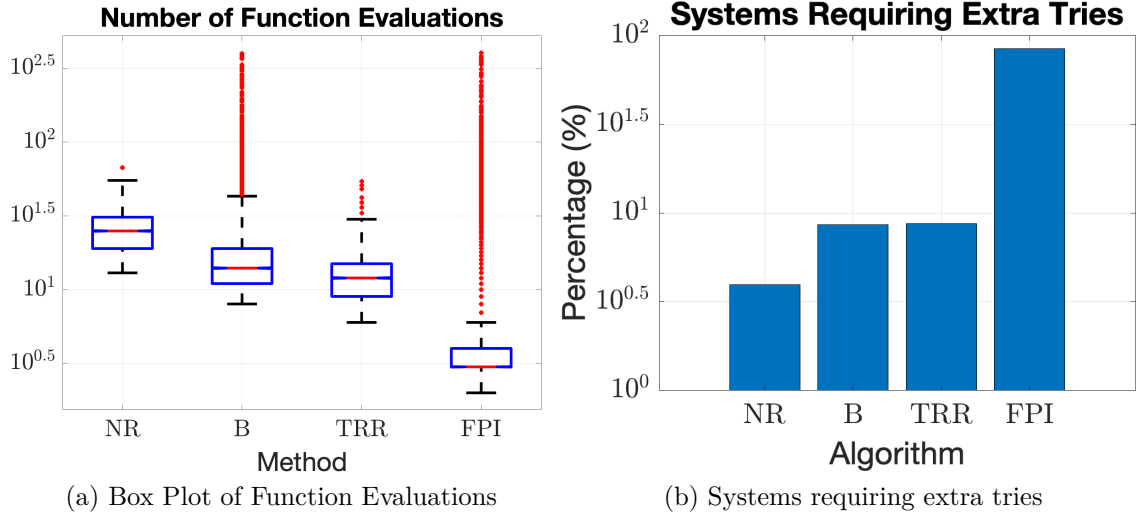
Figure 5.6: Computation of SL coefficients

5.5.3 Improving Computation through Coordinate Transformation

The idea of coordinate transformation is to allow solvers to have access to a larger space for variables than what is allowed in the base coordinate system, such that function evaluations do not result in undefined values. To ensure that the quasilinear gain N does not become negative in (5.3) and (5.4), $(N, \mu_{\hat{u}})$ can be transformed to a new coordinate system (N_t, M_t), which is defined through the following mapping: $N = f(N_t, M_t)$ and $\mu_{\hat{u}} = g(N_t, M_t)$, where f and g are transformations that satisfy these conditions: 1) f and g are bijective and differentiable such that the Jacobian of $\left[f\left(N_t, M_t\right) \ g\left(N_t, M_t\right) \right]^{\top}$ is invertible, 2) N_t and M_t can take all real values, and 3) The range of f is the interval $[0, 1]$, which is the range of allowable values for N in the case of SL for the saturation function. The first condition ensures that there is a one-one mapping between the coordinate systems and the function does not become

92

flat to avoid numerical issues. The second condition ensures that the solvers have access to an infinite space for the variables so that functional values do not become undefined.

Several forms of $f(N_t, M_t)$ are possible, including $f(N_t, M_t) = h(N_t)$, where $h(N_t)$ is one of the following (note that the function h is introduced, in addition to f, to simplify the discussion below, as I will show): $h(N_t) = 0.5 + \arctan(N_t)/\pi$, $h(N_t) = (1 + \text{erf}(N_t))/2$, and $h(N_t) = 1/(1 + e^{-N_t})$. However, as $N_t \to \pm\infty$, these functions $h(N_t)$ tend to 0 or 1 asymptotically, which may result in numerical issues if $N \approx 0$ or $N \approx 1$ as the function becomes flat at these extremes. Hence, the third requirement on f is modified to: the range of f is $[0 - \epsilon, 1 + \epsilon] \cap \mathcal{N}_s$, where $\epsilon \geq 0$ is a small number and $\mathcal{N}_s$ is the set of values of N that makes the closed-loop SL system stable (it can be verified that $\mathcal{N}_s = \{N : N > -1/P_0 C_0\}$ for the classes of systems considered in Section 6.2a, where P_0 and C_0 are the DC gains of the plant and controller respectively). For $\epsilon \neq 0$, this is essentially done by defining f such that $f(N_t, M_t) := h(N_t)(l - u) + l$, where $h(N_t)$ are as mentioned above, l represents the lower limit of $\mathcal{N}_s$, $\mathcal{N}_{s,\text{min}}$, and $u = 1 + \epsilon$. See Fig. 5.7a for graphs of these modified functions. For $g(N_t, M_t)$, possible functions are $g(N_t, M_t) = C_0(\mu_r - M_t P_0)$ (where M_t is actually M, as mentioned in Section 5.1), $g(N_t, M_t) = (C_0\mu_r - C_0 M_t P_0)/(1 + C_0 f(N_t)P_0)$ (where M_t is actually m) or $g(N_t, M_t) = M_t$ (when M_t is actually $\mu_{\hat{u}}$ and is not transformed).

In our investigation on the same systems considered in Section 5.5.2, it was found that out of all the above-mentioned combinations of the forms of $f(N_t, M_t)$ and $g(N_t, M_t)$, the forms of $f(N_t, M_t) = (0.5 + \tan^{-1}(N_t)/\pi)(l - u) + l$ and $g(N_t, M_t) = M_t$, with some $\epsilon > 0$, leads to the best results. The Monte Carlo experiment mentioned in

(a) Graphs of common $f(N_t)$ (b) Systems requiring extra tries
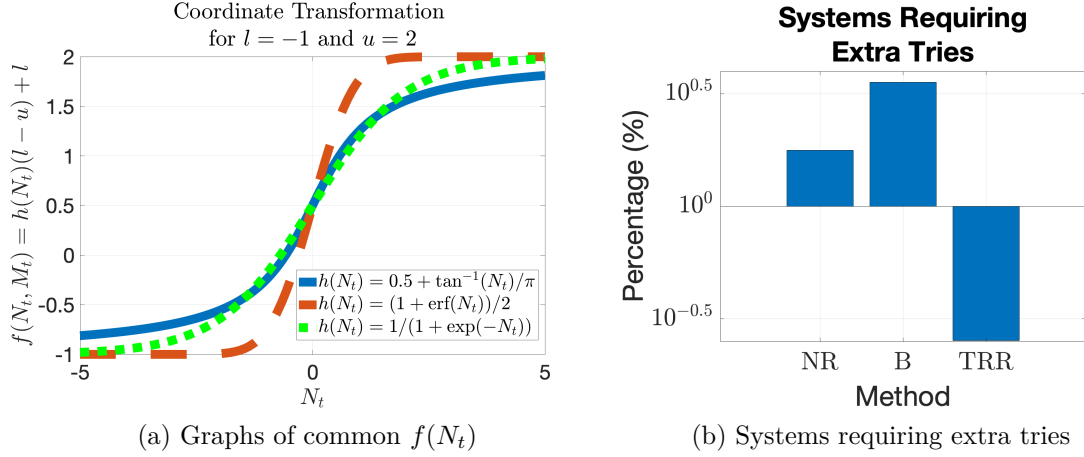
Figure 5.7: Coordinate Transformation for SL

Section 5.5.2 was performed again with these transformed coordinates for $\epsilon = 1$. The fixed point iteration method was not attempted again since the coordinate transformations destroy the contraction property. This is because the derivative of the inverse of arctan, erf and exp functions are greater than unity for the values of quasilinear gain considered. The results are shown in Fig. 5.7b. It can be seen that the number of systems requiring extra tries has reduced significantly for all methods (compared to Fig. 5.6b), with the lowest for the Trust-Region Reflective method. The number of function evaluations was similar on average.

Hence, for SL of asymmetric systems, it is our recommendation to use the transformations $f(N_t, M_t) = (0.5 + \tan^{-1}(N_t)/\pi)(l - u) + l$ and $g(N_t, M_t) = M_t$, with an $\epsilon \approx 1$, $u = 1 + \epsilon$, l as defined above, and the optimization-based Trust-Region Reflective method for quick convergence.

(a) Sensitivity of signal statistics to N

(b) Sensitivity of signal statistics to m

(c) Sensitivity of signal statistics to N and m.
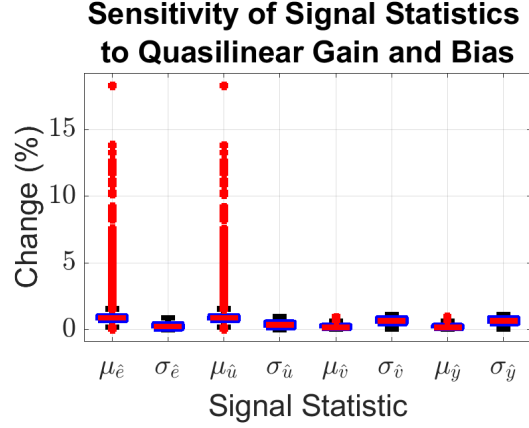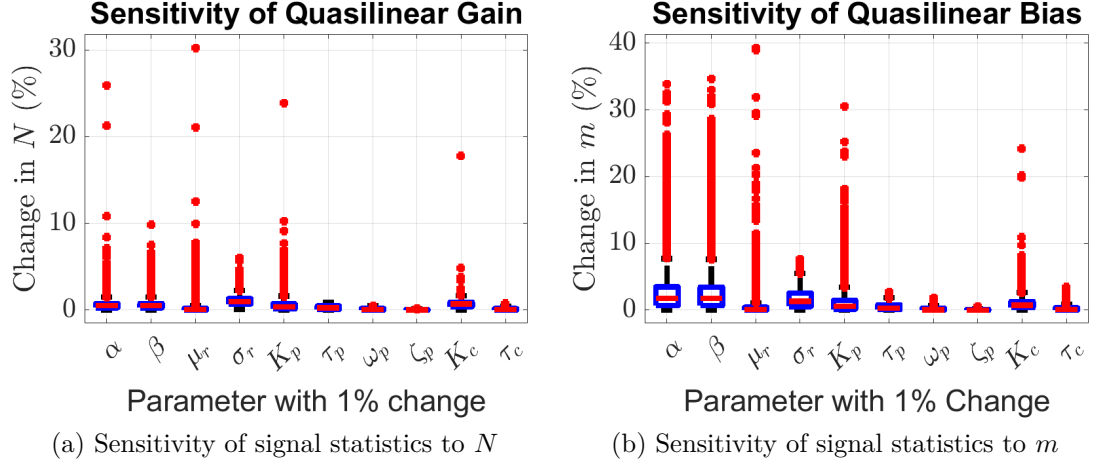
Figure 5.8: Sensitivity of SL coefficients

5.5.4 Results for Robustness Analysis

Recall that the procedure of SL in the case of asymmetric systems results in a value of N and $\mu_{\hat{u}}$ from (5.3) and (5.4). From the value of $\mu_{\hat{u}}$ found, both M and $m = M - N\mu_{\hat{u}}$ can be found (in fact, from any of $\mu_{\hat{u}}$, M and m, the other two can be found). Physically, $\mu_{\hat{u}}$ refers to the mean of the actuator input, M the mean of the actuator output, and m an external bias term that needs to be injected into the system as

shown in Fig. 5.1b. Since out of $\mu_{\hat{u}}$, M, and m, only m represents an external input, its value can be manipulated physically in a practical system, and hence, I performed the sensitivity analysis concerning N and m. The results for the sensitivity of the solved quasilinear gain N and $m = M - N\mu_{\hat{u}}$ to a 1% change in various system parameters (the definition of % change is the same as in Section 5.4.2) are shown in Figs. 5.8a and 5.8b respectively. The sensitivities of signal statistics (μ denoting the mean and σ the standard deviation of the signal) to a 1% change introduced in N and m at the solution are shown in Fig. 5.8c. As before, those cases are removed where the magnitude of the parameters whose sensitivities are being found are less than 0.1 since the percentage change metric does not reliably portray the change when the original value is close to zero. From Fig. 5.8a, it can be seen that compared to the symmetric case, the sensitivity has increased for many systems to more than 20%. Also, from both Figs. 5.8a and 5.8b it can be observed that while the sensitivities of N and m to system parameters are, on average, close to zero, there are many systems where the bias term m is highly sensitive to the system parameters. Again, as in the symmetric case, it is found that sensitivities are higher for those parameters that directly affect the magnitude of the actuator input and its saturation authority, e.g., the controller or plant gains, and the actuator authorities.

From Fig. 5.8c, it can be seen that while the sensitivities of the signal statistics to the computed N and m are, on average, low, although the sensitivity of the mean of the tracking error, $\hat{e}$, and of the actuator input, $\hat{u}$, is higher for many systems. This is due to the effect of feedback, and the fact that the magnitude of the mean of the error is typically small for a reference tracking problem. The results indicate that if an optimization problem uses the mean of the tracking error or the actuator

input in the objective function, then the numerical tolerance of the solver should be carefully chosen and the parameters of the system accurately identified to avoid sensitivity issues. Note that such issues do not arise if only the standard deviation of the error and that of the actuator input are used in the objective function, as done, for example, in a standard LQR problem. I have not found a clear correlation of the outliers with known system parameters, and that is a topic for future investigation.

Remark 6. *Similar to the symmetric case, the sensitivity of the open-loop approximation error* (5.8) *for the stochastically linearized system was found to be, in general, close to zero for all system parameters, except for the plant time constants, in which case, the sensitivity was higher.*

CHAPTER 6

OPTIMAL PRIMARY FREQUENCY CONTROL OF POWER SYSTEMS WITH GENERATOR SATURATION

In this chapter, SL is applied to the droop control of power systems with generator saturation. The organization of the chapter is as follows. In Section 6.1, the system model is described and the optimization problem formulated. The description of the QLC design procedure is given in Section 6.2. Section 6.3 illustrates the design process using numerical simulations.

6.1 Modeling and Problem Formulation

6.1.1 Primary Frequency Control in Power Systems

Consider a simple two-area power system, which appears in [1] and is shown in Fig. 6.1. This is a simplified model to represent the dominant behavior of a large, interconnected power system having many control zones. It consists of two single-bus systems Σ_1 and Σ_2, each characterized by six parameters and connected with a tie-line in between them. The block diagram of system Σ_i is shown in Fig. 6.2a. Here the parameter T_{ti} represents the effective time constant of the governor/turbine dynamics, and H_i the total inertia constant of the area, which is rated at the base power S_{bi}. The parameter D_{Li} models the motor loads and W_{0i} the frequency-dependent loads. Finally, the parameter S_i, also known as speed regulation or droop, determines the effective steady-state speed vs. load characteristic of the generating units. Modifying this parameter affects the proportional droop controller gain $^1/s_i$, thereby regulating the change in frequency from the nominal value of f_0. The block $\text{sat}_{\alpha_i}^{\beta_i}(u_i)$ models the saturating actuator and is explained in 6.1.2. Each individual control area Σ_i has effectively two inputs, the mechanical power set-point P_{m0i} and the effective change in load power P_{di}, which acts as a power disturbance. The change in frequency Δf_i is the controlled output. As shown in Fig. 6.1, any mismatch in frequency between the two areas gives rise (through the block modeled by the parameter $\hat{P}_t$ related to the tie-line reactance) to a power flow ΔP_{tie} between the two areas. This power, when combined with the local load power disturbance ΔP_{Li} and fed back as the effective
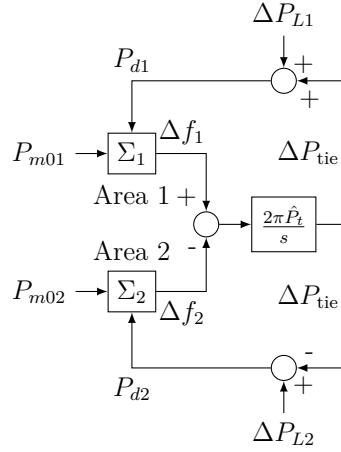
Figure 6.1: Block diagram of primary frequency control of a two-area interconnected power system

change in load power P_{di} to each area, regulates the frequency to a new steady state value, according to the following equations:

$$P_{d1} = \Delta P_{L1} + \Delta P_{\text{tie}} \quad \text{and} \quad P_{d2} = \Delta P_{L2} - \Delta P_{\text{tie}}$$

6.1.2   NONLINEARITY IN THE ACTUATOR

In the block diagram of Fig. 6.2a, it is assumed that the turbine output u_i, which is the change in mechanical power, is saturated by an asymmetric saturation nonlinearity, shown in Fig. 2.4. This situation can arise, for example, when the position of the gate or valve controlling the flow of steam into the turbine is restricted, resulting in specific power limits. The saturation is assumed to be asymmetric, with an upper bound $\beta_i > 0$ and a lower bound $\alpha_i < 0$, such that $|\alpha_i| > |\beta_i|$. This is a reasonable assumption since a turbine nominally produces mechanical power P_0 close to its designed capacity, $P_0 + \beta_i$. In the event of a frequency deviation, it can thus produce an output power
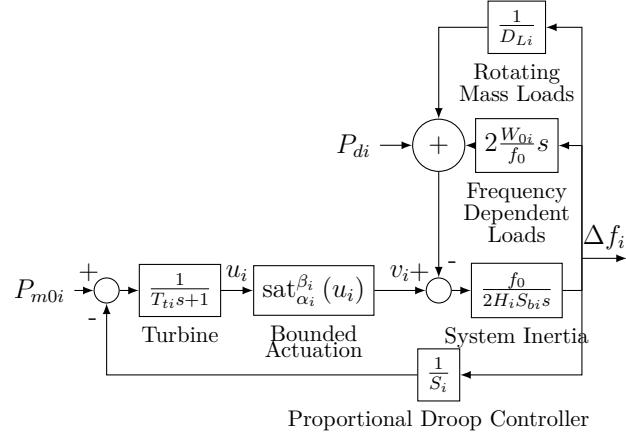
(a) Block diagram of each control area Σ_i
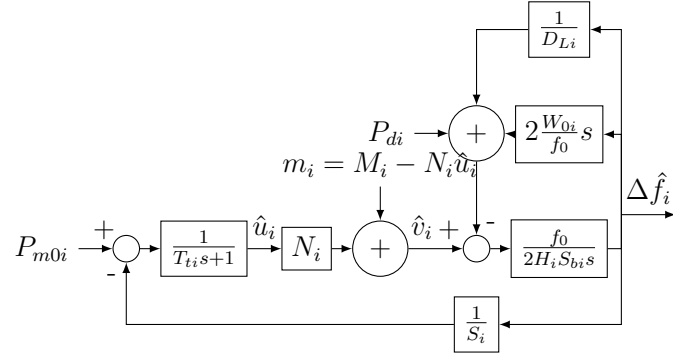
(b) Stochastically linearized system corresponding to Fig. 6.2a

Figure 6.2: Droop Control System

between $P_0 + \alpha_i < P_0$ and $P_0 + \beta_i > P_0$. Since this model is linearized around the nominal power P_0, the change in mechanical power output v_i of turbine is restricted between α_i and β_i, as modeled by the asymmetric saturation. Note that here, v_i does not refer to voltage, but I am using this notation to be consistent with earlier works in the literature of QLC.
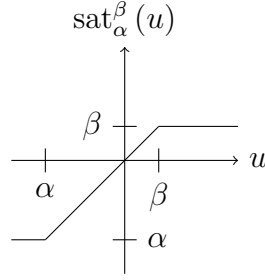
Figure 6.3: Asymmetric Saturation Nonlinearity

6.1.3 PROBLEM STATEMENT

The problem is to design optimal droop parameters S_1, S_2 that would improve the combined frequency and actuator input performance of the power system, compared to a baseline design, should any frequency deviation take place. This involves using stochastic linearization to find an equivalent quasilinear system, selecting a suitable cost function to minimize and then optimizing over an admissible region to find the optimal droop parameters. These are done in the sections to follow.

6.2 QLC BASED DROOP CONTROLLER DESIGN

In this section, the method of QLC is leveraged to design the optimal droop controller. It is appropriate to do so in this context since the load disturbance in power systems is stochastic in nature and QLC requires that all exogenous inputs to the system be random processes. The change in load power is thus first modeled accordingly. The nonlinear actuator block is then replaced by the corresponding stochastically linearized block for further analysis. The design process is explained below.

$$\mu_{Li}$$

$$w_i \rightarrow \boxed{F_{\Omega_d}\,(s)} \rightarrow \boxed{\sigma_{Li}} \rightarrow \left(+\right) \rightarrow \Delta P_{Li}$$

$$\|F_{\Omega_d}\,(s)\|_2 = 1$$
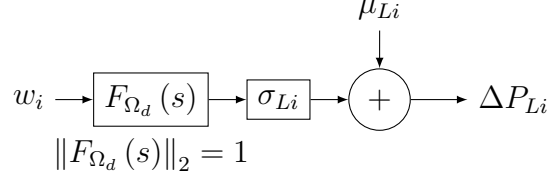
Figure 6.4: Modeling the change in load power

6.2.1   MODELING THE LOAD POWER DISTURBANCE

The change in load power ΔP_{L_i} in area i is modeled as a wide sense stationary Gaussian white noise with mean μ_{Li} and standard deviation σ_{Li}. The Gaussian distribution is a reasonable modeling assumption for a power system load disturbance having small temporal scales due to the central limit theorem and has been used in [111] to model wind farm power disturbance. Similar reasoning can be applied in solar applications. The noise ΔP_{L_i} is modeled as a standard white Gaussian noise w_i, as shown in Fig. 6.4, passed through a coloring filter $F_{\Omega_d}\,(s)$ of bandwidth Ω_d, multiplied by a gain σ_{Li}, and added to a bias μ_{Li}. To ensure a realistic disturbance signal, the filter bandwidth is chosen to equal the closed loop bandwidth of the control area for the system to be able to detect the change in load power. Also, by choosing the filter such that its H_2-norm equals unity, the final signal ΔP_{Li} is ensured to have mean μ_{Li} and standard deviation σ_{Li}.

6.2.2   STOCHASTIC LINEARIZATION OF THE NONLINEAR ACTUATOR

To analyze the system and determine the optimal droop parameters, the nonlinear actuator needs to be linearized. Leveraging the method of stochastic linearization, the

nonlinear system of area i described by Fig. 6.2a can be reduced using equations (2.2) and (2.3) to an equivalent linear system shown in Fig. 6.2b, where the nonlinearity $\text{sat}_{\alpha_i}^{\beta_i}$ has been replaced by an equivalent quasilinear gain N_i and a bias $m_i = M_i - N_i\mu_{\hat{u}_i}$ such that M_i is the quasilinear bias and $\mu_{\hat{u}_i}$ the mean of actuator input. Here,

$$N_i = \frac{1}{2}\left[\text{erf}\left(\frac{\beta_i - \mu_{\hat{u}_i}}{\sqrt{2}\sigma_{\hat{u}_i}}\right) - \text{erf}\left(\frac{\alpha_i - \mu_{\hat{u}_i}}{\sqrt{2}\sigma_{\hat{u}_i}}\right)\right] \tag{6.1}$$

and

$$M_i = \frac{\alpha_i + \beta_i}{2} + \frac{\mu_{\hat{u}_i} - \beta_i}{2}\text{erf}\left(\frac{\beta_i - \mu_{\hat{u}_i}}{\sqrt{2}\sigma_{\hat{u}_i}}\right)$$

$$-\frac{\mu_{\hat{u}_i} - \alpha_i}{2}\text{erf}\left(\frac{\alpha_i - \mu_{\hat{u}_i}}{\sqrt{2}\sigma_{\hat{u}_i}}\right) - \frac{\sigma_{\hat{u}_i}}{\sqrt{2\pi}}\left\{\exp\left[-\left(\frac{\beta_i - \mu_{\hat{u}_i}}{\sqrt{2}\sigma_{\hat{u}_i}}\right)^2\right]\right.$$

$$\left. - \exp\left[-\left(\frac{\alpha_i - \mu_{\hat{u}_i}}{\sqrt{2}\sigma_{\hat{u}_i}}\right)^2\right]\right\} \tag{6.2}$$

where $\sigma_{\hat{u}_i}$ is the standard deviation of $\hat{u}_i$, $\hat{u}_i$ is the actuator input in the stochastically linearized system, and

$$\text{erf}(x) = \frac{2}{\sqrt{\pi}}\int_0^x e^{-t^2}dt$$

is the error function. Recall that α_i and β_i are the generator saturation limits in area i. For more details, please refer to [89, 111].

As seen from equations (6.1) and (6.2), calculation of N_1, N_2, M_1 and M_2 requires knowledge of $\mu_{\hat{u}_1}$, $\mu_{\hat{u}_2}$, $\sigma_{\hat{u}_1}$ and $\sigma_{\hat{u}_2}$. Since the system is interconnected, these values depend on each other. For the sake of illustration, I assume that the disturbance in load power takes place only in the first area, i.e., $\Delta P_{L2} = 0$. Considering that the system is operating in the stationary regime, the values of $\sigma_{\hat{u}_1}$ and $\sigma_{\hat{u}_2}$ can be found using the transfer function $T_1(s)$ from the change in load power ΔP_{L1} to the actuator

input $\hat{u}_1$:

$$\sigma_{\hat{u}_1} = \|F_{\Omega_d}(s) T_1(s)\|_2 \sigma_{L1} = f_1(N_1, N_2, S_1, S_2) \tag{6.3}$$

where $\| \cdot \|_2$ is the H_2-norm. Similarly, using the transfer function $T_2(s)$ from the change in load power ΔP_{L1} to the second actuator input $\hat{u}_2$:

$$\sigma_{\hat{u}_2} = \|F_{\Omega_d}(s) T_2(s)\|_2 \sigma_{L1} = f_2(N_1, N_2, S_1, S_2) \tag{6.4}$$

The values of $\mu_{\hat{u}_1}$ and $\mu_{\hat{u}_2}$ can be found by first finding the transfer functions from P_{m01}, P_{m02}, μ_{L1}, m_1 and m_2 to $\hat{u}_1$ and $\hat{u}_2$ and then evaluating the DC gains, which leads to:

$$\mu_{\hat{u}_1} = P_{m01} + \frac{L}{S_1} = f_3(M_1, M_2, S_1) \tag{6.5}$$

$$\mu_{\hat{u}_2} = P_{m02} + \frac{L}{S_2} = f_4(M_1, M_2, S_2) \tag{6.6}$$

where:

$$L = \frac{D_{L1}D_{L2}}{D_{L1} + D_{L2}} (\mu_{L1} - M_1 - M_2) \tag{6.7}$$

The values of N_1, N_2, M_1 and M_2 can thus be found by substituting (7.3)-(7.4) into (6.1) and (6.2), which results in a system of four transcendental equations in the four unknowns N_1, N_2, M_1 and M_2. MATLAB's `fsolve` command provides a convenient way to solve this numerically.

6.2.3   Selection of Suitable Cost Function

To find an optimal controller, a suitable cost function is required. It is desirable to have small change in frequency and low actuator input. Several possible objective

functions were plotted as a function of the droop parameters S_1 and S_2, which are the optimization variables. In each case, actuator saturation was neglected, as it mainly serves to impose constraints and does not change the nature or shape of the cost function. Also, no change in load power of area 2 was assumed, i.e., $\Delta P_{L2} = 0$.

An objective function defined as the sum of variances of frequency deviations in the two areas, i.e., $\sigma_{\Delta \hat{f}_1}^2 + \sigma_{\Delta \hat{f}_2}^2$, results in a surface shown in Fig. 6.5. Note that $\Delta \hat{f}_i$ are the outputs of the stochastically linearized system shown in Fig. 6.2b. For plotting this surface, the values of $\sigma_{\Delta \hat{f}_1}$ and $\sigma_{\Delta \hat{f}_2}$ were calculated using the following equations, similar to equations (7.3) and (6.4):

$$\sigma_{\Delta \hat{f}_1} = \|F_{\Omega_d}(s) T_3(s)\|_2 \sigma_{L1}$$

$$\sigma_{\Delta \hat{f}_2} = \|F_{\Omega_d}(s) T_4(s)\|_2 \sigma_{L1}$$

where $T_3(s)$ and $T_4(s)$ are the transfer functions from ΔP_{L1} to $\Delta \hat{f}_1$ and $\Delta \hat{f}_2$ respectively.

The surface has an infimum at zero, leading to infinite gain in the proportional controller, as the control action is not penalized. A surface similar to that of Fig. 6.5 results when the objective function is defined as the sum of variances of frequency deviations: $\Delta \hat{f}_1$ and $\Delta \hat{f}_1$, and also the variances of rate of change of frequency (RO-COF): $\frac{d}{dt}\left(\Delta \hat{f}_1\right)$ and $\frac{d}{dt}\left(\Delta \hat{f}_2\right)$. Unlike the surface in Fig. 6.5, the surface shown in Fig. 6.6, which is generated using the objective function defined as the sum of variances of changes in frequency and lowly penalized variances of actuator inputs, is more suitable for implementation. This is because the surface has a specific minimum leading to a finite controller gain unlike the other. Hence, this surface is chosen for

formulating the optimization problem, as explained in the following subsection. This is also consistent with standard practice in optimal control, for example in designing a linear quadratic regulator (LQR), which optimizes the combined state and control costs for a system.

6.2.4   Optimization Problem

Using the surface explained in the previous subsection, the optimization problem is formulated as:

$$\min_{S_1,S_2} \sigma^2_{\Delta \hat{f}_1} + \sigma^2_{\Delta \hat{f}_2} + \rho \left(\sigma^2_{\hat{u}_1} + \sigma^2_{\hat{u}_2} \right)$$

$$\text{subject to (6.1)–(6.6) and } S_1, S_2 > 0 \tag{6.8}$$

where $\rho > 0$ is a sufficiently small scalar. Since this problem is non-convex, with transcendental constraints (6.1) and (6.2), it cannot be solved analytically. However, it can be approached numerically, for example, using MATLAB's `lsqnonlin` command.

6.3   Performance Evaluation and Discussion of Results

To evaluate the performance of the designed optimal controller, the two-area power system in Fig. 6.1 was simulated for a sufficiently long time, first with droop parameters from the baseline design of [1], and then with the designed optimal QLC controller. The value of ρ for the optimization was 1.27×10^{-8}, which was selected
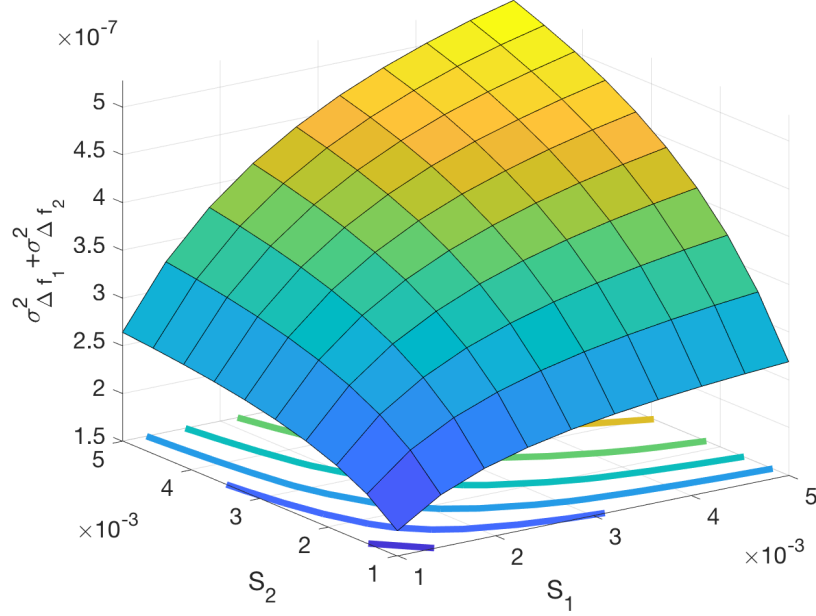
Figure 6.5: Surface contour plot of objective function $\sigma^2_{\Delta f_1} + \sigma^2_{\Delta f_2}$ neglecting actuator saturation. The surface can be seen to have an infimum at the origin.

by analyzing the Pareto optimal front discussed below. The system parameters of area 2 were chosen to equal those of area 1, as in Table 6.1, so that both areas were of the same size. In both cases, the load power change in area 1 was modeled as a zero-mean white Gaussian noise with a standard deviation of $\sigma_{L1} =$200 MW, passed through a 3rd-order Butterworth filter $F_{\Omega_d}(s)$, with bandwidth Ω_d chosen to be the same as the closed loop bandwidth of one of the power system areas (around 0.56 Hz):

$$F_{\Omega_d}(s) = \sqrt{\frac{3}{\Omega_d}} \left(\frac{\Omega_d^3}{s^3 + 2\Omega_d s^2 + 2\Omega_d^2 s + \Omega_d^3} \right), \Omega_d = 0.56 \text{ Hz} \tag{6.9}$$

For illustration, the load power change in the second area was assumed to be zero. For both areas, the value of α was chosen to be -100 MW and $\beta = 5$ MW, so that the saturation is asymmetric as explained in Section 6.1.2.
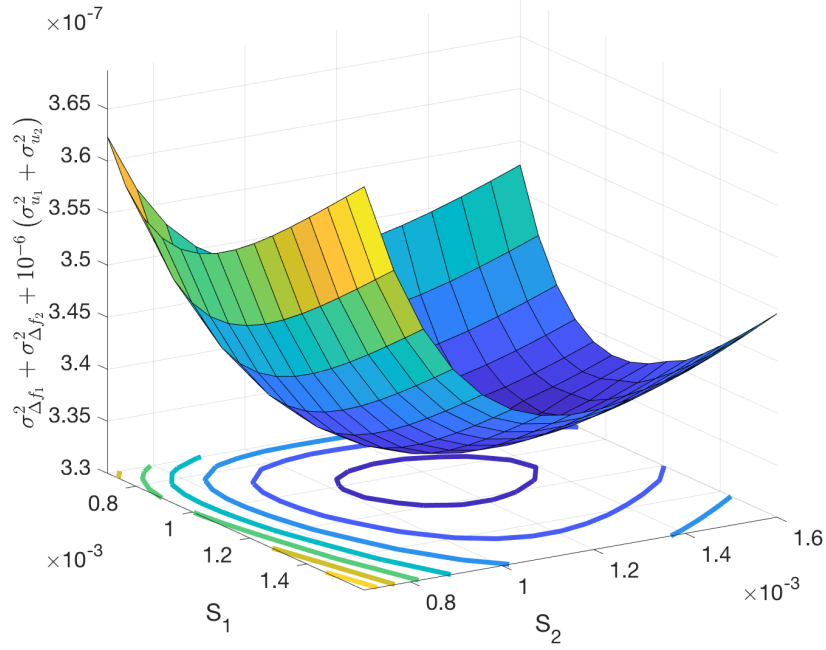
Figure 6.6: Surface contour plot of objective function $\sigma^2_{\Delta f_1} + \sigma^2_{\Delta f_2} + 10^{-6} \left(\sigma^2_{u_1} + \sigma^2_{u_2} \right)$ ne-glecting actuator saturation. The non-zero minimum of this surface allows for the design of a finite controller gain compared to the surface of Fig. 6.5.

The numerical optimization required trying several initial conditions before con-verging to the global minimum. The results, tabulated in Table 6.2, show that the optimal droop parameters reduced the objective function from 0.0197 to 0.0164, i.e., by 17%, compared to the baseline design. Note that the optimization results in an increase in S_2 (i.e., a decrease in $\frac{1}{S_2}$), which is reasonable, since the disturbance does not dynamically affect the second area as much as it does the first area. Although the sum of variances of changes in frequency (i.e., the state cost) increased by 4% from 0.0152 to 0.0158, the control effort reduced by 88% from 34.74×10^4 to 4.05×10^4. Hence, this optimal controller achieves a minimal combined state and control cost at the expense of a slight increase in state cost.

Table 6.1: Parameters and their values used for Simulation

Parameter	Value
$H_1 = H_2$	5 s
$S_{b1} = S_{b2}$	10 GW
f_0	50 Hz
$D_{l1} = D_{l2}$	$\frac{1}{200}$ Hz/MW
$W_{01} = W_{02}$	0 MW/Hz
$S_1 = S_2$	$\frac{1}{5000}$ Hz/MW
$\hat{P}_t$	533.33 MW

To demonstrate the trade-off between state and control costs, a Pareto optimal front was generated by varying the control penalty from $\rho = 10^{-10}$ to $\rho = 10^{-5}$, computing the quasilinear gains and biases for each ρ, and calculating the resulting costs using the QLC equations. The result is depicted by the curve in Fig. 6.7, where the optimal QLC gains are shown to produce a reduced combined cost compared to those in the baseline design of [1]. Note from Fig. 6.7 that, in contrast to the data above, the QLC equations predict a *reduction* in the state cost compared to the baseline design. This discrepancy is due to the inaccuracy of stochastic linearization for highly asymmetric systems [110], which will be a topic of future investigation. Nevertheless, at the optimum, the state cost of the nonlinear system is 0.0247, while that of the stochastically linearized version is 0.0231, indicating the high accuracy of stochastic linearization.

To illustrate the fact that QLC allows us to *systematically* redesign the controller upon parameter changes, I performed the following experiment. I assumed that σ_{L1} in the previous experiment increased from 200 MW to 300 MW due to, for example, increased renewable penetration. If the same QLC-based droop parameters are applied, the optimal value of the cost function increases from 0.0164 to 0.0481. This increase is reasonable, because a larger input forces the system to operate closer to its

Table 6.2: System Parameters Before and After Optimization

Parameter	Baseline	Optimal
S_1	0.00020	0.0006
S_2	0.00020	50.6705
N_1	0.0694	0.1979
N_2	1.0000	1.0000
M_1	-44.1950	-37.9331
M_2	0.0011	0.0000
$\sigma^2_{\Delta f_1} + \sigma^2_{\Delta f_2}$	0.0152	0.0158
$\sigma^2_{\Delta \hat{f}_1} + \sigma^2_{\Delta \hat{f}_2}$	0.0156	0.0160
$\sigma^2_{\Delta f_1} + \sigma^2_{\Delta f_2} + \rho\left(\sigma^2_{u_1} + \sigma^2_{u_2}\right)$	0.0197	0.0164
$\sigma^2_{\Delta \hat{f}_1} + \sigma^2_{\Delta \hat{f}_2} + \rho\left(\sigma^2_{\hat{u}_1} + \sigma^2_{\hat{u}_2}\right)$	0.0201	0.0166
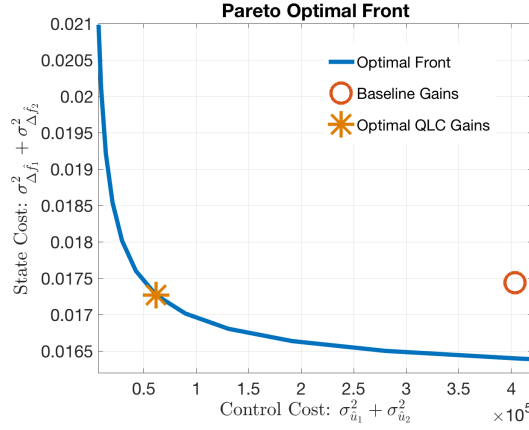
Figure 6.7: Pareto optimal front of cost function with ρ ranging logarithmically from 10^{-10} to 10^{-5}.

limits, which constrains achievable performance. However, if the droop parameters are re-designed with the new information on σ_{L1}, the value of the cost function is lowered to 0.0479, a decrease by 0.5%. Note that this decrease is small compared to that in the previous case, since the optimization is being performed on an already optimal QLC-based controller produced using $\sigma_{L1} = 200$ MW. This experiment illustrates the effectiveness of QLC in systematically redesigning controllers based on available information on system parameters, which can be found out experimentally.

Chapter 7

Optimal Control of Virtual Batteries using Stochastic Linearization

In this chapter, the optimal control of virtual batteries using stochastic linearization is described. The outline of this chapter is as follows. Section 7.1 describes the modeling of VBs and the optimization problem. Section 7.2 showcases the advantages of an SL-based optimization over a non-SL based optimization in improving VB usage while attaining the grid objective. In Section 7.3, analyses are provided to explore the effect of various parameters on the capabilities of this method. Finally, Section 7.4 extends the design to VBs with variable power limits.

7.1 Modeling and Problem Formulation

7.1.1 Virtual Battery Model

Aggregated distributed energy resources (DERs) can be modeled as a virtual battery (VB) (consistent with abstractions in [137, 177, 178]) with a saturation in power delivered, defined by the lower and upper power limits, $P_{\min}$ and $P_{\max}$, respectively. The VB is assumed to be operating at a nominal power set-point denoted by P_{set} (which can be computed, for example, optimally at a slower time-scale, as described in [142]). The input and output of the VB are related by the following transfer function:

$$\frac{P_u(s)}{P_{\text{in}}(s)} = \frac{e^{-T_d s}}{\tau s + 1} \tag{7.1}$$

where $P_u(s)$ is the Laplace transform of the unsaturated output of the VB, $p_u(t)$, and $P_{\text{in}}(s)$ that of the power desired (input) from the VB, $p_{\text{in}}(t)$, τ is a first-order lag, and T_d is a pure time delay.

The model of (7.1) is obtained by taking into account the following facts [142]: i) The DERs composing a VB turn on/off (possibly) sequentially, and power electronic components present inside each VB, both contribute to a net lag τ; ii) There are communication delays (generally of the order of 200 ms) between the head node of the feeder and each VB [132, 179], and delays associated with disaggregating the control signal into device-level signals [180]. The delays I consider in the VB model (T_d) are of both these types lumped together.

Defining $u(t) := P_u(t) - P_{\text{set}}$, the saturated output of the VB is then $P_b(t) =$
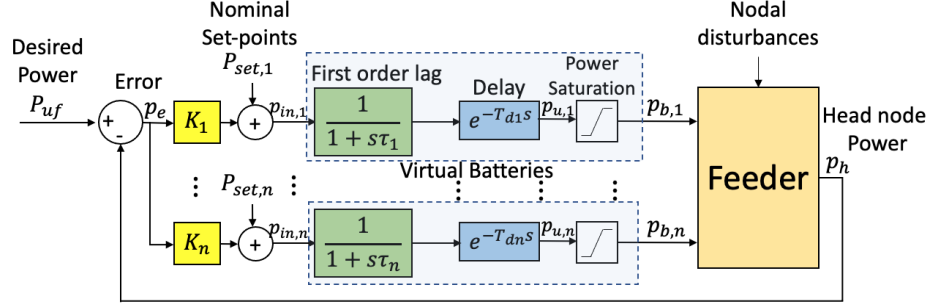
Figure 7.1: Nonlinear Feedback System
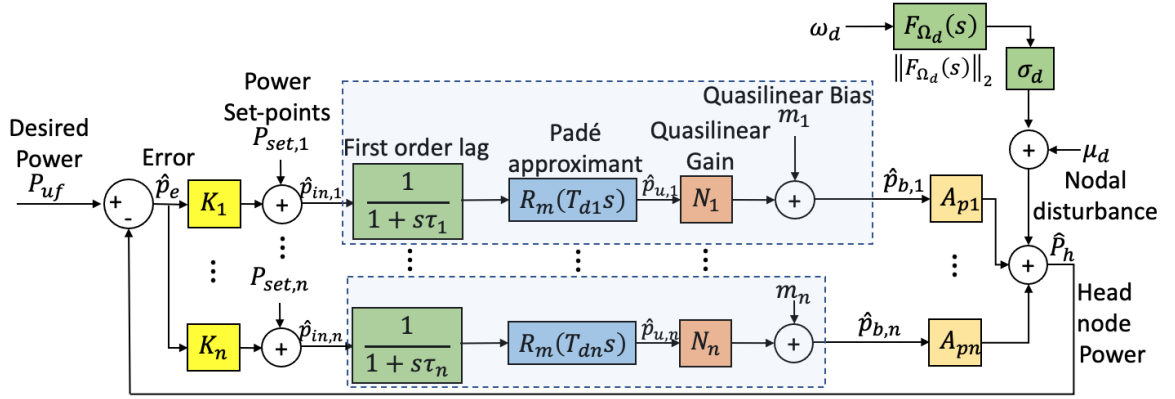
Figure 7.2: Stochastically Linearized System

$P_{\text{set}} + \text{sat}_\alpha^\beta(u(t))$, where $\alpha := P_{\min} - P_{\text{set}}$, $\beta := P_{\max} - P_{\text{set}}$, since the DC gains of the first-order transfer function and of the time delay are both unity, and $\text{sat}_\alpha^\beta(u)$ is as in (2.4).

7.1.2 PROBLEM SETUP

Consider a distribution feeder with sets of distributed energy resources (DERs) modeled by VBs (as in the previous subsection) located at its various nodes. The objective is to control the head node active power demand of the feeder, such that it tracks an economic reference by rejecting uncontrolled nodal disturbances, using available flexibility of the DERs. The control scheme is shown in Fig. 7.1, and is adapted

from [142]. It consists essentially of a bank of proportional controllers K_i that multiply the error between the head node power $p_h(t)$ of the feeder and a desired economic trajectory $P_{uf}(t)$ to control the ith VB with the model described in Section 7.1.1 (with suffix i added in all the parameters).

As described in [142, 146], the gains K_i in Fig. 7.1 can be designed optimally by first (Jacobian) linearizing the feeder at an operating point, depending on the nominal set-point $P_{\text{set},i}$ of the ith VB and the base load, neglecting the power saturation in the VBs (see Fig. 7.2, but with $N_i = 1$ and $m_i = 0$ - these will be defined later - essentially, this means locally linearizing all saturations and removing them from the analysis). This linearization leads to gains A_{pi}, which indicate the sensitivities of the head node active power of the feeder to the corresponding nodal active power injections. Next, a stationary Gaussian stochastic process is assumed as nodal disturbance (representing aggregate random fluctuations in solar PV over possibly a large geographic region [181]) with mean μ_d and standard deviation (SD) σ_d, and an mth order Padé approximation $R_m(T_{di}s)$ is assumed for the delay. The gains are then chosen by minimizing the sum of the variance of the tracking error, $\hat{p}_e(t)$, denoted by $\sigma_{\hat{p}_e}^2$, and a weighted sum of the variances of the control inputs to the VBs, $\hat{p}_{\text{in},i}(t)$, denoted by $\sigma_{\hat{p}_{\text{in},i}}^2$:

$$\text{minimize } \sigma_{\hat{p}_e}^2 + \rho \sum_{i=1}^{n} \sigma_{\hat{p}_{\text{in},i}}^2 \tag{7.2}$$

where the variances are computed using the $\mathcal{H}_2$-norm of the transfer functions from the standard white Gaussian noise $w_d(t)$ to $\hat{p}_e(t)$ and $\hat{p}_{\text{in},i}(t)$ (setting $\mu_d = 0$), and $\rho > 0$ is a constant chosen according to the power capacity of the VBs.

However, the optimization problem (7.2) does not include the saturation nonlinearities due to VB power limits. Note that while the nonlinear feeder can be linearized

with Jacobian linearization, the saturation nonlinearities in the VBs cannot. This is because the power flows in the nonlinear system due to nodal injections are close to that predicted by the linearized feeder and do not change their region of operation drastically. However, when VBs are nearly saturated, even a small disturbance can change the region of operation (by saturating), rendering a Jacobian linearization inaccurate. Moreover, although the control penalty ρ can be chosen to be inversely proportional to the power capacity of the VBs, as done in [142], it is difficult to choose it according to the saturation level of the VBs and is rather heuristic. Hence, the focus of this chapter is to overcome these problems by leveraging SL instead of Jacobian linearization to linearize the saturation functions. The method of SL provides a method to *systematically* include the saturation authorities and the saturation level (based on the operating point) of the VBs into the optimization problem. Also, it utilizes the statistical properties of the disturbance signal to linearize the system. In the next section, the procedure of SL is reviewed before using it to solve the above problem.

7.2 Optimal Controller Design for Virtual Batteries using Stochastic Linearization

7.2.1 Formulation using SL

Leveraging the method of SL, the nonlinear system in Fig. 7.1 can be approximated using (2.5)-(2.6) by an equivalent linear system shown in Fig. 7.2, where the saturation function for the ith VB, $\mathrm{sat}_{\alpha_i}^{\beta_i}(u_i)$, has been replaced by an equivalent quasilinear gain N_i and a bias $m_i = M_i - N_i \mu_{\hat{u}_i}$ such that M_i is the quasilinear bias and $\mu_{\hat{u}i}$ is the mean of the input to the saturation, $\hat{u}_i(t) = P_{\hat{u},i}(t) - P_{\mathrm{set},i}$.

As seen from (2.5)-(2.6), calculation of N_i, M_i requires knowledge of $\mu_{\hat{u}i}$, and $\sigma_{\hat{u}i}$, and hence, these variables depend on each other and all other system parameters. Considering that the system is operating in the stationary regime, the values of $\sigma_{\hat{u}i}$ can be found using the transfer function from the nodal disturbance $w_d(t)$ to $\hat{P}_{u,i}(t)$:

$$\sigma_{\hat{u}i} = \left\| \frac{F_{\Omega_d}(s) K_i \frac{1}{1+s\tau_i} R_m(T_{di}s)}{1 + \sum_{i=1}^{n} K_i \frac{1}{1+s\tau_i} R_m(T_{di}s) N_i A_{pi}} \right\|_2 \sigma_d \tag{7.3}$$

The values of $\mu_{\hat{u}_i}$ can be obtained by finding the transfer functions from μ_d, and m_i to $\hat{P}_{u,i}(t)$ and evaluating their DC gains, which leads to:

$$\mu_{\hat{u}i} = (P_{uf} - \mu_d - \sum_{j=1}^{n} M_j A_{pj}) K_i \tag{7.4}$$

117

where M_j are functions of $\mu_{\hat{u}i}$ and $\sigma_{\hat{u}i}$, obtained using (6.2).

The values of N_i, M_i can thus be found by substituting (7.3)-(7.4) into (2.5)-(2.6) for each N_i, M_i, $\sigma_{\hat{u}i}$ and $\mu_{\hat{u}_i}$, which results in a system of $2n$ transcendental equations in the unknowns N_i and M_i, for $i = 1, \ldots, n$. Note that compared to Jacobian linearization, which assumes $N_i = 1$, $m_i = 0$, SL provides $0 < N_i < 1$ and m_i not necessarily 0, such that the statistical properties of the signals in the linearized system and the nonlinear system match closely. Thus, SL-based optimization involves formulating the optimization problem described in (7.2) by *considering* the values of N_i, M_i (and thus $m_i = M_i - N_i\mu_{\hat{u}i}$) while evaluating $\sigma_{\hat{P}_e}$ and $\sigma_{\hat{P}_{\text{in},i}}$:

$$
\begin{aligned}
\text{minimize} \quad & \sigma_{\hat{P}_e}^2 + \rho \sum_{i=1}^{n} \sigma_{\hat{P}_{\text{in},i}}^2 \\
\text{subject to:} \quad & (7.3), (7.4), i = 1, 2, \ldots, n \\
& N_i = \mathcal{F}_N(\mu_{\hat{u}}(M_i), \sigma_{\hat{u}i}(N_i)), i = 1, 2, \ldots, n \\
& M_i = \mathcal{F}_M(\mu_{\hat{u}}(M_i), \sigma_{\hat{u}i}(N_i)), i = 1, 2, \ldots, n
\end{aligned}
\tag{7.5}
$$

where:

$$
\sigma_{\hat{P}_e} = \left\| \frac{F_{\Omega_d}(s)K_i}{1 + \sum_{i=1}^{n} K_i \frac{1}{1+s\tau_i} R_m(T_{di}s)N_i A_{pi}} \right\|_2 \sigma_d
$$

and $\sigma_{\hat{P}_{\text{in},i}} = K_i\sigma_{\hat{P}_e}$.

Note that (7.5) defines a static optimization problem that is dependent on system parameters (like σ_d) that can be estimated and/or measured. If the system parameters change, the optimization can be re-done. This adaptive nature of SL is discussed in more detail in Section 7.2.3.
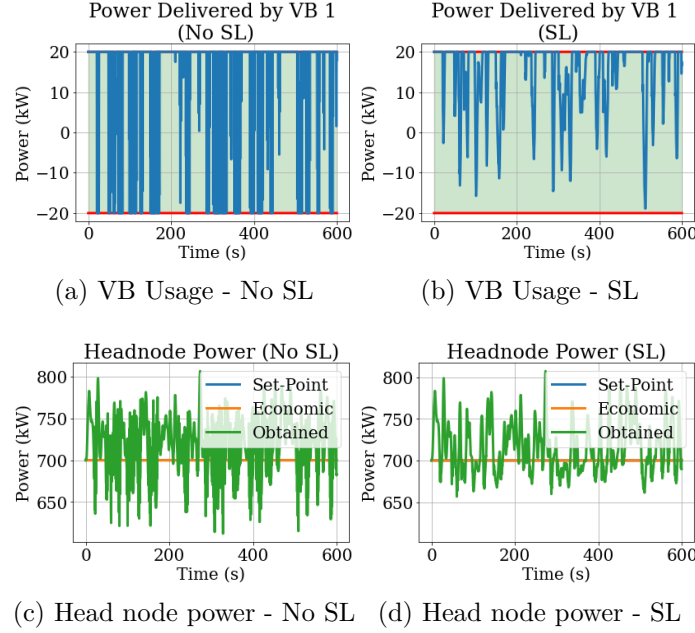
Figure 7.3: VB Usage and Head Node Power. This is for VBs with fixed power limits (i.e., univariate saturation).

7.2.2 SIMULATION

Setup

The simulation setup consists of an IEEE 37-node feeder (single-phase equivalent) [182], with two VBs at two different nodes (specifically, 701 and 737), where the base loads are 140 kW each. The upper and lower power limits of the VBs are taken to be 20 kW and -20 kW respectively. The nominal power set-points are optimally found to be 20 and 18 kW (using the optimal set-point dispatcher described in [142]) to meet a head node power demand of 700 kW, resulting in a highly saturated system. The maximum state-of-charge capacities of the VBs were taken to be 80 kWh (representing a maximum of four hours of operation at maximum power capacity) each.

119

Table 7.1: Signal Statistics

Quantity	With No SL	With SL	Improvement (%)
SD of VB 1 Power (P)	15.2 kW	9.9 kW	35.2
SD of VB 2 P	14.8 kW	10.3 kW	30.1
Mean of Head Node P	713.8 kW	709.2 kW	0.6
SD of Head Node P	33.9 kW	30.0 kW	11.8
Cost	3609.3 kW^2	1121.9 kW^2	68.9

The time constants of the first-order VB model were taken to be 600 ms and 400 ms respectively, and the time delays to be 100 ms and 200 ms respectively. I assume Gaussian random active and reactive power noise injected into certain locations of the feeder (as is expected, for example, due to random cloud cover). A 10 min simulation was performed using both the SL-based optimization and the non-SL-based optimization to illustrate the effectiveness of SL. The value of ρ was assumed to be 0.1 and a 3rd order Padé approximation was considered for the delays in both cases.

Results and Discussion

Fig. 7.3 shows the power delivered by one of the VBs, both by not using SL (Fig. 7.3a) and using SL (Fig. 7.3b). It can be seen that there is significant saturation using the controller gains designed without SL. This is because there is no knowledge of VB power bounds in that design. Moreover, the variability of the head node power shown in Fig. 7.3c is also high. However, with SL-based design, the saturation and variability of VB power are significantly reduced, along with a reduction in the head node power deviation (Fig. 7.3d) from the desired value of 700 kW. The mean and SDs of the signals were found numerically after the simulations, and the improvements are summarized in Table 7.1. Note that although a single simulation is reported

(a) Non-SL
(b) SL
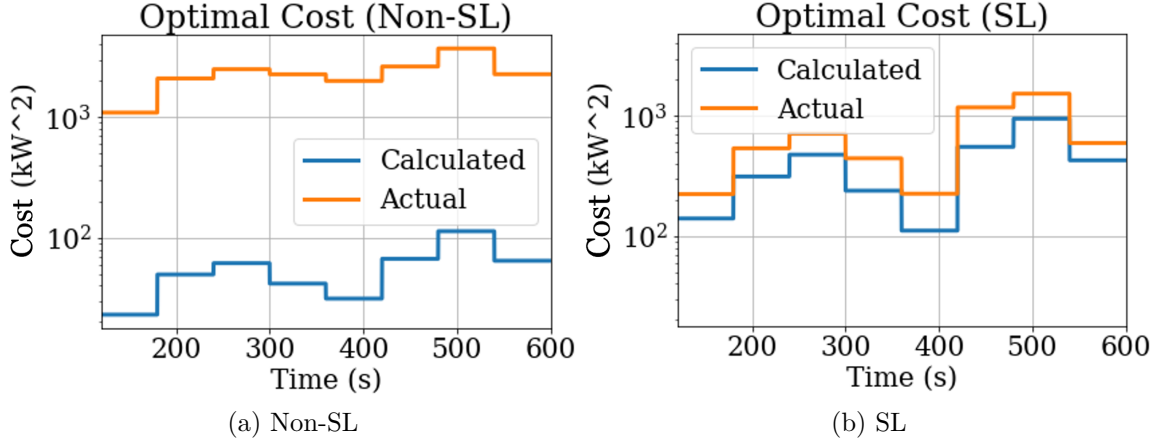
Figure 7.4: Optimal Cost, evaluated over one minute intervals. Y-axis is in log scale.

here to illustrate the effectiveness of SL, other simulations performed with the similar conditions also resulted in similar improvements with SL. Of course, the exact system parameters will dictate how effective SL will be in a given situation, and I discuss the effect of some system parameters in Section 7.3.

7.2.3 DATA DRIVEN SL FORMULATION

Since the SL process mentioned in the previous section takes into account all system parameters (as in (7.5)), the controller gains can be designed *adaptively*, considering changes in system parameters (such as saturation limits in VB power) or exogenous signal statistics (such as the mean and SD of the head node power). In situations when these parameters can be estimated using real-time data, e.g., using Kalman filters, recursive least squares, or running averages [183]), the controller gains can be adaptively re-tuned based on this data. If done sufficiently slowly, the system stability is not comprised, though the proof of this is a topic for future research. This subsection illustrates the effectiveness of SL for adaptive control of VBs by using
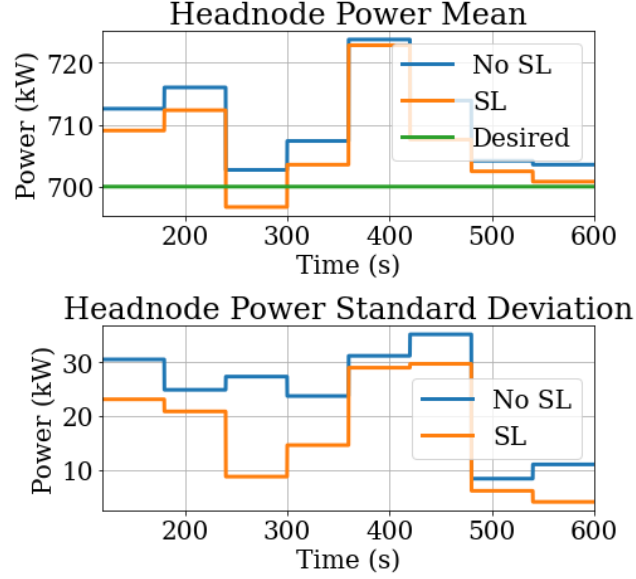
Figure 7.5: Headnode power. Statistics are evaluated over one minute intervals.
updated head node power statistics at regular intervals.

Setup

The same system is considered as described in Section 7.2.2. However, in this case, the disturbance statistics μ_d and σ_d are estimated over a running window of two minutes using measured head node statistics and the linearized system model. The VB optimization problem is run every minute using updated head node power (over the last two minutes), first by not using SL and then using SL. As before, ρ was assumed to be 0.1 in both cases.

Results and Discussion

First, the results indicate several advantages of an SL-based optimization over a non-SL based optimization. For instance, Fig. 7.4 shows the calculated (using (7.3)-(7.5)) and actual optimal cost (by numerical simulation) over every one minute interval. It

(a) Non-SL   (b) SL
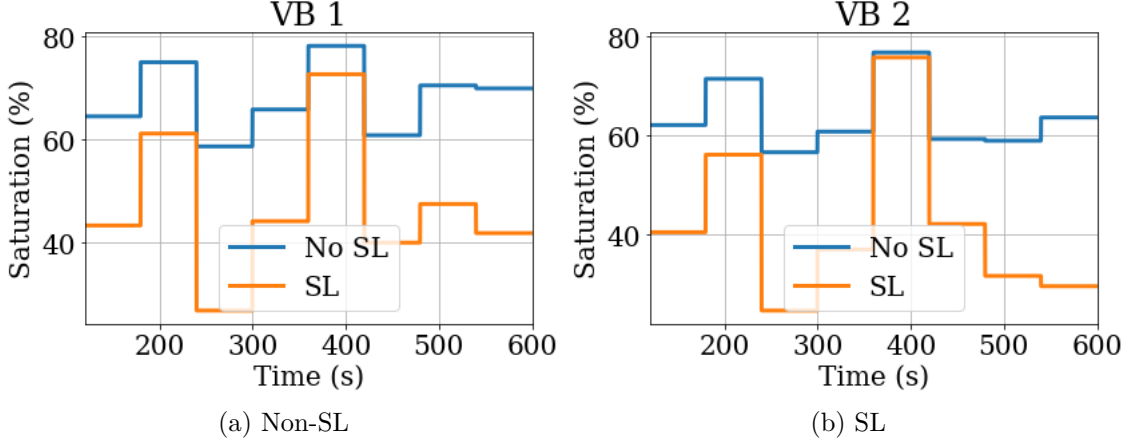
Figure 7.6: Saturation of VBs

can be seen that non-SL based optimization method *grossly underestimates* the cost

that it minimizes (Fig. 7.4), by more than an order of magnitude, whereas the SL

based optimization, due to knowledge of updated VB bounds and noise statistics,

estimates the cost more accurately. Moreover, using the improved estimation of the

statistics of the error and the control input in SL-based optimization, a slightly lower

value of SD can be obtained and the mean of the head node power with SL is also

slightly closer to the desired value (Fig. 7.5). The mean is lower due to the additional

bias term that is added due to SL in the operating points of the VBs. With SL, the

amount of saturation in VB power is reduced by about 10-30% (Fig. 7.6), indicating

that VBs are being pushed lesser to their limits. This is a major advantage of an SL-

based design compared to the non-SL-based design and results in much lesser usage

of power to achieve the same or better grid objective.

Second, the adaptive nature of SL is specifically highlighted in Fig. 7.7. Unlike

the non-SL based optimization, whose solution (i.e., optimal gains) is independent of

noise statistics or VB bounds (since σ_d^2 is just a multiplying factor for, and μ_d does

not feature in, the objective function (7.5), while $N_i = 1$ and $m_i = 0$ always), the

(a) Controller Gain 1   (b) Controller Gain 2
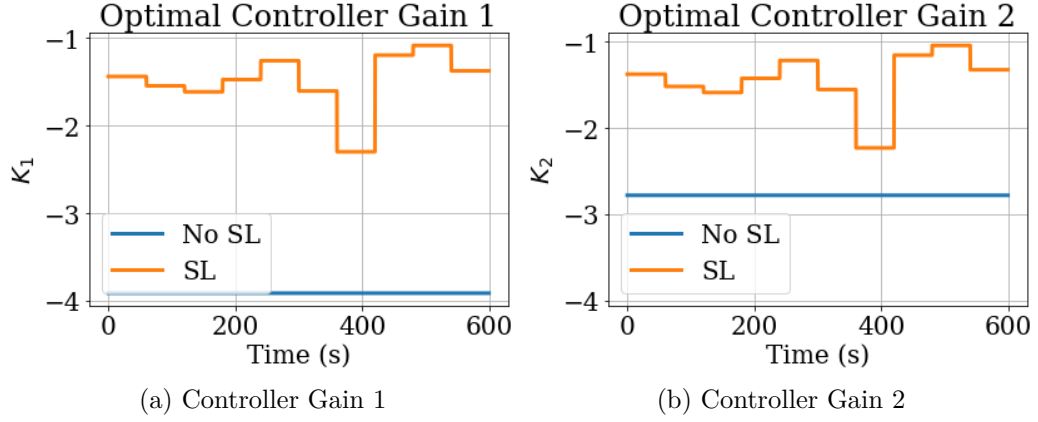
Figure 7.7: Controller Gains

SL-based optimization takes into account this information about the system to find the quasilinear gain/bias and updates the gain accordingly (Fig. 7.7). Hence, the SL-based optimization is adaptive, unlike the non-SL based optimization.

7.3   ANALYSIS ON EFFECT OF PARAMETERS

In this section, I provide the results of simulations to show the effect of various system parameters on the SL-based optimization procedure. This provides various insights into the design and analysis of nonlinear stochastic systems using SL.

7.3.1   EFFECT OF CONTROL PENALTY

First, the value of the control penalty ρ is varied. In this specific study, the delay is neglected. This is because delays are not accurately modeled when the bandwidth of the control system is high, which can occur with high values of controller gains, or due to modeling errors resulting from discrete-time simulation of the continuous-time system, unless the sampling time is very small.

124
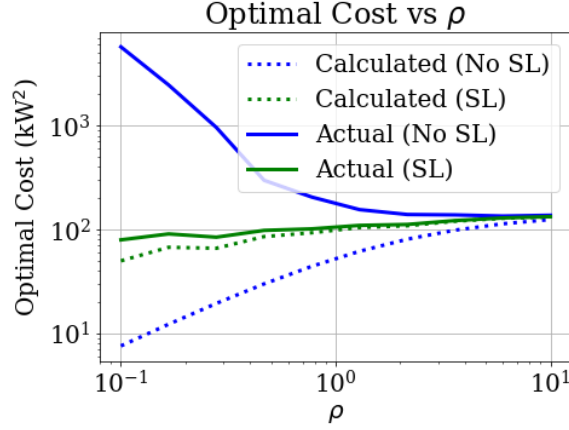
Figure 7.8: Effect of ρ. Axes are in log scale.

On Optimal Cost

The effect of ρ on the optimal cost is displayed in Fig. 7.11a. The solid lines show the value of the cost obtained numerically from a 10-minute simulation of the VBs, while the dotted lines show the calculated cost. It can be seen that with small ρ, the non-SL-based design is not able to reduce the actual cost due to no knowledge of bounds. Effectively, for very small ρ, the control input is not penalized much, and hence its variability is high and the VB ouput is saturated. For large ρ, the costs from both the non-SL and the SL-based optimizations converge since, for large ρ, the control action is highly penalized, and thus there is no VB saturation. However, SL captures the cost more accurately due to the knowledge of bounds, and hence, it can make the actual cost smaller even for small values of ρ.

On Head Node Power

With SL-based optimization, the mean of the head node power is generally closer to the desired value (it is still away from the desired value due to the fundamental limit
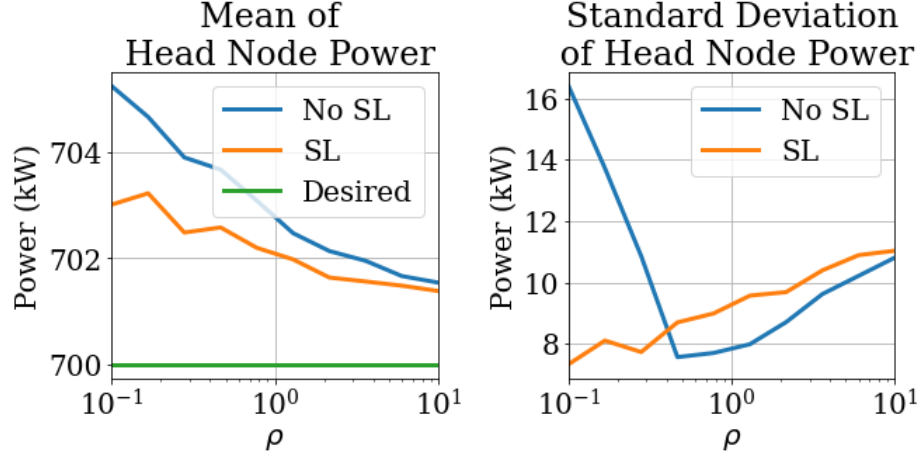
Figure 7.9: Effect of ρ on Head Node Power

of VB saturation). As mentioned earlier, the lower mean of the head node power is due to the additional bias term (m_i) that is added due to SL in the operating points of the VBs. The two methods converge for large ρ due to the same reason mentioned in the previous paragraph. Moreover, the SD of the head node power is much smaller for small values of ρ and is relatively the same as that obtained by not using SL for higher values of ρ. Note that the SD of the head node power sometimes increases and decreases since it forms only a part of the cost function in (7.5).

7.3.2 Effect of different saturation limits

Next, I investigate the effect of changing the power limit of one of the VB with respect to the other. Keeping the same time constants (= 400 ms), delays (= 400 ms), and feeder locations, the power limit of one VB (VB 2) was varied, keeping that of the other (VB 1) fixed, and the controllers were redesigned with new information on VB limits.
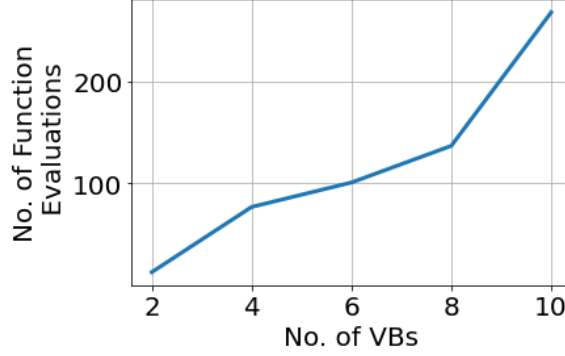
Figure 7.10: Effect of VBs on SL and optimization

(a) Effect of ρ. Axes are in log scale.

(b) No. of SL function evaluations vs. number of VBs
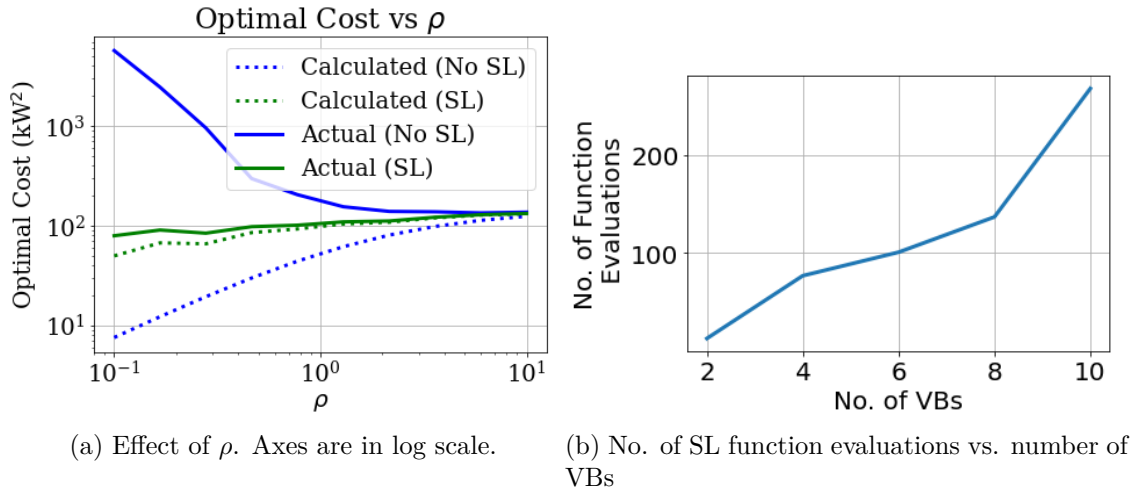
Figure 7.11: Effect of VBs on SL and optimization

7.3.3 EFFECT OF THE NUMBER OF VBS

Since SL involves solving a system of transcendental equations, the computational complexity increases as the number of equations increases. For each VB added, there are added two equations involving N_i and M_i. To quantify the computational complexity, the number of evaluations of the SL functions for fixed controller gains were noted as the number of VBs were increased. This would roughly indicate a lower bound on the number of evaluations required of the SL functions when they are part of

127

the optimization problem as equality constraints, as solving the optimization problem involves finding a solution to these SL equations. The equations were solved using a modification of the Powell hybrid method, as implemented in MINPACK [184] (other numerical methods were also tried, like the Broyden method, but this was the best in terms of the number of function evaluations). The results are shown in Fig. 7.11b. It can be seen that with the increase in the number of VBs, the number of function evaluations (for solving SL equations with fixed controller gains) also increases, indicating that SL becomes more computationally expensive, but grows polynomially rather than exponentially.

7.4 EXTENSION TO VARIABLE VIRTUAL BATTERY POWER BOUNDS

7.4.1 MODELING

In practice, the power limits of the VB's underlying DER aggregation are generally not constant [139]. The DERs that make up a VB can choose not to participate in providing grid services due to user preferences or to avoid Quality-of-Service (QoS) violations, leading to a change in the power and energy limits. To deal with such a case, a *trivariate* saturation in the VB model can be considered, where instead of the saturation authorities α and β being constants in (2.4), they are time-varying, i.e.,

$\alpha(t)$ and $\beta(t)$:

$$\mathrm{sat}_{\alpha(t)}^{\beta(t)}\left(u(t)\right) = \begin{cases} \beta(t), & u(t) \geq \beta(t) \\ u(t), & \alpha(t) < u < \beta(t) \\ \alpha(t), & u(t) \leq \alpha(t) \end{cases} \tag{7.6}$$

when $\alpha(t) < \beta(t)$, and 0 otherwise (since then there is no flexibility and the VB output is nominal, i.e., $p_b(t) = P_{\mathrm{set}}$).

7.4.2 MULTIVARIABLE SL

Open-Loop

Equation (7.6) describes a trivariate nonlinearity. To find SL of this nonlinearity, (2.2)-(2.3) is not applicable. Hence, I apply the procedure of multivariable SL described in [144], where instead of (2.2)-(2.3), the quasilinear gain N *vector* and the bias M are computed for a *multivariate* function $f : \mathbb{R}^n \to \mathbb{R}$ using:

$$N = E\left[\nabla f(u(t))\right] := \mathcal{G}_N(\mu, \Sigma), \quad M = E\left[f\left(u(t)\right)\right] := \mathcal{G}_M(\mu, \Sigma) \tag{7.7}$$

where $\mathcal{G}_N(\cdot, \cdot)$ and $\mathcal{G}_M(\cdot, \cdot)$ are functions representing the dependence of N and M on μ and Σ, the mean and covariance matrix of $u(t)$ respectively. Note that μ is composed of μ_u, μ_α, and μ_β (the means of the inputs $u(t)$, $\alpha(t)$, and $\beta(t)$, respectively), and the covariance matrix Σ is composed of σ_u, σ_α, and σ_β (their corresponding SDs), and $\rho_{u\alpha}$, $\rho_{\alpha\beta}$, and $\rho_{u\beta}$ (the correlation coefficient between $u(t)$ and $\alpha(t)$, that between $\alpha(t)$ and $\beta(t)$, and that between $u(t)$ and $\beta(t)$ respectively). Assuming that $\alpha(t)$, $\beta(t)$, and $u(t)$ form a trivariate Gaussian process, on substituting the

nonlinear function (7.6) for $f(\cdot)$ in (7.7), the value of N can be found as follows: $N = [N_1 \ N_2 \ N_3]^T = E[\nabla \text{sat}(u(t), \alpha(t), \beta(t))]$. Here note that since the saturation function is not differentiable at certain points, the gradient ∇ has to be taken piecewise.

Closed-Loop

Now consider the feedback system of Fig. 7.1, but with trivariate saturation in VBs instead of univariate saturation. Since $\alpha_i(t)$ and $\beta_i(t)$ are intrinsic properties of the ith VB and are not influenced by the nodal disturbance $d(t)$, I assume that the values of $\mu_{\alpha i}$, $\mu_{\beta i}$, $\sigma_{\alpha i}$, $\sigma_{\beta i}$, $\rho_{u\alpha i}$, $\rho_{\alpha\beta i}$, and $\rho_{u\beta i}$ are known (based on, e.g., historical data), and evaluate $\mu_{\hat{u}i}$ and $\sigma_{\hat{u}i}$ as before from (7.3)-(7.4), in place of μ_{ui} and σ_{ui} (due to the same reason mentioned in Section 3.2). Then, similar to (2.2)-(2.3), the SL of the closed-loop system is performed by solving:

$$N_i = \mathcal{G}_N(\hat{\mu}_i(M), \hat{\Sigma}_i(N)), \quad M_i = \mathcal{G}_M(\hat{\mu}_i(M), \hat{\Sigma}_i(N))$$

where $\hat{\mu}_i$ and $\hat{\Sigma}_i$ in the stochastically linearized system denote the moments corresponding to μ_i and Σ_i in the nonlinear system. This completes the SL procedure of the closed-loop system. For more details, please refer to [144].

7.4.3 SIMULATION

Setup

To illustrate the SL of the system with trivariate saturation, an IEEE 37-node feeder with a VB of 600 ms time constant and 100 ms time delay at one of its nodes was considered for the simulation. The time-varying upper and lower power limits of the
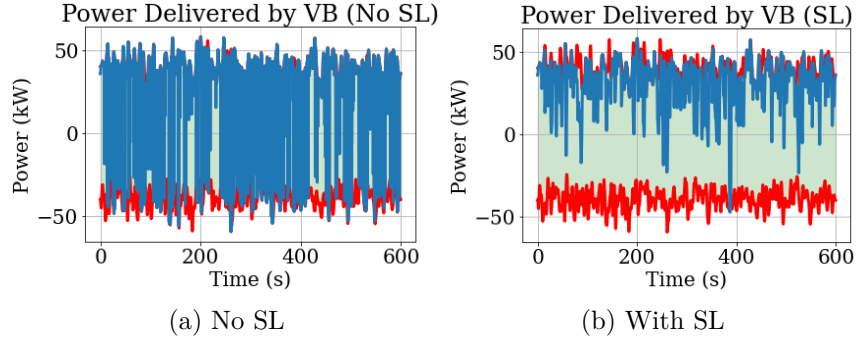
Figure 7.12: VB Actuation. The red lines indicate time-varying power limits.

VB were taken to Gaussian, with 40 and -40 kW as mean respectively, and 6 kW as the SD (for both limits). For the optimization, the value of ρ was taken to be 0.1. The power limits were assumed to be uncorrelated to the input to the saturation.

Results

The results are shown in Fig. 7.12. It can be seen that with SL, the VB power is significantly less variable than that by not using SL. The SD of the VB power in case of no SL is 28.5 kW and that with SL is 14.9 kW (an improvement of 47.7%). The mean head node power with no SL is 715.1 kW and with SL is 710.2 kW (an improvement of 0.7%) while the SD of the head node power with no SL is 32.6 kW and with SL, it is 29.7 kW (an improvement of 8.9%). The overall cost function improved from 9826.5 kW^2 (no SL) to 1042.3 kW^2 (SL), an improvement of 89%. Moreover, it was observed that if the VB power limits were *not* assumed stochastic while designing the controller gains, but in reality they were, the actual optimal cost would increase by 2.3%, the SD of VB power by 6%, and the head node power mean by 0.1%. These serve as preliminary results to illustrate that variable power bounds can be handled in the context of VBs. A full exposition of this idea is a topic for the future.

Chapter 8

Conclusion and Future Works

In this dissertation, the theory of QLC has been extended to systems with multivariate nonlinearities, the numerical properties of QLC have been investigated, and QLC has been applied to power system applications like frequency control and control of virtual batteries in distribution feeders. Detailed conclusions are discussed below.

8.1 QLC of Systems with Multivariate Nonlinearities

In Chapter 3, SL of systems with multivariate nonlinearities is discussed. The formulae for the equivalent gains and bias resulting from SL are derived. The formulae are then applied to a trivariate saturation nonlinearity and the SL coefficients are interpreted. The process of multivariable SL has been applied to find an equivalent realization of a stochastic system with stochastic parameters or state multiplicative noise, and its effectiveness in finding optimal controllers has been illustrated. A recipe

for finding the robustness of SL is also given. A numerical example is presented to show that the method can be used to design optimal controllers for systems with multivariate nonlinearities.

8.2 INVESTIGATION OF ACCURACY, ROBUSTNESS AND COMPUTATION OF SL

In Chapter 5, the open-loop accuracy, robustness, and computational performance of SL for a typical stochastic nonlinear feedback system with both asymmetric and symmetric saturation have been investigated. From the study on open-loop accuracy, a mathematical relationship has been established between the actuator authority and the worst-case error, and its implications on closed-loop accuracy described. From the study on the robustness of SL to system parameters, it is found out that the SL coefficients are more sensitive in the case of asymmetric saturation than in the case of symmetric saturation, and that the sensitivity is more towards those parameters that affect the saturation directly (e.g., gain, actuator authority, signal statistics). Also, in the case of asymmetric saturation, the mean of the actuator input and tracking error is more sensitive to changes in SL coefficients. Finally, from the study on computational efficiency, it is found that the Broyden method is best suited for applying SL to symmetric saturation in a reference tracking problem since it requires a low computational effort. In the case of asymmetric saturation, it is found that a coordinate transformation can lead to significant improvements in the number of tries required by an algorithm, and the Trust Region Reflective method requires the least number of tries. For both asymmetric/symmetric saturation, it is

found out that fixed point iteration is not an effective method for solving the SL gain/bias.

8.3   Droop Control of Power Systems

In Chapter 6, the method of QLC has been applied to design an optimal droop controller for primary frequency control of power systems with generator saturation. Numerical simulations show that the controller achieves a reduced combined state and control cost, compared to a baseline design, at the expense of a slightly increased state cost. Since the process depends on the values of all the system parameters, the optimal controller can dynamically update itself on change of parameters, for example, the load variability or the saturation limits, to produce optimal performance.

8.4   Optimal Control of VBs

In Chapter 7, an SL-based method of optimizing the power delivered by VBs in distribution feeders is described. Since SL takes into account VB power limits and other system parameters, it provides a superior method of analysis and design of gains optimally. Simulation results show that compared to a non-SL-based optimization, SL results in a more accurate estimation of signal statistics. They also indicate that SL-based optimization can reduce head node power deviation from the nominal while optimizing VB usage and can use updated information to change the gains, i.e., is adaptive. Some analysis on the effect of the control penalty ρ in the cost function shows that even at small values of this parameter, with proper models of the devices,

SL can lead to a reduction in the cost. Moreover, it is shown that with an increased number of VBs, the computational complexity of SL increases. Finally, the design is extended to VBs with variable power limits.

8.5 FUTURE WORKS

There are many interesting directions of investigation in this field, including:

- Investigation of the accuracy, robustness and computation of *multivariable* SL.

- Investigation of accuracy of SL for systems with low phase margin, and of the causes for outliers in the sensitivity studies of Chapter 5.

- SL of systems with nonlinearities other than saturation.

- Applications of QLC to handle saturation in the slew rate of generators and energy constraints, apart from power constraints, in virtual batteries.

- SL of systems in discrete-time and QLC theory for discrete-time systems.

- Comparison of SL with other common nonlinear control techniques.

- Exposition on data-driven SL, including methods of estimating the probability density function, and the effects on computed quasilinear gain/bias, as new data points are obtained on the fly.

- Effect of SL on the controllability and observability of control systems.

Bibliography

[1] Göran Anderson. Dynamics and Control of Electric Power Systems. *Lecture 227-0528-00, ITET ETH*, (February):32–35, 2012.

[2] R E Kalman. Lyapunov functions for the problem of Lur'e in automatic control. *Proceedings of the National Academy of Sciences*, 49:201–205, 1963.

[3] H K Khalil. *Nonlinear Systems*. Prentice Hall, third edition, 2002.

[4] A Isidori. *Nonlinear control systems*. Springer, third edition, 1995.

[5] S Boyd and H Hindi. Analysis of Linear Systems With Saturation Using Convex Optimization. *Proceedings of the 37th IEEE Conference on Decision and Control*, pages 903–908, 1998.

[6] T Hu, Z Lin, and B M Chen. An analysis and design method for linear systems subject to actuator saturation and disturbance. *Automatica*, 38(2):351–359, 2002.

[7] Karl J Åström. *Introduction to stochastic control theory*. Courier Corporation, 2012.

[8] Zhongwei Lin, Yan Lin, and Weihai Zhang. A unified design for state and output feedback H_∞ control of nonlinear stochastic Markovian jump systems with state and disturbance-dependent noise. *Automatica*, 45(12):2955–2962, 2009.

[9] Bor-Sen Chen and Weihai Zhang. Stochastic H_2/H_∞ control with state-dependent noise. *IEEE Transactions on Automatic Control*, 49(1):45–57, Jan 2004.

[10] Eduardo F Camacho and Carlos Bordons Alba. *Model predictive control*. Springer science & business media, 2013.

[11] Carlos E Garcia, David M Prett, and Manfred Morari. Model predictive control: Theory and practice—a survey. *Automatica*, 25(3):335–348, 1989.

[12] Manfred Morari and Jay H Lee. Model predictive control: past, present and future. *Computers & Chemical Engineering*, 23(4-5):667–682, 1999.

[13] Frank Allgöwer and Alex Zheng. *Nonlinear model predictive control*, volume 26. Birkhäuser, 2012.

[14] Lars Grüne and Jürgen Pannek. Nonlinear model predictive control. In *Nonlinear model predictive control*, pages 45–69. Springer, 2017.

[15] Wallace E Vander Velde et al. Multiple-input describing functions and nonlinear system design. *McGraw lill*, 1968.

[16] James H Taylor. Describing functions. *Electrical Engineering Encyclopedia*, 1999.

[17] A Mees and A Bergen. Describing functions revisited. *IEEE Transactions on Automatic Control*, 20(4):473–478, 1975.

[18] Nicolas Noiray, Daniel Durox, Thierry Schuller, and Sébastien Candel. A unified framework for nonlinear combustion instability analysis based on the flame describing function. *Journal of Fluid Mechanics*, 615:139–167, 2008.

[19] Paul Palies, Daniel Durox, Thierry Schuller, and Sébastien Candel. Nonlinear combustion instability analysis based on the flame describing function applied to turbulent premixed swirling flames. *Combustion and Flame*, 158(10):1980–1991, 2011.

[20] Mayuresh V Kothare, Peter J Campo, Manfred Morari, and Carl N Nett. A unified framework for the study of anti-windup designs. *Automatica*, 30(12):1869–1883, 1994.

[21] Sergio Galeani, Sophie Tarbouriech, Matthew Turner, and Luca Zaccarian. A tutorial on modern anti-windup design. In *2009 European Control Conference (ECC)*, pages 306–323. IEEE, 2009.

[22] Sophie Tarbouriech and Matthew Turner. Anti-windup design: an overview of some recent advances and open problems. *IET control theory & applications*, 3(1):1–19, 2009.

[23] Luca Zaccarian and Andrew R Teel. *Modern anti-windup synthesis*. Princeton University Press, 2011.

[24] Christopher Edwards and Ian Postlethwaite. Anti-windup and bumpless-transfer schemes. *Automatica*, 34(2):199–210, 1998.

[25] Laurent El Ghaoui and Silviu-Iulian Niculescu. *Advances in linear matrix inequality methods in control*. SIAM, 2000.

[26] Kazuo Tanaka and Hua O Wang. *Fuzzy control systems design and analysis: a linear matrix inequality approach*. John Wiley & Sons, 2004.

[27] Pascal Gahinet and Pierre Apkarian. A linear matrix inequality approach to h$_\infty$ control. *International journal of robust and nonlinear control*, 4(4):421–448, 1994.

[28] Carsten Scherer and Siep Weiland. Linear matrix inequalities in control. *Lecture Notes, Dutch Institute for Systems and Control, Delft, The Netherlands*, 3(2), 2000.

[29] Stephen Boyd, Laurent El Ghaoui, Eric Feron, and Venkataramanan Balakrishnan. *Linear matrix inequalities in system and control theory*. SIAM, 1994.

[30] Aaron D Ames, Xiangru Xu, Jessy W Grizzle, and Paulo Tabuada. Control barrier function based quadratic programs for safety critical systems. *IEEE Transactions on Automatic Control*, 62(8):3861–3876, 2016.

[31] Aaron D Ames, Jessy W Grizzle, and Paulo Tabuada. Control barrier function based quadratic programs with application to adaptive cruise control. In *53rd IEEE Conference on Decision and Control*, pages 6271–6278. IEEE, 2014.

[32] Xiangru Xu, Paulo Tabuada, Jessy W Grizzle, and Aaron D Ames. Robustness of control barrier functions for safety critical control. *IFAC-PapersOnLine*, 48(27):54–61, 2015.

[33] Aaron D Ames, Samuel Coogan, Magnus Egerstedt, Gennaro Notomista, Koushil Sreenath, and Paulo Tabuada. Control barrier functions: Theory and applications. In *2019 18th European Control Conference (ECC)*, pages 3420–3431. IEEE, 2019.

[34] Keng Peng Tee and Shuzhi Sam Ge. Control of nonlinear systems with partial state constraints using a barrier lyapunov function. *International Journal of Control*, 84(12):2008–2023, 2011.

[35] Petar Kokotović, Hassan K Khalil, and John O'reilly. *Singular perturbation methods in control: analysis and design*. SIAM, 1999.

[36] HAKAN ELMALI and NEJAT OLGAC. Sliding mode control with perturbation estimation (smcpe): a new approach. *International Journal of control*, 56(4):923–941, 1992.

[37] Petar V Kokotović. Applications of singular perturbation techniques to control problems. *SIAM review*, 26(4):501–550, 1984.

[38] Desineni S Naidu. *Singular perturbation methodology in control systems*. Number 34. IET, 1988.

[39] Yangmin Li and Qingsong Xu. Adaptive sliding mode control with perturbation estimation and pid sliding surface for motion tracking of a piezo-driven micromanipulator. *IEEE Transactions on control systems technology*, 18(4):798–810, 2009.

[40] Shankar Sastry. *Nonlinear systems: analysis, stability, and control*, volume 10. Springer Science & Business Media, 2013.

[41] Mathukumalli Vidyasagar. *Nonlinear systems analysis*. SIAM, 2002.

[42] Philip G Drazin and Philip Drazin Drazin. *Nonlinear systems*. Number 10. Cambridge University Press, 1992.

[43] Charles L Lawson and Richard J Hanson. *Solving least squares problems*. SIAM, 1995.

[44] Kenneth Levenberg. A method for the solution of certain non-linear problems in least squares. *Quarterly of applied mathematics*, 2(2):164–168, 1944.

[45] Åke Björck. *Numerical methods for least squares problems*. SIAM, 1996.

[46] Åke Björck. Least squares methods. *Handbook of numerical analysis*, 1:465–652, 1990.

[47] Johan AK Suykens and Joos Vandewalle. Least squares support vector machine classifiers. *Neural processing letters*, 9(3):293–300, 1999.

[48] Wilson J Rugh and Jeff S Shamma. Research on gain scheduling. *Automatica*, 36(10):1401–1425, 2000.

[49] Douglas J Leith and William E Leithead. Survey of gain-scheduling analysis and design. *International journal of control*, 73(11):1001–1025, 2000.

[50] Wilson J Rugh. Analytical framework for gain scheduling. In *1990 American Control Conference*, pages 1688–1694. IEEE, 1990.

[51] Pierre Apkarian and Richard J Adams. Advanced gain-scheduling techniques for uncertain systems. In *Advances in linear matrix inequality methods in control*, pages 209–228. SIAM, 2000.

[52] Jeff S Shamma and Michael Athans. Gain scheduling: Potential hazards and possible remedies. *IEEE Control Systems Magazine*, 12(3):101–107, 1992.

[53] Wei Kang and Arthur J Krener. Extended quadratic controller normal form and dynamic state feedback linearization of nonlinear systems. *SIAM Journal on Control and Optimization*, 30(6):1319–1337, 1992.

[54] Costas Kravaris and Prodromos Daoutidis. Nonlinear state feedback control of second-order nonminimum-phase nonlinear systems. *Computers & chemical engineering*, 14(4-5):439–449, 1990.

[55] Daizhan Cheng, Xiaoming Hu, and Yuzhen Wang. Non-regular feedback linearization of nonlinear systems via a normal form algorithm. *Automatica*, 40(3):439–447, 2004.

[56] Rajagopalan Devanathan. Linearization condition through state feedback. *IEEE transactions on Automatic Control*, 46(8):1257–1260, 2001.

[57] J O'reilly and MM Fahmy. The minimum number of degrees of freedom in state feedback control. *International Journal of Control*, 41(3):749–768, 1985.

[58] Bernard Charlet, Jean Lévine, and Riccardo Marino. On dynamic feedback linearization. *Systems & Control Letters*, 13(2):143–151, 1989.

[59] A Yeşildirek and Frank L Lewis. Feedback linearization using neural networks. *Automatica*, 31(11):1659–1664, 1995.

[60] Ali Bidram, Ali Davoudi, Frank L Lewis, and Josep M Guerrero. Distributed cooperative secondary control of microgrids using feedback linearization. *IEEE Transactions on Power Systems*, 28(3):3462–3470, 2013.

[61] Daewon Lee, H Jin Kim, and Shankar Sastry. Feedback linearization vs. adaptive sliding mode control for a quadrotor helicopter. *International Journal of control, Automation and systems*, 7(3):419–428, 2009.

[62] John Chiasson. Dynamic feedback linearization of the induction motor. *IEEE transactions on automatic control*, 38(10):1588–1594, 1993.

[63] K David Young, Vadim I Utkin, and Umit Ozguner. A control engineer's guide to sliding mode control. *IEEE transactions on control systems technology*, 7(3):328–342, 1999.

[64] Christopher Edwards and Sarah Spurgeon. *Sliding mode control: theory and applications.* Crc Press, 1998.

[65] Arie Levant. Sliding order and sliding accuracy in sliding mode control. *International journal of control*, 58(6):1247–1263, 1993.

[66] Yuri Shtessel, Christopher Edwards, Leonid Fridman, Arie Levant, et al. *Sliding mode control and observation*, volume 10. Springer, 2014.

[67] Wilfrid Perruquetti and Jean-Pierre Barbot. *Sliding mode control in engineering.* CRC press, 2002.

[68] Daniel Y Abramovitch. Lyapunov redesign of analog phase-lock loops. In *1989 American Control Conference*, pages 2684–2689. IEEE, 1989.

[69] Maruthi T Ravichandran and Arun D Mahindrakar. Robust stabilization of a class of underactuated mechanical systems using time scaling and lyapunov redesign. *IEEE Transactions on Industrial Electronics*, 58(9):4299–4313, 2010.

[70] Claudio De Persis and Romain Postoyan. A lyapunov redesign of coordination algorithms for cyber-physical systems. *IEEE Transactions on Automatic Control*, 62(2):808–823, 2016.

[71] Chang-Sei Kim, Keum-Shik Hong, and Moon-Ki Kim. Nonlinear robust control of a hydraulic elevator: experiment-based modeling and two-stage lyapunov redesign. *Control Engineering Practice*, 13(6):789–803, 2005.

[72] Ghazal Montaseri and Mohammad Javad Yazdanpanah. Adaptive control of uncertain nonlinear systems using mixed backstepping and lyapunov redesign techniques. *Communications in Nonlinear Science and Numerical Simulation*, 17(8):3367–3380, 2012.

[73] Jay A Farrell, Marios Polycarpou, Manu Sharma, and Wenjie Dong. Command filtered backstepping. *IEEE Transactions on Automatic Control*, 54(6):1391–1395, 2009.

[74] Tarek Madani and Abdelaziz Benallegue. Backstepping control for a quadrotor helicopter. In *2006 IEEE/RSJ International Conference on Intelligent Robots and Systems*, pages 3255–3260. IEEE, 2006.

[75] ZHONG-PING JIANGdagger and Henk Nijmeijer. Tracking control of mobile robots: A case study in backstepping. *Automatica*, 33(7):1393–1399, 1997.

[76] Rafael Fierro and Frank L Lewis. Control of a nonholomic mobile robot: Back-stepping kinematics into dynamics. *Journal of robotic systems*, 14(3):149–163, 1997.

[77] Hua Deng and Miroslav Krstić. Stochastic nonlinear stabilization—i: A back-stepping design. *Systems & Control Letters*, 32(3):143–150, 1997.

[78] Blake Hannaford and Jee-Hwan Ryu. Time-domain passivity control of haptic interfaces. *IEEE transactions on Robotics and Automation*, 18(1):1–10, 2002.

[79] Jee-Hwan Ryu, Dong-Soo Kwon, and Blake Hannaford. Stable teleoperation with time-domain passivity control. *IEEE Transactions on robotics and automation*, 20(2):365–373, 2004.

[80] Arjan J Van der Schaft and AJ Van Der Schaft. *L2-gain and passivity techniques in nonlinear control*, volume 2. Springer, 2000.

[81] Romeo Ortega and Eloisa Garcia-Canseco. Interconnection and damping assignment passivity-based control: A survey. *European Journal of control*, 10(5):432–450, 2004.

[82] Nikhil Chopra and Mark W Spong. Passivity-based control of multi-agent systems. In *Advances in robot control*, pages 107–134. Springer, 2006.

[83] Luca Zaccarian and Andrew R Teel. A common framework for anti-windup, bumpless transfer and reliable designs. *Automatica*, 38(10):1735–1744, 2002.

[84] Raymond Hanus, Michel Kinnaert, and J-L Henrotte. Conditioning technique, a general anti-windup and bumpless transfer method. *Automatica*, 23(6):729–739, 1987.

[85] PJ Campo, M Morari, and CN Nett. Multivariable anti-windup and bumpless transfer: A general theory. In *1989 American Control Conference*, pages 1706–1711. IEEE, 1989.

[86] Matthew C Turner and Daniel J Walker. Linear quadratic bumpless transfer. *Automatica*, 36(8):1089–1101, 2000.

[87] Dibakar Das, Gurunath Gurrala, and U Jayachandra Shenoy. Linear quadratic regulator-based bumpless transfer in microgrids. *IEEE Transactions on Smart Grid*, 9(1):416–425, 2016.

[88] William S Levine. *The Control Handbook (three volume set)*. CRC press, 2018.

[89] Shinung Ching, Yongsoon Eun, Cevat Gokcek, Pierre T. Kabamba, and Semyon M. Meerkov. *Quasilinear control: Performance analysis and design of feedback systems with nonlinear sensors and actuators.* Cambridge University Press, 2010.

[90] Leslaw Socha. *Linearization methods for stochastic dynamic systems*, volume 730. Springer Science & Business Media, 2007.

[91] J B Roberts and P D Spanos. *Random Vibration and Statistical Linearization.* Dover Publications, 2003.

[92] Isaac Elishakoff and Stephen H. Crandall. Sixty years of stochastic linearization technique. *Meccanica*, 52(1-2):299–305, 2017.

[93] Richard C Booton. Nonlinear control systems with random inputs. *IRE Transactions on Circuit Theory*, 1(1):9–18, 1954.

[94] IE Kazakov. An approximate method for the statistical investigation for nonlinear systems. *Trudy VVIA im Prof. NE Zhukovskogo*, 394:1–52, 1954.

[95] Yoshikazu Sawaragi. *Statistical Studies on non-linear control systems.* Nippon Print. and Publishing Company, 1962.

[96] Arthur Gelb and Wallace E. Vander Velde. *Multiple-input describing functions and nonlinear system design.* McGraw-Hill, New York, 1968.

[97] D. P. Atherton and George M. Siouris. Nonlinear control engineering. *IEEE Transactions on Systems, Man, and Cybernetics*, 7(7):567–568, 1977.

[98] N Sinitsyn. Method of statistical linearization (survey). *Avtom. Telemekh.*, pages 36–48, 1974.

[99] Vladimir Vasil'evič Bolotin. *Random vibrations of elastic systems*, volume 8. Springer Science & Business Media, 2013.

[100] Xiangting Zhang, Isaac Elishakoff, and Ruichong Zhang. A stochastic linearization technique based on minimum mean square deviation of potential energies. In *Stochastic Structural Dynamics 1*, pages 327–338. Springer, 1991.

[101] I Elishakoff and X Zhang. An appraisal of different stochastic linearization techniques. *Journal of Sound and Vibration*, 153(2):370–375, 1992.

[102] I.E. Kazakov. Generalization of Statistical Linearization Method to Multidimensional Systems. *Avtomat. i Telemekh.*, 26(7):1210–1215, 1965.

[103] T. Selcuk Atalik and Senol Utku. Stochastic linearization of multi-degree-of-freedom non-linear systems. *Earthquake Engineering & Structural Dynamics*, 4(4):411–420, 1976.

[104] Thomas K Caughey. Equivalent linearization techniques. *The Journal of the Acoustical Society of America*, 35(11):1706–1711, 1963.

[105] L. Socha and M. Pawleta. Are statistical linearization and standard equivalent linearization the same methods in the analysis of stochastic dynamic systems? *Journal of Sound and Vibration*, 248:387–394, 11 2001.

[106] PT D Spanos and WD Iwan. On the existence and uniqueness of solutions generated by equivalent linearization. *International Journal of Non-linear mechanics*, 13(2):71–78, 1978.

[107] Igor G Vladimirov and Ian R Petersen. Gaussian stochastic linearization for open quantum systems using quadratic approximation of hamiltonians. *arXiv preprint arXiv:1202.0946*, 2012.

[108] A Di Matteo, PD Spanos, and A Pirrotta. Approximate survival probability determination of hysteretic systems with fractional derivative elements. *Probabilistic Engineering Mechanics*, 54:138–146, 2018.

[109] PD Spanos, Ying Zhang, and Fan Kong. Formulation of statistical linearization for mdof systems subject to combined periodic and stochastic excitations. *Journal of Applied Mechanics*, 86(10), 2019.

[110] P.T. Kabamba, S.M. Meerkov, and H.R. Ossareh. Stochastic linearisation approach to performance analysis of feedback systems with asymmetric nonlinear actuators and sensors. *International Journal of Control*, 88(1):65–79, 2015.

[111] Yi Guo, Pierre T. Kabamba, Semyon M. Meerkov, Hamid R. Ossareh, and Choon Yik Tang. Quasilinear Control of Wind Farm Power Output. *IEEE Transactions on Control Systems Technology*, 23(4):1555–1562, July 2015.

[112] I.E. Kazakov and S Malczikow. Analysis of stochastic systems in state space. *Nauka, Moskwa*, 67:79, 1975.

[113] I.E. Kazakov. Statistical theory of control systems in state space (Russian). *Moscow, Izdatel'stvo Nauka, 1975. 432*, 1975.

[114] BN Naumov. Theory of nonlinear automatic systems: Frequency methods, 1972.

[115] Hamid R Ossareh. An LQR theory for systems with asymmetric saturating actuators. In *Proceedings of the American Control Conference*, volume 2016-July of *2016 American Control Conference (ACC)*, pages 6941–6946. IEEE, 7 2016.

[116] R F Curtain. *Stability of Stochastic Dynamical Systems: Proceedings of the International Symposium Organized by 'The Control Theory Centre', University of Warwick, July 10-14, 1972.* Lecture Notes in Mathematics. Springer Berlin Heidelberg, 2006.

[117] S. P. Nandanoori, I. Chakraborty, T. Ramachandran, and S. Kundu. Identification and validation of virtual battery model for heterogeneous devices. In *2019 IEEE Power Energy Society General Meeting (PESGM)*, pages 1–5, 2019.

[118] S Ching, S M Meerkov, and T Runolfsson. Gaussianization of Random Inputs by Filtering Plants: The Case of Poisson White and Telegraph Processes. In *Decision and Control (CDC), 2010 49th IEEE Conference on*, pages 2650–2655. Ieee, 2010.

[119] C Gokcek, P T Kabamba, and S M Meerkov. Disturbance rejection in control systems with saturating actuators. *Nonlinear Analysis*, 40:213–226, 2000.

[120] S. Brahma, M. R. Almassalkhi, and H. R. Ossareh. A stochastic linearization approach to optimal primary control of power systems with generator saturation. In *2018 IEEE Conference on Control Technology and Applications (CCTA)*, pages 982–987, August 2018.

[121] C Gokcek, P T Kabamba, and S M Meerkov. An LQR/LQG Theory for Systems With Saturating Actuators. *IEEE Transactions on Automatic Control*, 46(10), 2001.

[122] L Socha and TT Soong. Sensitivity and linearization techniques in analysis of non-linear stochastic systems. *Journal of sound and vibration*, 156(1):79–97, 1992.

[123] P. Kundur. *Power Systems Stability and Control.* 1994.

[124] Allen J. Wood and Bruce F. Wollenberg. *Power Generation, Operation, and Control*, volume 37. John Wiley & Sons, 1996.

[125] PW Sauer, MA Pai, and JH Chow. *Power System Dynamics and Stability: With Synchrophasor Measurement and Power System Toolbox.* 2017.

[126] Enrique Mallada, Changhong Zhao, and Steven Low. Optimal Load-Side Control for Frequency Regulation in Smart Grids. *IEEE Transactions on Automatic Control*, 62(12):6294–6309, 12 2017.

[127] Florian Dörfler, John Simpson-Porco, and Francesco Bullo. Breaking the Hierarchy: Distributed Control & Economic Optimality in Microgrids. *IEEE Transactions on Control of Network Systems*, 3(3):241–253, 1 2014.

[128] Florian Dorfler, John W. Simpson-Porco, and Francesco Bullo. Plug-and-play control and optimization in microgrids. In *Proceedings of the IEEE Conference on Decision and Control*, volume 2015-Febru, pages 211–216. IEEE, 12 2014.

[129] Seungil You and Lijun Chen. Reverse and forward engineering of frequency control in power networks. In *53rd IEEE Conference on Decision and Control*, pages 191–198. IEEE, 12 2014.

[130] Enrique Mallada. IDroop: A Dynamic Droop controller to decouple power grid's steady-state and dynamic performance. In *2016 IEEE 55th Conference on Decision and Control, CDC 2016*, pages 4957–4964. IEEE, 12 2016.

[131] Changhong Zhao, Ufuk Topcu, Na Li, and Steven Low. Design and stability of load-side primary frequency control in power systems. *IEEE Transactions on Automatic Control*, 59(5):1177–1189, 5 2014.

[132] Mahraz Amini and Mads Almassalkhi. Investigating delays in frequency-dependent load control. In *IEEE PES Innovative Smart Grid Technologies Conference Europe*, pages 448–453. IEEE, 11 2016.

[133] A. Ghafouri, J. Milimonfared, and G. B. Gharehpetian. Coordinated control of distributed energy resources and conventional power plants for frequency control of power systems. *IEEE Transactions on Smart Grid*, 6(1):104–114, 2015.

[134] V Ravikumar Pandi, A Al-Hinai, and Ali Feliachi. Coordinated control of distributed energy resources to support load frequency control. *Energy conversion and management*, 105:918–928, 2015.

[135] A. D. Dominguez-Garcia, C. N. Hadjicostis, and N. H. Vaidya. Resilient networked control of distributed energy resources. *IEEE Journal on Selected Areas in Communications*, 30(6):1137–1148, 2012.

[136] E. Mayhorn, K. Kalsi, M. Elizondo, W. Zhang, S. Lu, N. Samaan, and K. Butler-Purry. Optimal control of distributed energy resources using model predictive

control. In *2012 IEEE Power and Energy Society General Meeting*, pages 1–8, 2012.

[137] Justin T Hughes, Alejandro D Domínguez-García, and Kameshwar Poolla. Identification of virtual battery models for flexible loads. *IEEE Transactions on Power Systems*, 31(6):4660–4669, 2016.

[138] Feng Ju, Junwen Wang, Jingshan Li, Guoxian Xiao, and Stephan Biller. Virtual battery: A battery simulation framework for electric vehicles. *IEEE Transactions on Automation Science and Engineering*, 10(1):5–15, 1 2013.

[139] S. P. Nandanoori, I. Chakraborty, T. Ramachandran, and S. Kundu. Identification and validation of virtual battery model for heterogeneous devices. In *2019 IEEE Power Energy Society General Meeting (PESGM)*, pages 1–5, 2019.

[140] Kristin Dietrich, Jesus M Latorre, Luis Olmos, and Andres Ramos. Modelling and assessing the impacts of self supply and market-revenue driven virtual power plants. *Electric Power Systems Research*, 119:462–470, 2015.

[141] Ali Bidram and Ali Davoudi. Hierarchical structure of microgrids control system. *IEEE Transactions on Smart Grid*, 3(4):1963–1976, 2012.

[142] S. Brahma, N. Nazir, H. Ossareh, and M. Almassalkhi. Optimal and resilient coordination of virtual batteries in distribution feeders. *IEEE Transactions on Power Systems*, pages 1–1, 2020.

[143] Karl Johan Åström, Tore Hägglund, and Karl J Astrom. *Advanced PID control*, volume 461. ISA-The Instrumentation, Systems, and Automation Society Research Triangle Park, 2006.

[144] Sarnaduti Brahma and Hamid R. Ossareh. Quasilinear Control of Feedback Systems with Multivariate Nonlinearities. In *58th IEEE Conference on Decision and Control (CDC)*, Nice, France, 2019.

[145] Wei-Ping Huang, Sarnaduti Brahma, and Hamid R. Ossareh. Quasilinear Control of Systems with Time-Delays and Nonlinear Actuators and Sensors. In *American Control Conference (ACC)*, Philadelphia, 2019.

[146] Mads Almassalkhi, Sarnaduti Brahma, Nawaf Nazir, Hamid Ossareh, Pavan Racherla, Soumya Kundu, Sai Pushpak Nandanoori, Thiagarajan Ramachandran, Ankit Singhal, Dennice Gayme, and et al. Hierarchical, grid-aware, and economically optimal coordination of distributed energy resources in realistic distribution systems. *Energies*, 13(23):6399, Dec 2020.

[147] Rosario Toscano. *Structured Controllers for Uncertain Systems*. Springer, 2013.

[148] Jorge J Moré and Danny C Sorensen. Computing a trust region step. *SIAM Journal on scientific and statistical computing*, 4(3):553–572, 1983.

[149] I Kazakov. Statistical Analysis of Multidimensional Nonlinearities Systems. *Avtomat. i Telemekh.*, 26(3):463–469, 1965.

[150] P. D. Spanos. Formulation of Stochastic Linearization for Symmetric or Asymmetric M.D.O.F. Nonlinear Systems. *Journal of Applied Mechanics*, 47(1):209, 2009.

[151] O Il'chenko. Stochastically bounded solutions of a linear nonhomogeneous stochastic differential equation. *Theory of Probability and Mathematical Statistics*, 68:41–48, 2004.

[152] Simo Särkkä and Arno Solin. *Applied Stochastic Differential Equations*. Cambridge University Press, 2019.

[153] Roger Brockett. Stochastic control. *Lecture Notes, Harvard University*, 2009.

[154] Elias Jarlebring. Methods for Lyapunov equation. *Lecture notes in numerical linear algebra*, pages 1–15, 2017.

[155] D R Smart. *Fixed Point Theorems*. Cambridge University Press, 1980.

[156] Weinian Zhang and Shuzhi Sam Ge. A global Implicit Function Theorem without initial point and its applications to control of non-affine systems of high dimensions. *Journal of Mathematical Analysis and Applications*, 313(1):251–261, 2006.

[157] Michael J D Powell. A FORTRAN subroutine for solving systems of nonlinear algebraic equations. *The Computer Journal*, 24:87–91, 11 1968.

[158] R H Byrd, J.Ch. Gilbert, and J Nocedal. A Trust Region Method Based on Interior Point Techniques for Nonlinear Programming. *Mathematical Programming*, 89(1):149–185, 2000.

[159] C. Soize. Stochastic linearization method with random parameters for SDOF nonlinear dynamical systems: prediction and identification procedures. *Probabilistic Engineering Mechanics*, 10(3):143–152, 1995.

[160] V.S. Pugachev, I.N. Sinitsyn, and I.V. Sinitsyna. *Stochastic Differential Systems Analysis and Filtering*. Analysis and Filtering. Wiley, 1987.

[161] W iM Wonham and WF Cashman. A computational approach to optimal control of stochastic saturating systems. *International Journal of Control*, 10(1):77–98, 1969.

[162] Fouad Mesquine, Fernando Tadeo, and Abdellatif Benlamkadem. Constrained regulator problem for linear uncertain systems: control of a pH process. *Mathematical Problems in Engineering*, 2006, 2006.

[163] Weihai Zhang, Yong Zhao, and Li Sheng. Some remarks on stability of stochastic singular systems with state-dependent noise. *Automatica*, 51:273–277, 2015.

[164] E. Gershon, D. J.N. Limebeer, U. Shaked, and I. Yaesh. Robust H_∞ filtering of stationary continuous-time linear systems with stochastic uncertainties. *IEEE Transactions on Automatic Control*, 46(11):1788–1793, 2001.

[165] U Paraev. Introduction in statistical dynamics of control and filtration processes. *Sovetskoe radio, Moscow*, 1976.

[166] Thomas F. Coleman and Yuying Li. An Interior Trust Region Approach for Nonlinear Minimization Subject to Bounds. *SIAM Journal on Optimization*, 6(2):418–445, 2005.

[167] John A. Gubner. *Probability and Random Processes for Electrical and Computer Engineers*. Cambridge University Press, 2006.

[168] H. Minkowski. *Geometrie Der Zahlen*. Creative Media Partners, LLC, 2018.

[169] Richard L. Burden and J. Douglas Faires. 2.1 the bisection algorithm. In *Numerical Analysis (3rd ed.)*. PWS Publishers, 1985.

[170] Graham R Wood. The bisection method in higher dimensions. *Mathematical programming*, 55(1-3):319–337, 1992.

[171] T. Ypma. Historical development of the newton–raphson method. *SIAM Review*, 37(4):531–551, 1995.

[172] C. G. Broyden. Quasi-newton methods and their application to function minimisation. *Mathematics of Computation*, 21(99):368–381, 1967.

[173] Thomas F Coleman and Yuying Li. An interior trust region approach for nonlinear minimization subject to bounds. *SIAM Journal on optimization*, 6(2):418–445, 1996.

[174] John E Dennis Jr and Robert B Schnabel. *Numerical methods for unconstrained optimization and nonlinear equations*. SIAM, 1996.

[175] BE Rhoades. Some fixed point iteration procedures. *International Journal of Mathematics and Mathematical Sciences*, 14(1):1–16, 1991.

[176] Huibert Kwakernaak and Raphael Sivan. *Linear optimal control systems*, volume 1. Wiley-interscience New York, New York, NY, 1972.

[177] He Hao, Borhan M Sanandaji, Kameshwar Poolla, and Tyrone L Vincent. Aggregate flexibility of thermostatically controlled loads. *IEEE Transactions on Power Systems*, 30(1):189–198, 2014.

[178] L. A. D. Espinosa, A. Khurram, and M. R. Almassalkhi. A virtual battery model for packetized energy management. In *2020 59th IEEE Conference on Decision and Control (CDC)*, pages 42–48, 2020.

[179] B. Naduvathuparambil, M. C. Valenti, and A. Feliachi. Communication delays in wide area measurement systems. In *Proceedings of the Thirty-Fourth Southeastern Symposium on System Theory (Cat. No.02EX540)*, pages 118–122, 2002.

[180] S. P. Nandanoori, S. Kundu, D. Vrabie, K. Kalsi, and J. Lian. Prioritized threshold allocation for distributed frequency response. In *2018 IEEE Conference on Control Technology and Applications (CCTA)*, pages 237–244, 2018.

[181] Richard Perez, Mathieu David, Thomas E. Hoff, Mohammad Jamaly, Sergey Kivalov, Jan Kleissl, Philippe Lauret, and Marc Perez. Spatial and temporal variability of solar energy. *Foundations and Trends® in Renewable Energy*, 1(1):1–44, 2016.

[182] K. P. Schneider, B. A. Mather, B. C. Pal, C. Ten, G. J. Shirek, H. Zhu, J. C. Fuller, J. L. R. Pereira, L. F. Ochoa, L. R. de Araujo, R. C. Dugan, S. Matthias, S. Paudyal, T. E. McDermott, and W. Kersting. Analytic considerations and design basis for the ieee distribution test feeders. *IEEE Transactions on Power Systems*, 33(3):3181–3188, 2018.

[183] Dan Simon. *Optimal state estimation: Kalman, H infinity, and nonlinear approaches*. John Wiley & Sons, 2006.

[184] J J Moré, B S Garbow, and K E Hillstrom. User guide for MINPACK-1. Technical Report ANL-80-74, Argonne Nat. Lab., Argonne, IL, Aug 1980.